PERGAMON

Progress in Energy and Combustion Science 26 (2000) 459–505

PROGRESS IN ENERGY AND COMBUSTION SCIENCE

www.elsevier.com/locate/pecs

Structure, aerodynamics, and geometry of premixed flamelets ☆

C.K. Law[a,*], C.J. Sung[b]

[a]*Department of Mechanical and Aerospace Engineering, Princeton University, Princeton, NJ 08544, USA*
[b]*Department of Mechanical and Aerospace Engineering, Case Western Reserve University, Cleveland, OH 44106, USA*

Abstract

Recent advances in the understanding of the structure, dynamics, and geometry of laminar premixed flames under the influence of stretch, as manifested by aerodynamic straining, flame curvature, and flame/flow unsteadiness, are reviewed and presented in a tutorial manner. The discussion first treats the flame as a structureless surface which propagates into the fresh mixture with a constant velocity—the laminar flame speed, and the phenomena of cusp formation and volumetric burning rate augmentation through flame wrinkling are demonstrated. It is then shown that by considering the effects of stretch on the flame structure, and by allowing for mixture nonequidiffusion, the flame responses, especially the flame speed, can be quantitatively as well as qualitatively modified. By using the stretch-affected flame speed, we then describe the phenomena of cusp broadening, of tip opening of the Bunsen flame, and of the intrinsic hydrodynamic, body-force and diffusional—thermal modes of flamefront cellular instabilities. Additional topics covered include forced and intrinsic oscillatory flame dynamics, and quantitative extraction of the global flame parameters represented by the activation energy, the Markstein length, and the Lewis number.

Keywords: Flame dynamics; Stretch; Nonequidiffusion; Markstein length

Contents

☆ This review is an updated version of an earlier paper by Law et al. (Law CK, Sung CJ, Sun CJ. On the aerodynamics of flame surfaces. In: Tien C-L, editor. Annual review of heat transfer, vol. VIII. Begell House, 1997. p. 93–151). Permission was granted by the publisher for the use of materials from this earlier paper.

* Corresponding author. Tel.: + 1-609-258-5271; fax: +1-609-258-6233.
E-mail address: cklaw@princeton.edu (C.K. Law).

0360-1285/00/$ - see front matter
PII: S0360-1285(00)00018-6

1. Introduction

The structure and propagation of laminar premixed flames are governed by convection, diffusion, and chemical reactions that are frequently characterized by large activation energies and high heat release rates. Early studies on premixed flames have pursued along two directions. The first is aerodynamic in nature, treating the flame as a structureless surface which releases a certain amount of heat according to the mixture composition, propagates with a given, constant, speed, and is passively convected by the flow field in which it is embedded. Transport and chemistry are absent. The second is the study of the flame structure, allowing for transport and chemical processes to various degrees of detail, but keeping the description of aerodynamics to the simplest level. Frequently the study is based on the idealized situation of the steady propagation of the one-dimensional planar flame in the doubly infinite domain. As such, there is basically no aerodynamics in the problem. Such analyses usually yield the speed with which the flame propagates, which is the constant flame speed needed by the aerodynamic analyses.

However, it was also recognized quite early that the characteristics of premixed flames could be profoundly affected by aerodynamics. For example, the phenomena of flame extinction, stabilization, and blowoff cannot be described if the flame had a constant flame speed. Furthermore, a constant flame speed would also fail to describe the curvature variation over the surface of a conventional closed-tipped Bunsen flame. In response of such concerns, Karlovitz [1] proposed the concept of flame stretch to describe flame extinction in nonuniform flow fields, while Markstein [2] allowed the flame speed to vary with the flame curvature in order to describe the observed flamefront cellular instability phenomena.

Over the past 25 years, since the inception of PECS, significant progress has been made in flame theory in general, and the structure and dynamics of stretched flame in particular [3–6]. For example, Karlovitz's definition of flame stretch due to flow nonuniformity has been generalized to include flame curvature and flame/flow unsteadiness [7–9], rigorous asymptotic analyses have been conducted for stretched flames [10–14], the strong coupling between diffusion and stretch has been identified, and systematic formulation to describe the dynamics of flame surfaces has been initiated [4,15]. Perhaps equally important are the results from the parallel experimental [16–23] and computational [23–26] investigations of stretched flames, providing the needed scrutiny, guidance, and verification of the analytically predicted phenomena. Thus most of the fundamental framework towards an eventual mature description of stretched flames are now in place.

There are two objectives for the present review. First, we shall update an earlier review by the first author on the dynamics of stretched flames [5]. Notable new developments are the improved interpretations of the various stretched flame phenomena, additional computational results made possible with the recent advances in computational combustion, the systematic description of the dynamics, geometry, and stability of flame surfaces, and the quantitative extraction of global flame parameters useful for the simulation of such complex phenomena as turbulent flames. The second objective is to provide tutorial material adaptable for graduate-level instruction on the subject matters covered. Being mindful of the latter objective, some of the key results are derived, instead of quoted, such that the underlying physics can be clearly exposed. The emphasis here, however, is on the physical insight and phenomenology, rather than mathematical manipulation.

In the next section we shall phenomenologically describe the structure of the one-dimensional and three-dimensional

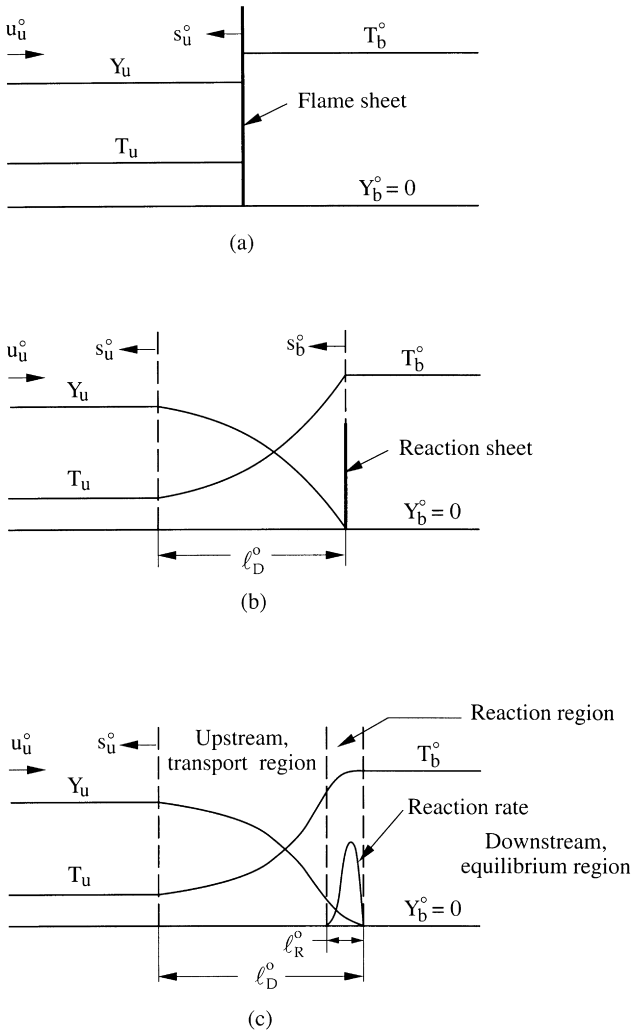

Fig. 1. Structure of the adiabatic, one-dimensional, freely propagating planar premixed flame at increasingly detailed levels of description: (a) hydrodynamic level; (b) transport level; and (c) reaction level.

flames. In Section 3 the dynamics of structureless stretched flame surfaces in hydrodynamic flow fields are discussed. The phenomena of cusp formation and burning rate augmentation through flame wrinkling are analyzed. In Sections 4–6 the influences of stretch on the flame structure and response are described and compared with experimental and computational results. A rational approach towards quantitative extraction of global flame parameters and quantitative description of the global flame responses to stretch rate variations are presented. In Section 7 we integrate results from the flame structure analysis to the dynamics of flame surfaces through the model problems of cusp broadening and the configurations of Bunsen flames. In Section 8 a unified analysis of the hydrodynamic, body-force, and diffusional–thermal flamefront cellular instabilities is presented, while in Section 9 the unsteady flame dynamics, as a result of either forced oscillation or intrinsic diffusional–thermal pulsating instability, are described. Most of the discussions on the dynamics and geometry of flame surfaces in the above topics are conducted via the *G*-equation formulation, where *G*, a constant, is a level surface in a flow field. The review closes with a discussion on some research problems and issues, in Section 10.

2. Qualitative flame structure

2.1. The one-dimensional flame

We consider the steady, adiabatic propagation of a planar flame into a combustible mixture with velocity s_u^o in the doubly infinite domain of $-\infty < x < \infty$. Designating the

unburnt and burnt states of the mixture far upstream and downstream of the nonequilibrium region of reaction and diffusion by the subscripts u and b, respectively, in the flame-stationary frame (Fig. 1a) the upstream mixture approaches the flame with velocity $u_u^o = s_u^o$ and temperature T_u, and leaves the flame with velocity $u_b^o = s_b^o$ and temperature T_b^o. If we assume that the mixture is sufficiently off-stoichiometric such that the reaction is governed by the mass fraction Y_u of the deficient reactant, then a one-reactant reaction described by Reactant → Products can be used. The superscript "o" is used to designate this particular flame.

The flame structure can be considered at three levels of detail. At the hydrodynamic level of the Rankin–Hugoniot relations, the flame is simply an interface separating two thermodynamic states of unburnt and burnt gases related by overall conservations of mass and energy. At this flame surface the temperature and the reactant concentration change discontinuously from T_u to T_b^o, and from Y_u to $Y_b^o = 0$, respectively (Fig. 1a). The states of the unburnt and burnt gases are in complete thermodynamic equilibrium.

At the next, more detailed, transport-dominated level of description, the flame sheet of Fig. 1a is expanded to reveal a so-called preheat zone of characteristic thickness $\mathcal{L}_D^o$ and dominated by heat and mass diffusion, as shown in Fig. 1b. Here as the mixture approaches the flame, it is gradually heated up by the heat conducted forward from the chemical heat release region, resulting in a continuously increasing temperature profile until T_b^o is reached. The profile is not linear because of the presence of convective transport. The continuous heating of the mixture will eventually lead to its ignition and subsequent reaction. Since combustible mixtures of interest to combustion are characterized by large activation energies, we expect that the reaction be activated only when the gas temperature is close to its maximum value. Furthermore, once reaction is initiated, it is completed rapidly as the deficient reactant is depleted. Thus at this transport-dominated level, the reaction zone can be considered to be concentrated at an interface—a reaction sheet, which serves as a source of heat and a sink for the reactant. At this surface the temperature and reactant concentration assumes their respective burnt values in the downstream, while their slopes change discontinuously.

Vanishing of the reactant concentration at the reaction sheet establishes a concentration gradient in the preheat zone. Thus the reactant concentration decreases continuously in the preheat zone. Furthermore, for mixtures whose Lewis number, *Le*, is close to unity, the similar values of the heat and mass diffusivities imply that the rate of temperature increase should be similar to that of concentration decrease; Lewis number is defined as the ratio of thermal diffusivity to a representative mass diffusivity of the mixture. For $Le = 1$ mixtures, the two profiles, when properly normalized, should span the same width (Fig. 1b). For *Le* sufficiently deviating from unity, however, the thermal and concentration thicknesses will necessarily be very different.

At the third, and most detailed level of flame description, the reaction sheet is expanded to reveal the reaction rate profile (Fig. 1c), which has a characteristic thickness $\mathcal{L}_R^o$. The reaction rate is a highly peaked function, consisting of a rapidly increasing portion due to activation of the reaction, followed by a rapidly decreasing portion because of the depletion of the reactant. Since this reaction zone is much thinner than the preheat zone, we also expect that in this zone diffusion, which is a second-order transport process, dominates over convection, which is a first-order transport process.

The one-dimensional flame structure can therefore be considered to consist of two distinct zones, namely the preheat zone in which convection and diffusion dominate and balance, and the reaction zone in which reaction and diffusion balance. Since $\mathcal{L}_R^o \ll \mathcal{L}_D^o$, the entire flame thickness representing the nonequilibrium processes of reaction and diffusion can be basically identified as $\mathcal{L}_D^o$. Across this flame, the overall conservation of mass and energy holds. Because of the low subsonic nature of the flame propagation, momentum conservation can frequently be represented by the simple condition of isobaricity.

Thus, from continuity, $\mathrm{d}(\rho u)/\mathrm{d}x = 0$, we have

$$f^o = \rho u = \rho_u u_u^o = \rho_b^o u_b^o \tag{1}$$

for the overall mass conservation, where ρ is the density and f^o the constant mass flux, which we shall call the laminar burning flux. Eq. (1) demonstrates that the fundamental flame propagation parameter is the laminar burning flux f^o instead of the propagation speed u_u^o, or s_u^o, by itself. This is a parameter of particular interest in studies of laminar flame propagation because it contains the basic information on the reactivity, diffusivity, and exothermicity of the mixture.

For energy conservation across the flame, we note that as all the deficient reactant is consumed, and because the system is adiabatic, for constant specific heat c_p we have

$$c_p(T_b^o - T_u) = q_c Y_u, \tag{2}$$

where q_c is the chemical heat release per unit mass of fuel consumed. Eq. (2) simply states that all the chemical heat liberated is used to heat the incoming gas. Therefore the downstream temperature T_b^o is just the adiabatic flame temperature T_{ad}.

In order to determine f^o, we need to consider the nonequilibrium processes of diffusion and reaction occurring within the flame structure. Since the reaction and diffusion balance in the reaction zone in general, and recognizing that the reaction is represented by a characteristic reaction time $\tau_R^o \sim (w_b^o/\rho_b^o)^{-1}$, where w_b^o is a characteristic reaction rate evaluated at the flame temperature T_b^o, while diffusion is represented by the diffusivity $(\lambda/c_p)_b/\rho_b^o$, where λ is the thermal conduction coefficient, the characteristic propagation speed of the thin reaction zone is simply $s_b^o \sim [(\lambda/c_p)_b/(\tau_R^o\rho_b^o)]^{1/2} = [(\lambda/c_p)_b w_b^o]^{1/2}/\rho_b^o$ based on dimensional

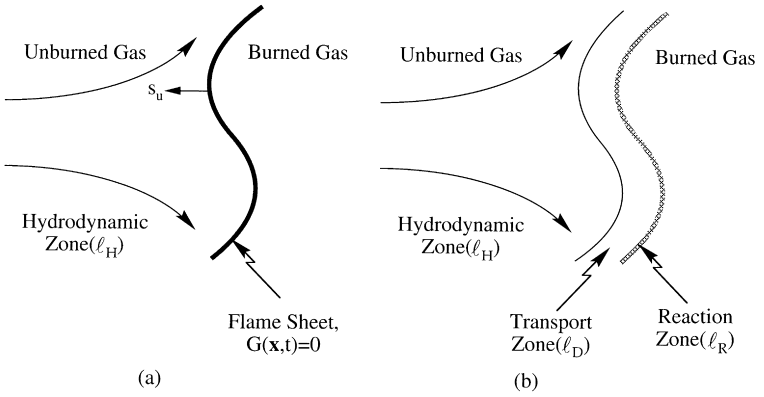

Fig. 2. Structure of a wrinkled flame at increasingly detailed levels of description: (a) hydrodynamic level of flame sheet; and (b) transport and reaction levels of detailed description.

considerations. Thus we have

$$(f^{o})^2 = (f_b^{o})^2 = (\rho_b^{o} s_b^{o})^2 \sim (\lambda/c_p)_b w_b^{o}. \tag{3}$$

From τ_R^{o} and $(\lambda/c_p)_b/\rho_b^{o}$ we can also form a characteristic length scale, which is the thickness of the reaction zone, as $(\mathcal{L}_R^{o})^2 \sim \tau_R^{o}(\lambda/c_p)_b/\rho_b^{o}$, or

$$(\mathcal{L}_R^{o})^2 \sim (\lambda/c_p)_b/w_b^{o}. \tag{4}$$

Eqs. (3) and (4) show that the laminar flame responses depend on the flame kinetics through the characteristic reaction rate w_b^{o}, and on the transport processes through the density-weighted transport coefficient $(\lambda/c_p)_b$.

Recognizing that $w_b^{o} \sim \exp(-T_a/T_b^{o})$, where $T_a = E_a/\Re$ is the activation temperature, E_a the activation energy, and $\Re$ the universal gas constant, that $\mathcal{L}_R^{o}$ and $\mathcal{L}_D^{o}$ can be approximately related through the temperature variations across the reaction and preheat zones, $(\mathcal{L}_R^{o}/\mathcal{L}_D^{o}) = \Delta T_R/(T_b^{o} - T_u)$, and that the characteristic temperature change across the reaction zone can be estimated by $\Delta T_R \sim [w/(\mathrm{d}w/\mathrm{d}T)]_{T_b^{o}}$, $\mathcal{L}_D^{o}$ can be related to $\mathcal{L}_R^{o}$ through

$$(\mathcal{L}_R^{o}/\mathcal{L}_D^{o}) \sim \frac{(T_b^{o})^2}{(T_b^{o} - T_u)T_a} = \epsilon^{o}. \tag{5}$$

In Eq. (5) we have defined a parameter ϵ^{o}, which basically compares the thermal energy available for the reaction ($\sim T_b^{o}$) to the activation energy ($\sim T_a$) of the reaction. Furthermore, since $T_a \gg T_b^{o}$, we have $\epsilon^{o} \ll 1$ provided that the heat release is substantial ($T_b^{o} \gg T_u$), which is usually the situation. The inverse of ϵ^{o} is the Zeldovich number, *Ze*. We have therefore obtained the order-of-magnitude estimates for f^{o}, $\mathcal{L}_R^{o}$ and $\mathcal{L}_D^{o}$.

Detailed derivations of f^{o} with non-unity *Le*, using either the rigorous activation energy asymptotic analysis, or less rigorous methods such as that of Frank-Kamenetskii, or the control volume analysis [14] which we shall use later in the study of stretched flames, yield a similar, but more detailed expression

$$f^{o} = \epsilon^{o}[Le(\lambda/c_p)B_C \exp(-T_a/T_b^{o})]^{1/2} \tag{6}$$

where B_C is a collision frequency having the unit (gm/cm^3/s).

Eq. (6) shows that $f^{o} \sim \sqrt{Le}$ for non-unity *Le* mixtures. Furthermore, if $Le \neq 1$, then instead of using a single diffusion length $\mathcal{L}_D^{o}$, we also need to distinguish the thermal diffusion length $\mathcal{L}_T^{o}$ from the mass diffusion length $\mathcal{L}_M^{o}$. From the control volume analysis we have

$$(\mathcal{L}_T^{o}/\mathcal{L}_M^{o}) = Le. \tag{7}$$

2.2. The wrinkled flame

It is clear that practical flames do not conform to the idealized planar configuration discussed earlier. Instead they can be wrinkled and unsteady, and can also exist in flow fields that are nonuniform and unsteady. It is therefore reasonable to expect that the various flame responses, such as the burning rate and thickness, can be quantitatively and qualitatively affected by these so-called stretch effects.

The influence of stretch on the flame response can be discussed based on the scales as well as the tangential and normal components of the flow field at the flame. Let us first consider stretch at the hydrodynamic scale (Fig. 2a). Here, analogous to the situation of Fig. 1a, diffusion and reaction are not resolved and the entire flame is considered to collapse into a flame sheet, with $\mathcal{L}_D = 0$. The flame propagates into the fresh mixture with a local propagation speed, which is normal to the flame surface and can also differ from s_u^{o}. The presence of stretch, through the tangential velocity gradient at the flame, changes the flame surface area *A* and consequently the volumetric burning rate $f_u A$. Depending on whether the local tangential velocity increases or decreases with distance along the surface, the local volumetric burning rate can also increase or decrease with stretch. The role of the normal velocity gradient is to allow adjustment of the flame location in the normal direction so that the flame

situates where the local flame speed, s_u, balances the local normal velocity, s_u. Thus the combined effects of the tangential and normal velocity gradients are the displacement of the flame surface, distortion of its geometry, and modification of the volumetric burning rate. We shall refer to stretch at this level of consideration as hydrodynamic stretch.

Resolving the transport and reaction zones (Fig. 2b), the tangential velocity variation in the transport zone directly affects the normal mass flux f_b entering the reaction zone. Furthermore, through interaction with heat and mass diffusion, it can also modify the temperature and concentration profiles in the transport zone and consequently the burning intensity, T_b and f_b, in the reaction zone, as will be shown later. We shall refer to stretch at this level as flame stretch. The normal velocity variation also affects the residence time within the reaction zone and consequently T_b and the completeness of reaction. It is however also important to note the flexibility with which a premixed flame can adjust its location to accommodate changes in the normal velocity gradient and to achieve the local stabilization requirement of $s_u = u_u$. Thus a change in the stretch rate does not necessarily lead to a change of corresponding extent in the residence time. We shall refer to a flame with total freedom of adjustment as either a freely propagating or freely standing flame, depending on whether the flame is in motion in the frame of reference under consideration.

The hydrodynamic stretch and flame stretch are strongly coupled in that the hydrodynamic stretch imposes the stretch intensity within the flame, constituting the flame stretch, while the flame stretch not only yields the propagation speed of the hydrodynamic flame surface, but it also predicts such critical phenomena as flame extinction. The direct influence of stretch in the reaction zone is expected to be small because of the secondary importance of convective transport in this very thin zone.

3. Hydrodynamic stretch

3.1. The G-equation

Let us now consider the situation wherein the flame is much thinner than the hydrodynamic length scale such that it can be treated as a surface propagating in the hydrodynamic flow. Let the geometry of the surface be described by

$$G(\mathbf{x}, t) = 0. \tag{8}$$

This surface is assumed to be smooth and continuous so that its unit normal vector,

$$\mathbf{n} = -\nabla G/|\nabla G|, \tag{9}$$

is uniquely defined everywhere. If we further define $\mathbf{n}$ to be positive when pointed in the upstream direction of the flame, a flame segment that is convex towards the unburnt mixture will have a positive curvature. On this surface, the relation

$$\frac{\mathrm{d}G}{\mathrm{d}t} = \frac{\partial G}{\partial t} + \mathbf{V}_f \cdot \nabla G = 0 \tag{10}$$

must hold, where $\mathbf{V}_f = \mathrm{d}\mathbf{x}/\mathrm{d}t$ is the local propagation velocity of the surface. Furthermore, the local propagation speed of the flame, s_u, is by definition

$$s_u = (\mathbf{V}_f - \mathbf{v}|_{G=0^-}) \cdot \mathbf{n}, \tag{11}$$

where $\mathbf{v}$ is the flow velocity. Substituting Eq. (11) into Eq. (10), and using Eq. (9), we obtain the G-equation [2,7,15]

$$\frac{\partial \hat{G}}{\partial \hat{t}} + \tilde{\mathbf{v}}|_{\hat{G}=0^-} \cdot \hat{\nabla} \hat{G} = \tilde{s}_u |\hat{\nabla} \hat{G}|, \tag{12}$$

where $\tilde{s}_u = s_u/s_u^o$ and we have also nondimensionalized $\mathbf{v}$ by s_u^o, all space variables by the hydrodynamic scale $\mathscr{L}_H$, and t by $\mathscr{L}_H/s_u^o$. For consistency all quantities referenced to the hydrodynamic length scale $\mathscr{L}_H$ and flame properties are superscripted by " $\wedge$ " and " $\sim$ ", respectively.

The G-equation, Eq. (12), describes the dynamics and geometry of the flame surface G in the flow field $\mathbf{v}$. We shall call such a flame as a premixed flamelet. We note that the LHS of Eq. (12) is simply the substantial derivative of $\hat{G}$ while the RHS represents a source term that causes the flame surface to propagate with the normal flame speed s_u relative to the unburnt mixture. The G-equation is coupled to the governing equations in the hydrodynamic regions through the term $|\tilde{\mathbf{v}}|_{\hat{G}=0^-}$. The coupling is quite complicated, representing the interaction between the flame front and the outer hydrodynamic flow: the outer flow convects the front while the front affects the outer flow through thermal expansion. The problem, however, can be decoupled and hence significantly simplified by assuming that s_u is not affected by stretch such that $s_u = s_u^o$ over the entire flame surface. We shall term this mode of flame propagation as the Landau limit, recognizing that Landau was among the first in employing this limit in the study of flame dynamics. The G-equation then becomes

$$\frac{\partial \hat{G}}{\partial \hat{t}} + \tilde{\mathbf{v}}|_{\hat{G}=0^-} \cdot \hat{\nabla} \hat{G} = |\hat{\nabla} \hat{G}|. \tag{13}$$

Further simplification in the analysis can also be achieved by making the constant density assumption such that the surface is a passive scalar being convected and distorted by $\tilde{\mathbf{v}}|_{\hat{G}=0^-}$, which can be considered to be prescribed. The constant density assumption is equivalent to the statement that there is negligible heat release in crossing the flame [27]. While such an assumption is obviously violated in real flames, it facilitates analysis and yields results that are readily amenable to physical interpretation. There are also reactive liquid systems in which the spreading of the chemical front is indeed almost thermally neutral [28].

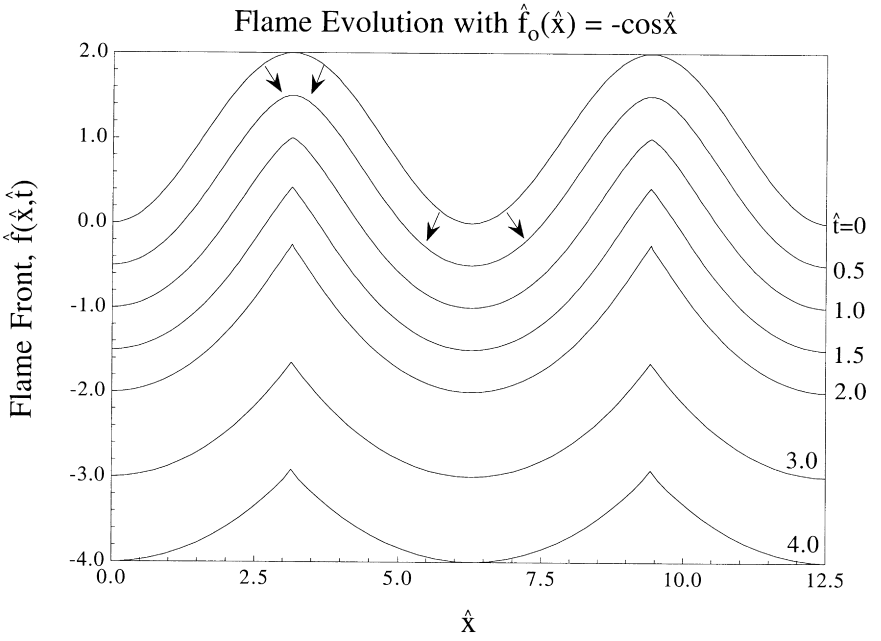

Fig. 3. Evolution and propagation of an initially sinusoidal flame surface in a quiescent medium, showing the formation of cusps over the flame surface.

3.2. Cusp formation

A characteristic of the Landau limit is the propensity of cusp[1] formation over the flame surface. Fig. 3 shows the evolution of a flame surface with an initial sinusoidal profile in a quiescent environment [29]. It is seen that, since the flame surface propagates normal to itself, it spreads out in the protruding, crest region, but steepens in the receding, trough region, as viewed from the unburnt side of the flame. Thus depending on the initial flame shape and the flow field, cusps can develop in the trough region.

To study this problem in a more general manner, we consider the evolution of a flame surface in a quiescent flow field [29]. Eq. (13) then becomes

$$\frac{\partial \hat{G}}{\partial \hat{t}} = |\hat{\nabla}\hat{G}|. \tag{14}$$

If we assume that the flame is not folded or multiply connected, then in two dimension the flame surface can be described by $\hat{G}(\hat{x},\hat{y},\hat{t}) = \hat{y} - \hat{f}(\hat{x},\hat{t})$, where $\hat{f}(\hat{x},\hat{t})$ is the flame shape function with $\hat{f}(\hat{x},0) = \hat{f}_0(\hat{x})$ being its initial shape. Eq. (14) can thus be expressed as

$$\frac{\partial \hat{f}}{\partial \hat{t}} = -\left[1 + \left(\frac{\partial \hat{f}}{\partial \hat{x}}\right)^2\right]^{1/2}. \tag{15}$$

Take the partial derivative of Eq. (15) with respect to $\hat{x}$ and let $\hat{g} = \partial\hat{f}/\partial\hat{x}$, Eq. (15) becomes

$$\frac{\partial \hat{g}}{\partial \hat{t}} + \frac{\hat{g}}{(1+\hat{g}^2)^{1/2}}\frac{\partial \hat{g}}{\partial \hat{x}} = 0, \tag{16}$$

with the initial condition $\hat{g}(x,0) = \hat{g}_0(x) = \mathrm{d}\hat{f}_0/\mathrm{d}\hat{x}$.

Eq. (16) is a quasi-linear wave equation whose solution can be obtained by using the method of characteristics in the same manner as that for shock formation from compressive Mach waves in supersonic flows. Thus the general solution for $\hat{g}$ is

$$\hat{g}(\hat{x},\hat{t}) = \hat{g}_0\left(\hat{x} - \frac{\hat{g}}{(1+\hat{g}^2)^{1/2}}\hat{t}\right), \tag{17}$$

while the minimum time $\hat{t}^*$ for cusp formation is

$$\hat{t}^* = \min\left\{\frac{-(1+\hat{g}_0^2)^{3/2}}{(\mathrm{d}\hat{g}_0/\mathrm{d}\hat{x})}\right\}, \tag{18}$$

and the propagation velocity $\hat{\mathbf{v}}^*$ of the cusp after it is formed is

$$\hat{\mathbf{v}}^* = \frac{[(1+g^2)^{1/2}]}{[g]} \tag{19}$$

[1] Mathematically, a cusp is defined as the intersection point of two branches of a curve, with coincident tangents on both sides. However, in the combustion literature the term "cusp" has been used to describe the sharp corner along the flame front, corresponding to a discontinuity in the slope of the flame front.

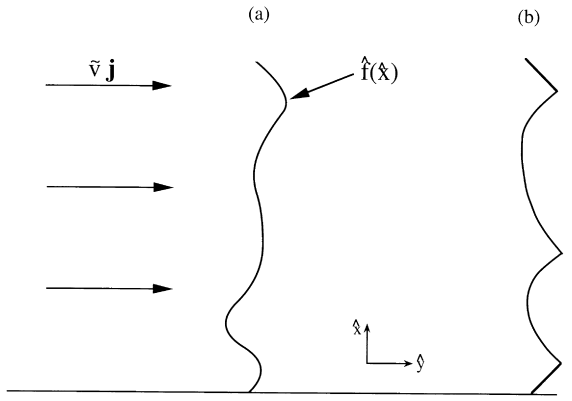

Fig. 4. Schematic demonstrating the increase of bulk flame propagation rate due to flame wrinkling: (a) before cusp formation; (b) after cusp formation.

where $[\cdot]$ in Eq. (19) represents the jump in the bracketed quantity across the cusp.

For the example given in Fig. 3, the initial sinusoidal flame shape is described by $\hat{f}_0(\hat{x}) = -\cos\hat{x}$, such that $\hat{g}_0(\hat{x}) = \sin\hat{x}$. Eq. (18) then readily shows that the cusp is formed at $\hat{t}^* = 1$, as shown in the figure. Furthermore, $\hat{v}^* = 0$ due to the symmetry of $\hat{g}$.

3.3. Burning rate increase through flame wrinkling

Conceptually, it can be readily accepted that, by wrinkling a flame through hydrodynamic stretch, the total flame surface area is increased. Thus if the burning flux at the flame surface is not affected by stretch, then the burning rate of a combustible mixture through which the wrinkled flame propagates will increase with increasing wrinkling simply due to the increase in the flame surface area. Indeed, this is the primary mechanism through which the volumetric burning rate of a turbulent flame is increased over that of the planar flame in the regime of thin flamelets.

To demonstrate such an increase in the burning rate [29], Fig. 4a shows an arbitrarily wrinkled flame situated in a flow field of uniform velocity $\tilde{v}\mathbf{j}$ in the y-direction. For $\partial\hat{G}/\partial\hat{t} = 0$, use of $\tilde{v}\mathbf{j}$ for $\mathbf{v}$ in Eq. (13) readily yields

$$\tilde{v} = \left[1 + \left(\frac{\partial\hat{G}}{\partial\hat{x}}\right)^2 \Big/ \left(\frac{\partial\hat{G}}{\partial\hat{y}}\right)^2\right]^{1/2}, \tag{20}$$

which shows that $\tilde{v} = v/s_u^o > 1$, hence demonstrating that the global propagating velocity of a wrinkled flame is higher than that of the laminar flame.

If the flame is also not folded, then $\hat{G}(\hat{x},\hat{y}) = \hat{y} - \hat{f}(\hat{x})$. Substituting $\hat{G}$ into Eq. (20) yields

$$\tilde{v} = \left[1 + \left(\frac{d\hat{f}}{d\hat{x}}\right)^2\right]^{1/2}. \tag{21}$$

Extending Eq. (21) to an arbitrary three-dimensional flame surface, we have

$$\tilde{v} = \left[1 + |\hat{\nabla}_\perp \hat{f}|^2\right]^{1/2}, \tag{22}$$

where $\hat{\nabla}_\perp$ is the two-dimensional gradient operator in the x and z directions. For a weakly wrinkled flame, Eq. (22) can be expanded to yield

$$\tilde{v} = 1 + \tfrac{1}{2}|\hat{\nabla}_\perp \hat{f}|^2, \tag{23}$$

which is basically the quadratic relation derived by Clavin and Williams [12] for the propagation speed of weakly turbulent flames.

It is also of interest to note that, for the particular problem of a uniform and steady upstream velocity, the convex segment continuously grows, while the concave segment continuously shrinks until it is totally eliminated when the cusp is formed. Subsequently the increase in the surface area and hence the burning rate relative to the planar flame are

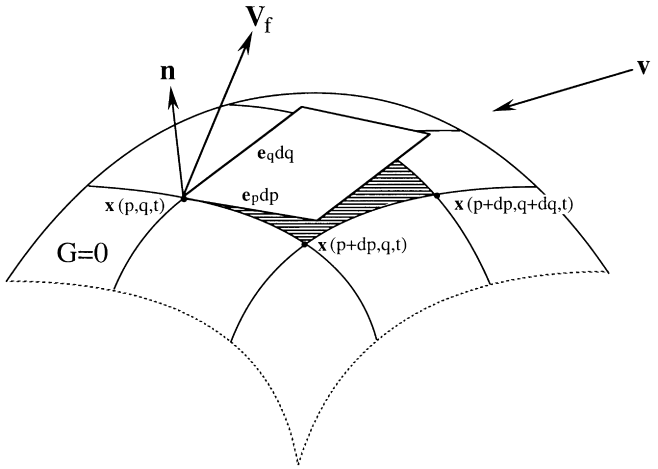

Fig. 5. Schematic of a surface element with velocity $\mathbf{V}_f$ and unit normal vector n in a flow field of $\mathbf{v}$.

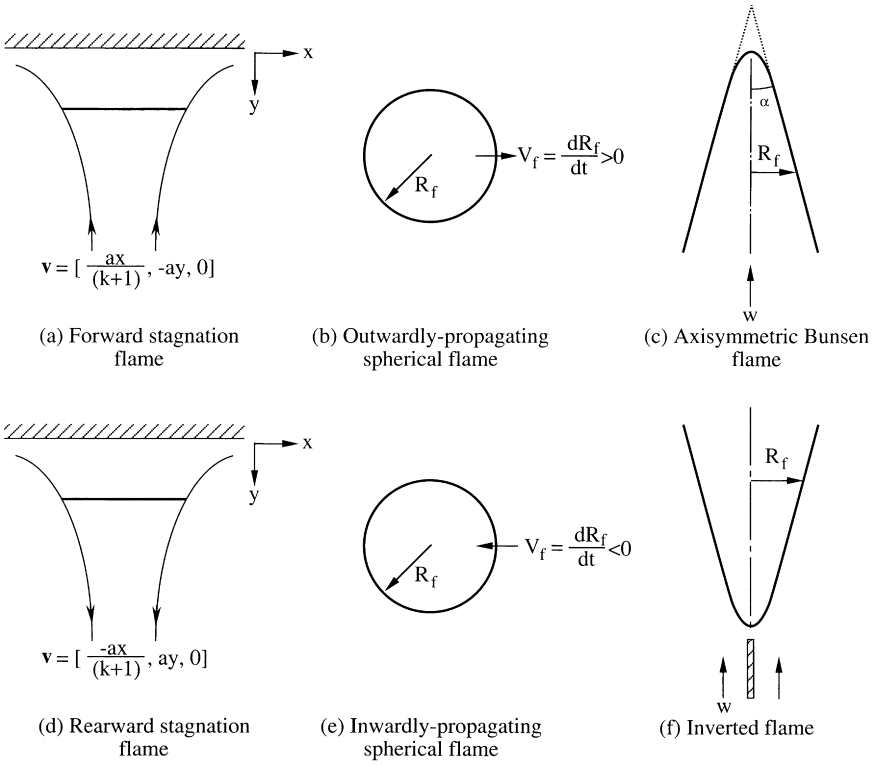

Fig. 6. Configurations of various model stretched flames.

solely contributed by the convex flame segments (Fig. 4b). Furthermore, the area of such a convex segment will continuously decrease as the opposite sides of the cusp collide and annihilate each other. Based on the above consideration *alone*, we can then say that in a uniform and steady flow a wrinkled flame tends to "smooth out" after the initial formation of cusps.

3.4. The stretch rate

The *G*-equation describes the dynamics and geometry of the flame surface through the knowledge of the flow velocity at the flame surface, $\mathbf{v}|_{G=0^-}$, the flame propagation speed s_u, and the geometry of the flame through its unit normal vector **n**. However, for an observer stationed on the flame surface, the individual influences of the flow and flame motion cannot be distinguished. Rather, the observer simply perceives an unsteady and nonuniform flow approaching it with some effective velocity. Its influence on the flame response, either the flame surface area in the hydrodynamic limit or the flame speed s_u and thereby the burning intensity, is through the extent of the unsteadiness of the flow and the nonuniform tangential velocity over the flame surface. Consequently it is reasonable to expect that the various influences due to flow nonuniformity, flame curvature, and flame/flow unsteadiness can be collectively described by a single parameter—the stretch rate, to be defined later in the article [7,8].

Fig. 5 shows a general flame surface $G = 0$. This surface has a velocity $\mathbf{V}_f$ while the fluid has a velocity **v**. A general definition of stretch at any point on this surface is the Lagrangian time derivative of the logarithm of the area A of an infinitesimal element of the surface [4],

$$\kappa = \frac{1}{A}\frac{\mathrm{d}A}{\mathrm{d}t}, \tag{24}$$

with the boundary of this surface element moving tangentially along the surface at the local tangential component of the fluid velocity. Thus κ has the unit of s^{-1}.

The deceptively simple expression of Eq. (24) actually contains the various factors that contribute to the influence of stretch [7,8]. To demonstrate this we now express Eq. (24) in terms of the dynamics of the general surface defined by $\mathbf{x}(p, q, t)$ as shown in Fig. 5, where (p, q) are the two curvilinear coordinates on it. The instantaneous velocity of the surface is therefore $\mathbf{V}_f(p, q, t) = \partial\mathbf{x}(p, q, t)/\partial t$. Since $\mathrm{d}\mathbf{x} = \mathbf{e}_p\,\mathrm{d}p + \mathbf{e}_q\,\mathrm{d}q$, where $\mathbf{e}_p$ and $\mathbf{e}_q$ are the unit vectors in the directions of p and q, an elemental area $A(p, q, t)$ of the surface at time t is simply

$$A(p, q, t) = (\mathbf{e}_p\,\mathrm{d}p) \times (\mathbf{e}_q\,\mathrm{d}q) = (\mathrm{d}p\,\mathrm{d}q)\mathbf{n}, \tag{25}$$

where $\mathbf{n} = \mathbf{e}_p \times \mathbf{e}_q$ is the unit vector of the elemental surface

pointed in the direction in which the surface is propagating, as defined earlier.

At a later time $(t + \delta t)$, the surface area becomes

$$A(p,q,t+\delta t) = \left[\mathbf{e}_p + \left(\frac{\partial \mathbf{V}_f}{\partial p}\right)\delta t\right] \times \left[\mathbf{e}_q + \left(\frac{\partial \mathbf{V}_f}{\partial q}\right)\delta t\right] \mathrm{d}p\,\mathrm{d}q. \tag{26}$$

Therefore with $A = \mathbf{A}\cdot\mathbf{n}$, the stretch rate can be expressed as

$$\kappa = \frac{1}{A(t)} \lim_{\delta t \to 0} \frac{A(t+\delta t) - A(t)}{\delta t} = \left[\mathbf{e}_p \cdot \frac{\partial \mathbf{V}_f}{\partial p} + \mathbf{e}_q \cdot \frac{\partial \mathbf{V}_f}{\partial q}\right], \tag{27}$$

which can be further developed to yield

$$\kappa = \nabla_t \cdot \mathbf{V}_f + (\mathbf{V}_f \cdot \mathbf{n})(\nabla \cdot \mathbf{n}), \tag{28}$$

where ∇_t is the tangential gradient operator over the flame surface. If we next decompose $\mathbf{V}_f$ into its tangential and normal components as $\mathbf{V}_f = \mathbf{V}_{f,t} + (\mathbf{V}_f \cdot \mathbf{n})\mathbf{n}$, where $\mathbf{V}_{f,t}$ is the tangential velocity of the surface, and assume that $\mathbf{V}_{f,t}$ is equal to the tangential component of the flow velocity $\mathbf{v}_s = \mathbf{v}|_{G=0^-}$ at the flame,

$$\mathbf{V}_{f,t} = \mathbf{v}_{s,t}, \tag{29}$$

Eq. (28) becomes

$$\kappa = \nabla_t \cdot \mathbf{v}_{s,t} + (\mathbf{V}_f \cdot \mathbf{n})(\nabla \cdot \mathbf{n}). \tag{30}$$

Eq. (30) shows the two sources of stretch a flame can be subjected to. The first term represents the influence of flow nonuniformity along the flame surface. Since $\mathbf{v}_{s,t} = \mathbf{n} \times (\mathbf{v}_s \times \mathbf{n})$, this term embodies the effects due to flow nonuniformity through v_s and flame curvature through the variation in $\mathbf{n}$. Furthermore, it exists only if the flow is oblique to the flame surface such that $\mathbf{v}_s \times \mathbf{n} \neq 0$. The second term in Eq. (30) represents stretch experienced by a nonstationary flame through $\mathbf{V}_f$, although the flame also has to be curved because $\nabla \cdot \mathbf{n}$ vanishes otherwise. These three stretch-induced effects can be separately referred to as those caused by aerodynamic straining, flame curvature, and flame motion. We further note that as (heat and mass) diffusion is in the direction of $\mathbf{n}$, the non-orthogonality requirement of $(\mathbf{v}_s \times \mathbf{n}) \neq 0$ leads us to anticipate the importance of diffusive transport in the dynamics of stretched flames, although the discussion so far has been kinematic in nature.

Although the use of the tangential gradient operator at the surface, ∇_t, provides a clear physical interpretation of stretch, mathematical specification of ∇_t can be somewhat cumbersome, especially for curved flames. However, since $\nabla = \nabla_t + \nabla_n$, where ∇_n is the normal component of the gradient operator on the surface, and $\nabla_n \cdot \mathbf{v}_{s,t} \equiv 0$, Eq. (30) can be alternately expressed as

$$\kappa = \nabla \cdot \mathbf{v}_{s,t} + (\mathbf{V}_f \cdot \mathbf{n})(\nabla \cdot \mathbf{n}). \tag{31}$$

As examples, let us compute the stretch rate κ for some common flame configurations shown in Fig. 6. The flames are infinitely thin so that the stretched surface is the flame.

(a) *Stationary planar flame in stagnation flow*—Fig. 6a shows a planar flame situated in a divergent stagnation flow. Assuming potential flow, the velocity vector is

$$\mathbf{v} = \{[a/(k+1)]x, -ay, 0\}, \tag{32}$$

where a is the strain rate of the flow, $k = 0, 1$ for Cartesian and cylindrical coordinates, respectively, and the x- and y-velocities in the cylindrical coordinates are those in the radial and axial directions, respectively. Using Eq. (30), since $(\mathbf{V}_f \cdot \mathbf{n}) = 0$ while $\nabla_t \cdot \mathbf{v}_{s,t} = a$, we have

$$\kappa = a. \tag{33}$$

(b) *Nonstationary spherical flame*—we again use Eq. (30) for evaluation. Here the flame propagates normal to its surface, implying that $\mathbf{v}_{s,t} = 0$ and $\mathbf{V}_f \cdot \mathbf{n} = V_f = \mathrm{d}R_f/\mathrm{d}t$, where R_f is the instantaneous flame radius. Furthermore,

$$(\nabla \cdot \mathbf{n}) = \pm\left(\frac{1}{R_1} + \frac{1}{R_2}\right), \tag{34}$$

where $\pm$, respectively, refer to outwardly and inwardly propagating flames because by definition $\partial \mathbf{e}_p/\partial p$ and $\partial \mathbf{e}_q/\partial q$ are the two principal radii of curvature, R_1 and R_2, pointed away from the flame surface towards the center of curvature, and $\mathbf{n}$, respectively, points outward and inward for these flames. Note that as the flame propagates, the stretch effect becomes weaker for an expanding flame and stronger for an inwardly propagating flame.

If the flame is spherically symmetric (Fig. 6b and e), $R_1 = R_2 = R_f$, we have

$$\kappa = \pm\frac{2}{R_f}\frac{\mathrm{d}R_f}{\mathrm{d}t}. \tag{35}$$

(c) *Axisymmetric flame*—this configuration includes the Bunsen flame (Fig. 6c). Adopting the cylindrical (r, θ, z) coordinate, and using Eq. (30) in which $\mathbf{V}_f = 0$, $\mathbf{v} = (0, 0, -w)$, and $\mathbf{n} = (-\cos\alpha, 0, \sin\alpha)$, we have

$$\kappa = -\left\{\frac{\sin\alpha}{r}\frac{\partial}{\partial r}(rw\cos\alpha) + \cos\alpha\frac{\partial}{\partial z}(w\cos\alpha)\right\} \tag{36}$$

evaluated at the flame surface. This result is general in that w and α can be general functions of r and z. If we further assume that w and α are constants such that the flame surface is a circular cone with a sharp apex, then

$$\kappa = -\frac{w\sin 2\alpha}{2R_f}. \tag{37}$$

Stretch in this case is derived from the three-dimensional nature of the curved surface. Note that while the forward stagnation flame and the outwardly propagating spherical flame are positively stretched, the stretch for the axisymmetric Bunsen flame is negative. This indicates that the Bunsen flame actually suffers compression. The intensity of compression also increases with the decreasing R_f as the flow moves towards the apex. The expression breaks down around the apex of the cone where $R_f \to 0$.

Similar to the outwardly and inwardly propagating

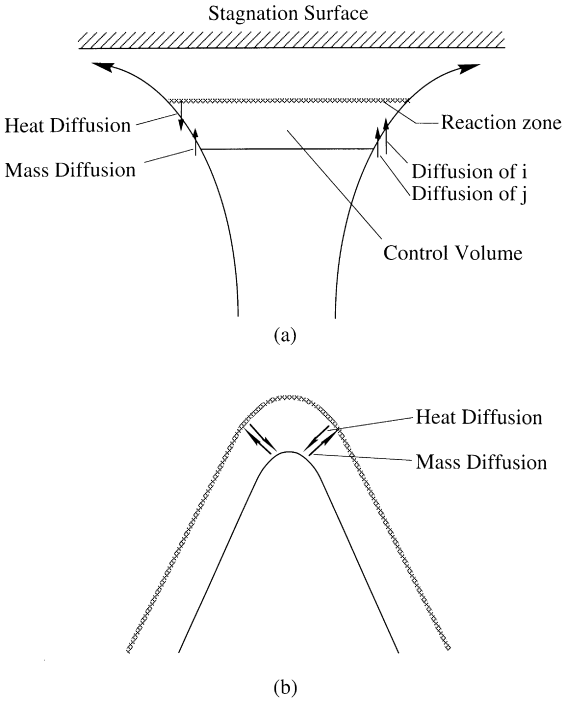

Fig. 7. Conceptual demonstration of the nonconservative nature of stretched flame response in the presence of nonequidiffusion: (a) stagnation flame; (b) tip of Bunsen flame.

flames, the counterpart of the forward stagnation flame is the rearward stagnation flame (Fig. 6d), while that of the Bunsen flame is the inverted flame, whose stretch rate is positive based on curvature alone.

There are also stretchless flames. Examples are the stationary and nonstationary one-dimensional planar flames, and the stationary cylindrical and spherical flames, respectively sustained by line and point sources [30].

Finally, for discussions on the flame stretch in the next section, we shall define a nondimensional stretch rate, the Karlovitz number, as

$$Ka = \tau_D \kappa \sim \frac{\ell_D}{s_u}\kappa \sim \frac{(\lambda/c_p)_u}{f_u^2}(\rho_u \kappa) \sim \frac{(\lambda/c_p)_b}{\epsilon f_b^2}(\rho_u \kappa), \quad (38)$$

which is simply the ratio of the flame time, τ_D, to the hydrodynamic time, $1/\kappa$. It also shows that the natural unit to measure the effect of stretch is a density-weighted stretch rate $\rho_u \kappa$, indicating the essential nature of convective transport. De Goey et al. [9] have developed expressions for the density-weighted stretch rate.

4. Flame stretch: phenomenology

We now study the effects of stretch on the flame structure and response [10–14]. Such effects can modify the flame responses such as the flame speed s_u used in the G-equation. The response has been found to be particularly strong for mixtures with unequal diffusivities because the flame temperature is directly affected. The structure itself, however, turns out to be affected to a much less extent. For mixtures with equal diffusivities, the influence has also been found to be quite subtle, as we shall show later.

To demonstrate the influence of nonequidiffusion on the response of stretched flames, we first note that there are at least three diffusivities of interest for an inert-abundant mixture, namely those associated with heat D_T, the deficient reactant D_i, and the excess reactant D_j. From these three diffusivities two interpretations for the effects of different diffusivities have been developed, based on comparing D_i with D_T, and D_i with D_j, for sufficiently off- and near-stoichiometric situations, respectively. These two interpretations can be, respectively, termed nonunity Lewis number effect, $Le = D_T/D_i$, and preferential diffusion effect, $(D_i/D_j) \neq 1$. The general phenomena related to unequal diffusion rates will be referred to as nonequidiffusion effects.

We first consider the flame response in a forward stagnation flow (Fig. 7a), and draw a control volume enclosing the transport zone and the divergent streamline as shown. By assuming that the stagnation surface is adiabatic, and that the flame can freely adjust its location in response to changes in stretch such that a complete reaction can be achieved; we can study the coupled effects of flow straining and mixture nonequidiffusion without complications from the system heat loss, flame curvature, and incomplete reaction.

Recognizing that the diffusive transport is normal to the reaction surface, then with the nonunity Lewis number interpretation, the control volume loses thermal energy to the external streamlines while it gains chemical energy from them due to an increase of the deficient reactant concentration. Thus the flame behavior, especially its temperature, depends on the relative rates of heat and mass diffusion. If the diffusivities are equal such that $Le = 1$, then total energy is conserved and the flame temperature is the adiabatic flame temperature. However, if $Le > 1$, heat loss exceeds mass gain and we expect $T_b < T_{ad}$. Conversely $T_b > T_{ad}$ if $Le < 1$.

We next take the preferential diffusion interpretation. Then if the leaner reactant is also the more diffusive one, the reactant concentration in the reaction zone will become more stoichiometric such that the flame temperature is higher and the burning more intense. The converse holds if the leaner reactant is less diffusive.

In the following we shall adopt the nonunity Lewis number interpretation because off-stoichiometric burning is more prevalent and because heat diffusion is a crucial mechanism in flame propagation.

If we now attempt to extinguish this stagnation flame by increasing the stretch rate, the flame will be pushed closer to the stagnation surface in order to maintain kinematic balance between the local flame speed and the flow velocity normal to the flame surface. At the same time it will suffer stronger flame stretch and thereby nonequidiffusion effects. Thus it is clear that for $Le > 1$, there exists a critical stretch

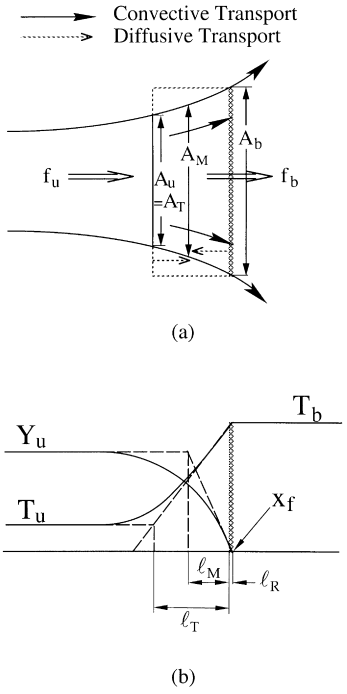

Fig. 8. Schematic for the control volume analysis of the planar stretched flame.

rate at which T_b will be reduced to such an extent that steady burning is not possible. Extinction occurs when the flame is at a finite distance away from the surface, with the lean reactant completely depleted in crossing the flame. On the other hand, for a $Le < 1$ flame, increasing stretch elevates T_b and therefore extinction cannot occur until the downstream boundary of the reaction zone is pushed onto the stagnation surface and the flame movement becomes restrained. With further stretching, reaction cannot be completed because of the reduced residence time. Only then will the flame temperature start to decrease, leading eventually to extinction.

The second situation illustrating flame stretch effects involves the burning intensity over the curved surface of an axisymmetric Bunsen cone (Fig. 7b). Here if we assume for simplicity that the flow is uniform, then flame stretch is manifested through curvature effects, especially in the tip region which has the strongest curvature. Thus for a closed tip, its concave nature towards the fresh mixture focuses the heat ahead of the flame, and therefore tends to raise the flame temperature to a value above T_{ad}. On the other hand, this curvature has a defocusing effect on the concentrations of the reactants approaching the flame, and therefore tends to reduce the flame temperature. Thus the temperature of the flame again depends on the relative rates of heat and mass diffusion. The deviation increases progressively from the flame base towards the flame tip because of the corresponding increase in the stretch intensity. Thus for $Le > 1$, the tip will burn more intensely relative to the shoulder region of the flame, while for $Le < 1$ the burning is less intense and can lead to local extinction, commonly known as the tip opening phenomenon. Note that because of the compressive nature of the Bunsen flame, its response to Lewis number variations is completely opposite to that of the positively stretched stagnation flame.

5. Flame stretch: analysis

We shall now derive the various flame responses to stretch, and thereby confirm the phenomenological discussions presented above. Asymptotic analyses have been performed for the structure and response of a wrinkled premixed flame situated in a general nonuniform flow field [10–13], although the complexity of derivation precludes their presentation here. Instead, we shall use the simpler, though somewhat less rigorous, control volume analysis [14]. Furthermore, we shall break the analysis into two parts. In Section 5.1 we shall capture the effects of stretch on the flame response through the model problem of the freely standing planar flame situated in a strained flow field that is not affected by the flame. In Section 5.2 we shall study the unstretched, stationary spherical flame to show that there is a pure curvature effect which can also modify the flame speed. Since the analyses are linear in the sense that the stretch rates and curvatures are considered to be small, results form these two separate analyses are then added in Section 5.3 to yield the final expression for the flame speed. The occurrence of extinction through nonlinear response is also discussed. These analyses are fairly straightforward, providing clear quantification of the various phenomena described above. Finally, in Section 5.4 we present results from a generalized analysis including the effect of thermal expansion on the flame structure and response.

5.1. Flame stretch effects

The problem analyzed is shown schematically in Fig. 8a. Here we shall treat the flow motion in traversing the flame structure as quasi-one-dimensional, with a varying streamtube area $A(x)$. The flame boundaries are planar. The quasi-one-dimensional governing equations are the following.

Continuity:

$$\frac{\mathrm{d}(fA)}{\mathrm{d}x} = 0. \tag{39}$$

Energy conservation:

$$\frac{\mathrm{d}}{\mathrm{d}x}\left[A\left(fc_pT - \lambda\frac{\mathrm{d}T}{\mathrm{d}x}\right)\right] = A_b q_c B_C Yk. \tag{40}$$

Species conservation:

$$\frac{\mathrm{d}}{\mathrm{d}x}\left[A\left(fY - \rho D\frac{\mathrm{d}Y}{\mathrm{d}x}\right)\right] = -A_b B_C Yk, \tag{41}$$

where A_b is the area of the thin reaction zone, $f = \rho u$ the local mass flux, and $k = \exp(-T_a/T)$ the Arrhenius factor.

Eq. (39) readily yields the constant flow rate, and hence the mass burning rate m in the streamtube,

$$m = f_u A_u = f_b A_b. \tag{42}$$

We next integrate Eq. (40) over the preheat zone, from the unburnt state where $A = A_u$ to x_f^-. The integration, however, is performed by recognizing (Fig. 8a) that while convective transport follows the streamline over the entire streamtube such that A varies from A_u to A_b and m is fixed, diffusive transport occurs only in the direction normal to the reaction "sheet" such that only the diffusion heat flux from the projection of A_u to A_b is utilized in heating the unburnt mixture. Thus diffusive transport takes place only over an area A_u. Consequently we have

$$mc_p(T_b - T_u) - \lambda\left(\frac{dT}{dx}\right)_{x_f^-} A_u = 0. \tag{43}$$

We then integrate Eq. (40) across the reaction zone, which has a constant area A_b and uniform downstream temperature T_b, to obtain

$$\lambda\left(\frac{dT}{dx}\right)_{x_f^-} = q_c B_C \int_{x_f^-}^{x_f^+} Yk\, dx. \tag{44}$$

By multiplying Eq. (44) by A_b, and adding the resulting expression to Eq. (43), we obtain overall energy transport across the entire flame,

$$mc_p(T_b - T_u) + \lambda\left(\frac{dT}{dx}\right)_{x_f^-}(A_b - A_u) = A_b q_c B_C \int_{x_f^-}^{x_f^+} Yk\, dx. \tag{45a}$$

Although Eq. (45a) is not an additional, independent relation, it clearly shows the nonconservative nature of the thermal energy transport. That is, if thermal energy were conserved, then all the chemical heat release is used to heat the mixture from the freestream. The diffusion term should then identically vanish, as for the one-dimensional planar flame in which $A_u \equiv A_b$. For the present problem, however, a finite amount of the thermal energy is lost from the control volume because of the change in the streamtube area and the fact that the diffusive transport occurs normal to the reaction zone.

A similar manipulation for the species concentration Y yields the expression indicating the nonconservative nature of species transport:

$$mY_u + \rho D\left(\frac{dY}{dx}\right)_{x_f^-}(A_b - A_u) = -A_b B_C \int_{x_f^-}^{x_f^+} Yk\, dx. \tag{45b}$$

However, if we add the expressions for the overall transport of thermal energy and species, and if we further assume equal diffusivities ($Le = 1$), then the loss in thermal energy is balanced by the gain in chemical energy such that the system is again rendered conservative, and the resulting flame temperature would be the adiabatic flame temperature. For $Le \neq 1$, such a compensation does not exist and the system would be nonconservative, as discussed phenomenologically.

By defining effective thicknesses for the thermal and mass diffusion zones as (Fig. 8b)

$$\ell_T = \frac{(T_b - T_u)}{(dT/dx)_{x_f^-}},\quad \ell_M = \frac{-Y_u}{(dY/dx)_{x_f^-}},$$

Eqs. (43) and (44), respectively, become

$$f_u \ell_T = (\lambda/c_p), \tag{46}$$

$$\lambda\frac{(T_b - T_u)}{\ell_T} = q_c B_C \int_{x_f^-}^{x_f^+} Yk\, dx. \tag{47}$$

A similar integration for the species equation yields

$$f_u \ell_M = (\rho D)(A_M/A_u), \tag{48}$$

$$(\rho D)\frac{Y_u}{\ell_M} = B_c \int_{x_f^-}^{x_f^+} Yk\, dx \tag{49}$$

Eqs. (45)–(49) provide four relations to solve the four flame responses, f_u, T_b, ℓ_T and ℓ_M in terms of the area ratio (A_M/A_u). It may be noted that the definitions of ℓ_T and ℓ_M simply replace the flame parameters $(dT/dx)_{x_f^-}$ and $(dY/dx)_{x_f^-}$; no additional independent relations are introduced.

If we assume that the change in the streamtube area is gradual (see Fig. 8b), then

$$\frac{A_b - A_u}{\ell_T} \approx \frac{A_b - A_M}{\ell_M}, \tag{50}$$

which relates A_M to A_u. Finally, recognizing that the Karlovitz number is simply a nondimensional measure of the extent of flow nonuniformity across the flame, it can be represented by the fractional area change along the streamtube. We can thus identify Ka as

$$Ka \approx \frac{\Delta A}{A_u} = \frac{A_b - A_u}{A_u} = \frac{A_b}{A_u} - 1, \tag{51}$$

which relates A_b to A_u through Ka. The problem is now completely defined in terms of the Karlovitz number Ka.

Approximating the reaction integral in Eqs. (47) and (49) by $(\epsilon^o Y_u)\ell_R^o \exp(-T_a/T_b)$, we obtain for $Ka^o = [(\lambda/c_p)_u/(f_u^o)^2](\rho_u \kappa) \ll 1$ the linearized solution

$$(A_u/A_M) = 1 + S^o \tag{52}$$

$$(\ell_T/\ell_M) = (1 + S^o)Le \tag{53}$$

$$T_b = T_b^o + (T_b^o - T_u)S^o \tag{54}$$

$$\tilde{f}_u = (f_u/f^o) = \tilde{s}_u = 1 + \sigma^o \tag{55}$$

$$\tilde{f}_b = (f_b/f^o) = 1 + \sigma^o - Ka^o/Le \tag{56}$$

$$\tilde{\ell}_T = (\ell_T/\ell_T^o) = 1 - \sigma^o, \tag{57}$$

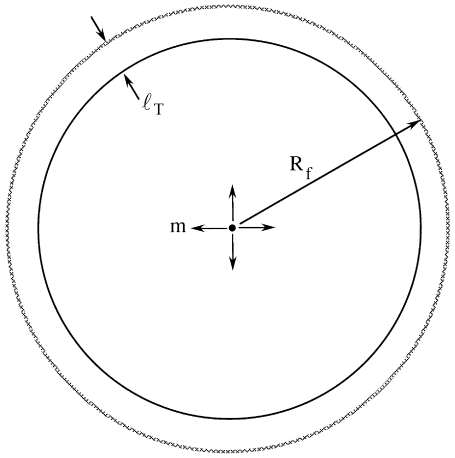

Fig. 9. Schematic for the control volume analysis of the stationary spherical flame supported by a point source.

where we have defined the two stretch-related parameters

$$S^o = \left(\frac{1}{Le} - 1\right)Ka^o, \quad \sigma^o = \frac{S^o}{2\epsilon^o} = Ma^o Ka^o \tag{58}$$

and a Markstein number

$$Ma^o = \frac{(Le^{-1} - 1)}{2\epsilon^o}. \tag{59}$$

The above results degenerate to those of the one-dimensional planar flame for $Ka^o = 0$, as should be. Furthermore, although the above derivation was performed only for the aerodynamically stretched planar flame, the general nature with which κ and hence the Karlovitz number Ka^o is defined implies that these results are applicable to flames subjected to various sources of stretch, as imposed by flow nonuniformity, flame curvature, and flame motion.

Several interesting observations can be made regarding the above results. First, we have identified two reduced parameters, namely S^o and σ^o. The parameter $S^o = (Le^{-1} - 1)Ka^o$ represents the combined effects of stretch and nonequidiffusion, and directly affects the flame temperature through energy conservation. Furthermore, since deviation of the flame temperature from the adiabatic flame temperature can occur only in the simultaneous presence of stretch ($Ka^o \neq 0$) and nonequidiffusion ($Le \neq 1$), and since Ka^o can be positive and negative, while Le can be greater or less than unity, we expect

$$T_b > T_b^o = T_{ad} \text{ for } \{Ka^o > 0,\ Le < 1\}$$
$$\text{or } \{Ka^o < 0,\ Le > 1\}$$

$$T_b < T_b^o = T_{ad} \text{ for } \{Ka^o > 0,\ Le > 1\}$$
$$\text{or } \{Ka^o < 0,\ Le < 1\}.$$

Thus the flame behavior for a gas of given Le is completely opposite for the positively stretched stagnation flame and the negatively stretched Bunsen flame, as anticipated earlier from the phenomenological discussion.

The modification of T_b through S^o leads to corresponding modifications of the burning flux and flame thickness through the factor σ^o, which combines the influence of S^o and chemical activation through ϵ^o. Since the present analysis is a linearized one such that perturbation in the burning rate, σ^o, is at most $O(\epsilon^o)$, then perturbation in the flame temperature, S^o, is $O[(\epsilon^o)^2]$. The requirement of $S = O[(\epsilon^o)^2]$ for the present linearized analysis can be met by either a highly nonequidiffusive mixture, $(Le - 1) = O(1)$, and weakly stretched flame, $Ka^o = O[(\epsilon^o)^2]$, or a near-equidiffusive mixture, $(Le - 1) = O(\epsilon^o)$, and a moderately stretched flame, $Ka^o = O(\epsilon^o)$. In any case, the linearized results cannot exhibit the intrinsically nonlinear phenomena of extinction.

It is of particular significance to recognize that, for an equidiffusive mixture ($Le = 1$), the effects of stretch vanish identically such that $\tilde{T}_b = \tilde{T}_b^o$, $\tilde{f}_u = 1$, $\tilde{f}_b = 1 - Ka^o$ and $\tilde{\mathcal{L}}_T = 1$. Thus for an adiabatic, equidiffusive, freely propagating, strained planar flame, the flame temperature, the upstream burning flux, and the flame thickness are not affected by flow straining, being identical to their unstrained values. The downstream burning flux f_b is modified from the unstrained value, f^o, by an amount Ka^o, simply due to flow divergence. As corollaries, we then expect that the thermal and concentration structures of the flame, in the direction normal to its surface, should be insensitive to strain rate variations. Furthermore, since the burning intensity at the reaction zone, as indicated by the flame temperature $\tilde{T}_b$, is not affected by strain, we should also expect that this flame cannot be extinguished by strain alone.

The above observations are in variance with some well-held concepts in combustion theory, which suggest that flow straining is a major cause of flame extinction in a nonuniform flow field [31]. The most commonly accepted argument is that increasing straining convectively reduces the flow residence time within the flame, which leads to a reduction in the flame thickness and hence eventually flame extinction. While this still holds for nonpremixed flames, the above concept has overlooked the fact that a premixed flame can freely move with increasing straining. It can therefore relocate itself to achieve dynamic balance within the flow field such that its scalar structure remains largely unaffected.

5.2. Pure curvature effects

We next consider the situation of Fig. 9 in which a steady spherical flame is supported by a point source of constant mass flow rate $m = fA$. Since diffusion now occurs in the same direction as convection, the flame is not stretched ($\mathbf{v}_s \times \mathbf{n} \equiv 0$) and is basically the spherical analog of the one-dimensional planar flame [30].

A balance of thermal energy and species transport

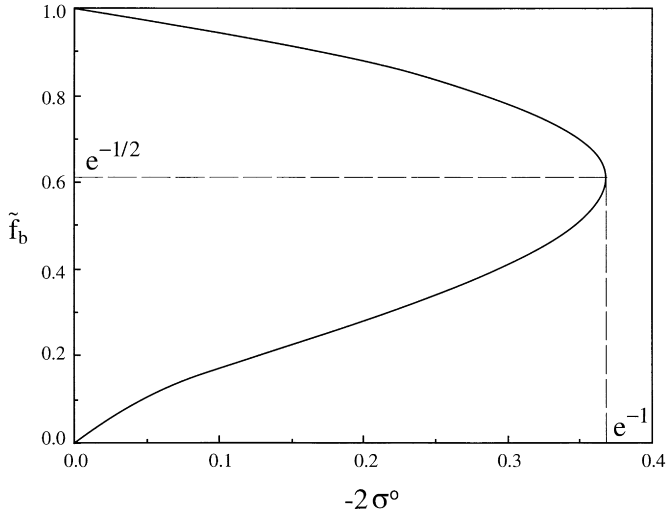

Fig. 10. Characteristic extinction turning point behavior for the nonlinear stretched flame.

through a radial streamtube across the entire flame respectively yields

$$mc_p(T_b - T_u) = A_b q_c B_C \int_{R_f^-}^{R_f^+} Yk \, dr \tag{60}$$

$$mY_u = A_b B_C \int_{R_f^-}^{R_f^+} Yk \, dr. \tag{61}$$

Comparing Eqs. (45a), (45b) and (60), we see that there is no diffusive loss in the present case and hence thermal energy is conserved across the flame. This is due to the fact that since diffusion now takes place along the streamline, the total amount of diffusive transport at A_u and A_b must be the same. A similar observation can be made for species conservation. Thus adding Eqs. (60) and (61) results in

$$c_p(T_b - T_u) = q_c Y_u, \tag{62}$$

which shows that $T_b = T_b^o$.

Analysis for the rest of the flame responses follows the same procedure as that for the stretched flame. In particular, we have

$$\tilde{\mathscr{L}}_T = 1, \ \frac{\mathscr{L}_T}{\mathscr{L}_M} = Le \tag{63}$$

$$\tilde{f}_u = \frac{A_b}{A_u} = \left(\frac{R_f}{R_f - \mathscr{L}_T}\right)^2 \approx 1 + \mathscr{L}_T^o\left(\frac{2}{R_f}\right), \ \text{for } \mathscr{L}_T^o \ll R_f \tag{64}$$

$$\tilde{f}_b = \left(\frac{A_u}{A_b}\right)\tilde{f}_u = 1. \tag{65}$$

Recognizing that $(-2/R_f)$ is simply the curvature term $\nabla\cdot\mathbf{n}$ for the spherical flame, $\tilde{f}_u$ can be generalized to

$$\tilde{f}_u = 1 - \mathscr{L}_T^o \nabla\cdot\mathbf{n} = 1 - \tilde{\nabla}\cdot\mathbf{n}. \tag{66}$$

We have therefore shown that for a purely curved flame, without stretch effects, the downstream burning flux remains the same as that of the one-dimensional planar flame, while the upstream burning flux is increased by an amount proportional to its curvature. Thus f_u is increased for a flame with negative curvature, and decreased otherwise. This is the factor that allows the burning flux at the tip of a $Le = 1$ Bunsen flame to exceed that at the shoulder [32]. It is also significant to note that, with $Le = 1$, while f_u is unaffected by straining for the planar stagnation flame, it is affected by the curvature for the purely curved flame. Consequently, through flow divergence f_b is affected for the strained planar flame but unaffected for the purely curved flame.

5.3. Linear and nonlinear solutions

Since the above solutions were obtained from linear analyses, it is reasonable to expect that a generalized linear solution would be the sum of the solutions for the stretched flame and unstretched but curved flame. Since T_b, $\tilde{\mathscr{L}}_T$, $\mathscr{L}_T/\mathscr{L}_M$ and $\tilde{f}_b$ are unaffected by curvature for the purely curved flame, their respective generalized responses are the same as those for the stretched flame, given by Eqs. (54), (57), (53) and (56), respectively. For $\tilde{f}_u$ and $\tilde{f}_b$, such a combination yields [14]

$$\tilde{f}_u = 1 - \tilde{\nabla}\cdot\mathbf{n} + \sigma^o \tag{67}$$

$$\tilde{f}_b = (f_b/f^o) = 1 + \sigma^o - Ka^o/Le. \tag{68}$$

The linearized solution is not capable to describe the

extinction phenomenon, as mentioned earlier. Furthermore, the validity of the analysis will necessarily breakdown as Ka^o increases. In particular, for the planar strained flame, the burning fluxes f_u and f_b will increase and decrease without bound for $Le < 1$ and >1, respectively.

A phenomenological analysis, however, can be readily performed based on previous results to describe the nonlinear extinction response. The crucial point to recognize is that for the strongly stretched, near-extinction flames, stretch-induced variations of the burning flux should be O(1), which implies that the corresponding variation of the flame temperature should be $O(\epsilon^o)$.

We next note that the characteristic time result of Eq. (3) for the one-dimensional adiabatic flame is equally applicable to a generalized flame of flame temperature T_b. Then we can write

$$f_b^2 \sim w_b \sim \exp(-T_a/T_b). \tag{69}$$

The flame temperature T_b is given for the stretched flame by Eq. (54), except now the perturbed amount is $O(\epsilon^o)$. Substituting T_b into Eq. (69) and expanding, we have

$$f_b^2 \sim \exp\left(-\frac{T_a}{T_b^o}\right)\exp\left(\frac{S^o}{\epsilon^o}\right). \tag{70}$$

The stretch parameter S depends on Ka, which in turn depends on the flame thickness and hence the burning flux, f_b, as shown in (38). This provides the needed feedback mechanism for extinction.

$$\frac{Ka}{Ka^o} \sim \frac{(f_b^o)^2}{f_b^2} \sim \frac{1}{\tilde{f}_b^2},$$

where $\tilde{f}_b = f_b/f^o$. Using the above Ka in f_b^2 in (70), and noting that $(f^o)^2 \sim \exp(-T_a/T_b^o)$, we have

$$\tilde{f}_b^2 \ln \tilde{f}_b^2 = 2\sigma^o. \tag{71}$$

For $\sigma^o < 0$, Eq. (71) exhibits the characteristic double valued extinction turning point behavior, as shown in Fig. 10. Here the upper branch is the physically realistic one while the lower branch is unstable. Thus for a stretchless flames, $\sigma^o = 0$ and $\tilde{f}_b = 1$. By decreasing σ^o, $\tilde{f}_b$ decreases until it reaches the turning point, at which extinction is expected. The extinction turning point is defined by $(d\sigma^o/d\tilde{f}_b)_{ex} = 0$, which yields $\tilde{f}_{b,ex} = e^{-1/2}$ and $2\sigma_{ex}^o = -e^{-1}$. Thus a flame is expected to extinguish, either globally or locally, as respectively exemplified by those of the counterflow flame and the opening of the Bunsen flame tips to be discussed later, when the global or local stretch parameter $2\sigma^o$ reaches $-e^{-1}$, at which the flame speed is reduced to $e^{-1/2}$ of its adiabatic value.

5.4. General solution with thermal expansion

While the above solutions are adequate to show the qualitative behavior of flames when subjected to stretch, they are quantitatively inaccurate. Perhaps the most severe assumption in the formulation is the suppression of the influence of thermal expansion on the flow velocity within the flame. Since the extent of thermal expansion is O(1), it is reasonable to expect that its influence is also O(1).

Recognizing that the temperature profile within the preheat zone is known to the leading order, the influence of thermal expansion has been incorporated in a generalized formulation of stretched flames, in the linearized limit [26] as well as allowing for nonlinearity and hence the description of extinction [33]. The major results in the linearized limit are given in the following equations.

$$\frac{T_b - T_u}{T_b^o - T_u} = 1 + \frac{\dot{R}(\tilde{\nabla}\cdot\mathbf{n} + \alpha^o Ka^o)}{Les_u^o}(\Lambda - \alpha^o) - \frac{\dot{R}(\tilde{\nabla}\cdot\mathbf{n} + \alpha^o Ka^o)}{s_u^o}\frac{\beta^o}{1-\beta^o}(\alpha^o - 1) + \alpha^o S^o \tag{72}$$

$$\frac{\ell_T}{\ell_T^o} = 1 + \frac{1}{2\epsilon^o}\left(\frac{T_b - T_b^o}{T_b^o - T_u}\right) \tag{73}$$

$$\frac{s_u}{s_u^o} = 1 + \left\{\frac{1}{2\epsilon^o}\left[\frac{\Lambda - \alpha^o}{Le} - \frac{\beta^o(\alpha^o - 1)}{1-\beta^o}\right] - \frac{\Lambda}{Le}\right\} \times \frac{\dot{R}(\tilde{\nabla}\cdot\mathbf{n} + \alpha^o Ka^o)}{s_u^o} + \alpha^o\sigma^o + \tilde{\nabla}\cdot\mathbf{n} \tag{74}$$

$$\frac{s_b}{s_b^o} = 1 + \left\{\frac{1}{2\epsilon^o}\left[\frac{\Lambda - \alpha^o}{Le} - \frac{\beta^o(\alpha^o - 1)}{1-\beta^o}\right] - \frac{\Lambda - \alpha^o}{Le}\right\} \times \frac{\dot{R}(\tilde{\nabla}\cdot\mathbf{n} + \alpha^o Ka^o)}{s_u^o} + \alpha^o\sigma^o - \frac{\alpha^o Ka^o}{Le}, \tag{75}$$

where $\dot{R} = dR/dt$ is the propagation speed of the flame front, $\beta^o = T_u/T_b^o = \rho_b^o/\rho_u$, $\alpha^o = 1 + \ln[\beta^o + (1-\beta^o)e^{-1}]$ is the factor accounting for the thermal expansion effect, and

$$\Lambda = \int_0^1 \frac{\beta^o(1 - e^{-\xi})}{\beta^o + (1-\beta^o)e^{-\xi/Le}}\, d\xi,$$

with $\xi \equiv x/\ell_M$ being in the flame coordinate.

For a stationary flame ($\dot{R} = 0$) and $\alpha^o = 1$, Eqs. (74) and (75) degenerate to Eqs. (67) and (68).

6. Flame stretch: experimental and computational results

6.1. Equidiffusive flames

Perhaps one of the most interesting properties predicted for stretched flames is that, for an equidiffusive ($Le = 1$), freely standing or freely propagating planar stretched flame, its flame temperature, thickness, and the upstream burning flux, are independent of the magnitude of stretch. This then

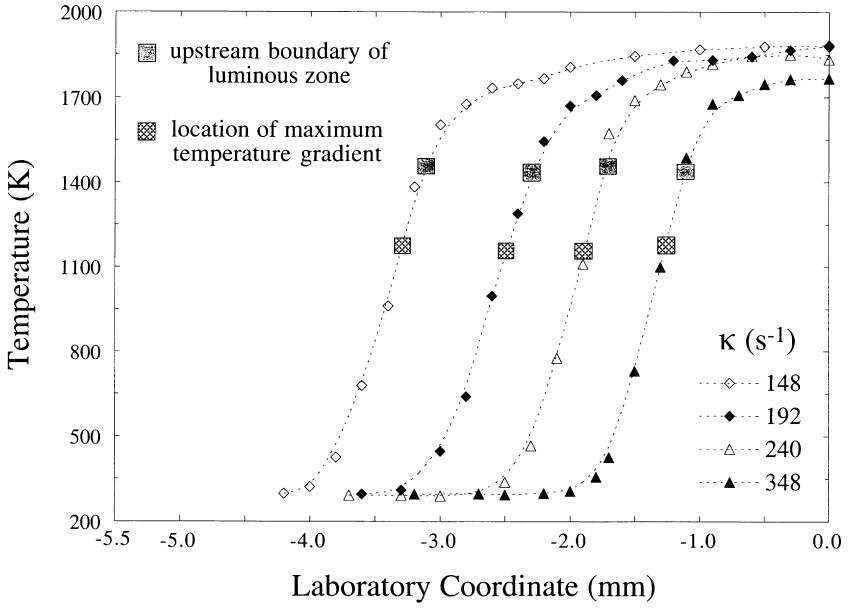

Fig. 11. Experimentally determined temperature profiles of counterflow flames with different strain rates, in the laboratory co-ordinate.

further implies that the flame structure in the direction normal to the flame surface should also be insensitive to strain rate variations. In order to verify this prediction, the temperature and major species profiles across an adiabatic, equidiffusive, nitrogen-diluted ($N_2/O_2 = 5$), $\phi = 0.95$ methane/air flame in a symmetrical counterflow has been experimentally determined by using laser Raman spectroscopy [23]. The symmetrical counterflow produces two identical flames situated on opposite sides of the stagnation surface. Owing to symmetry, all gradients vanish at the stagnation surface, hence providing well-defined "adiabatic" downstream boundary conditions. Fig. 11 shows the temperature profiles for four strain rates, with the highest strain rate (348/s) being close to the extinction state. It is

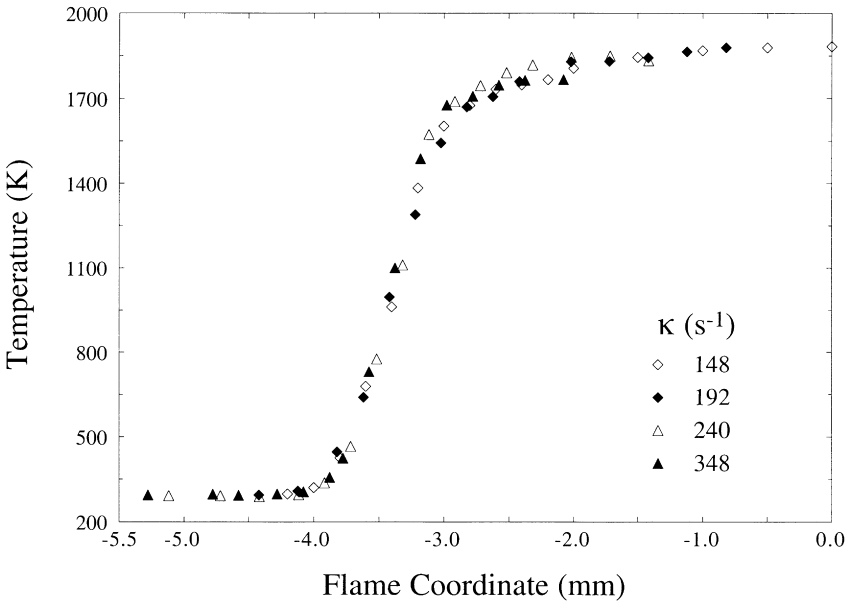

Fig. 12. Experimentally determined temperature profiles of counterflow flames with different strain rates, in the flame co-ordinate, demonstrating the insensitivity of the flame structure to strain rate variations.

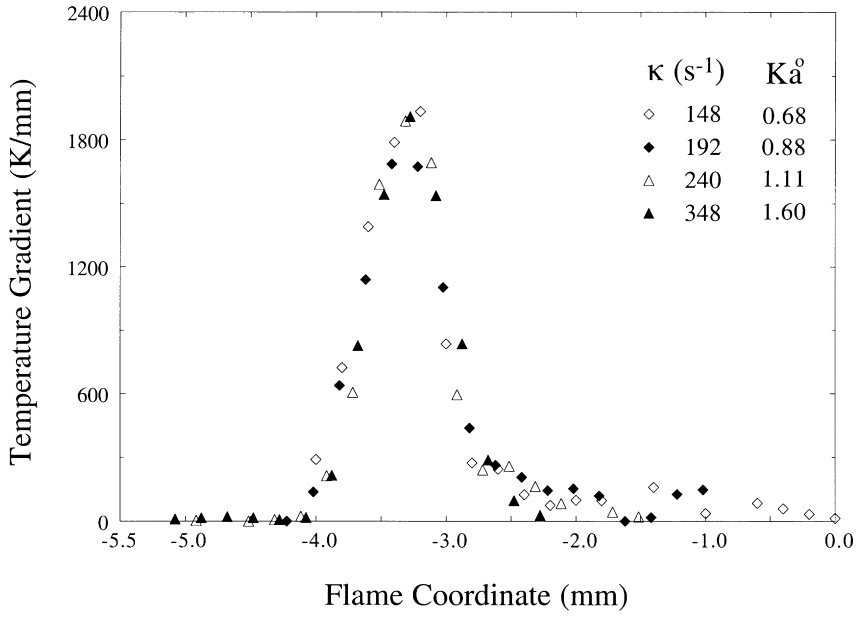

Fig. 13. Experimentally determined temperature gradient profiles of counterflow flames with different strain rates, in the flame co-ordinate.

seen that, with increasing straining, the flame recedes towards the stagnation surface (x = 0) in order to maintain dynamic balance. If we now superimpose these temperature profiles by shifting their spatial locations such that the locations of their maximum temperature gradients coincide, then Fig. 12 shows that, in this "flame coordinate", the temperature profiles basically overlap. To provide an even more stringent comparison, the temperature gradients were evaluated. Fig. 13 shows that their profiles again overlap. Similar results were obtained for the major species profiles. Furthermore, these experimental results also quantitatively agree well with the computed ones using detailed chemistry and transport [23]. As such, it is reasonable to conclude that the structure of equidiffusive, planar flames is insensitive to strain rate variations.

Fig. 13 also tabulates the computed Karlovitz numbers, $Ka^{o} = (\mathcal{L}_{T}^{o}/s_{u}^{o})\kappa$, for the four flames, with $s_{u}^{o} = 17.0$ cm/s independently calculated. The flame thickness is found to be 0.785 mm based on the definition $\mathcal{L}_{T}^{o} = (T_{ad} - T_{u})/(dT/dx)_{max}$. Using this value, Fig. 13 shows that the Karlovitz numbers including that for the near extinction state are either smaller than, or of the order of, unity.

6.2. Nonequidiffusive flames

For nonequidiffusive, stretched flames, theoretical results show that the flame response exhibits opposite behavior when the stretch changes from positive to negative, and when the mixture's effective Lewis number is greater or less than a critical value, which is unity for the flame temperature. These completely opposite trends should provide definitive verification of the concept of flame stretch with nonequidiffusion.

Two groups of mixtures are especially suitable for the study of nonequidiffusive effects (Table 1). The first group consists of lean hydrogen/air, lean methane/air, and rich propane/air mixtures. Estimates show that their effective Lewis numbers, based on the deficient species and freestream conditions, are less than unity. Thus positive (negative) stretch is expected to increase (decrease) the

Table 1
Mixtures for the study of nonequidiffusion effects

Mixture for simulation	$Le \neq 1$ interpretation	$D_i \neq D_j$ interpretation
Lean hydrogen/air	$Le_{H_2} < 1$	
Lean methane/air	$Le_{CH_4} < 1$	
Rich propane/air	$Le_{O_2} < 1$	$D_{H_2} > D_{CH_4} > D_{O_2} > D_{C_3H_8}$
Rich hydrogen/air	$Le_{O_2} > 1$	
Rich methane/air	$Le_{O_2} > 1$	
Lean propane/air	$Le_{C_3H_8} > 1$	

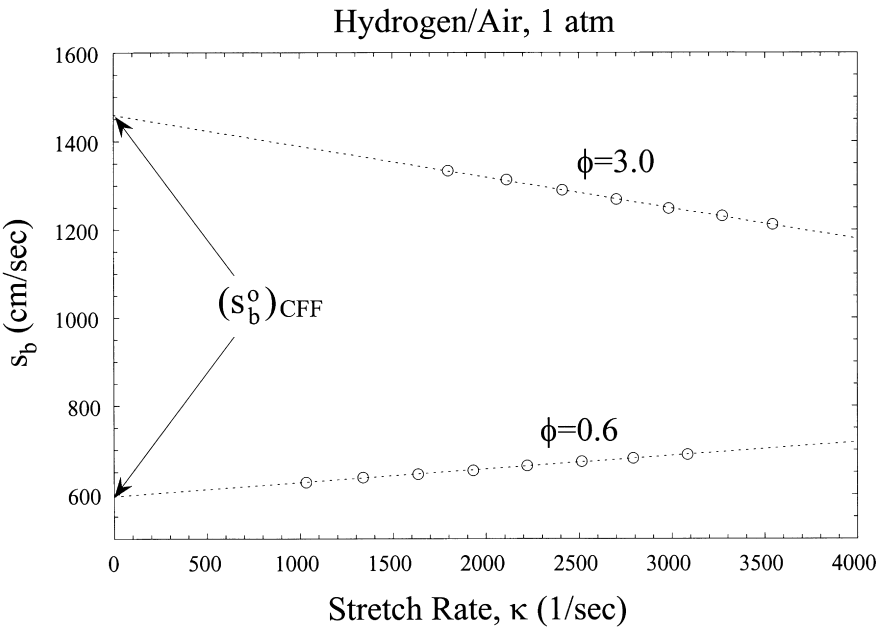

Fig. 14. Calculated s_b for weakly stretched counterflow hydrogen/air flames, showing its linear variation with stretch rate, and the opposite response for lean and rich flames.

flame intensity of such mixtures. This argument still holds even if we just consider the relative mass diffusivities of the fuel and oxidizer species. That is, based on molecular weight considerations, the diffusivities of the various reactants relative to nitrogen decrease in the order of propane, oxygen, methane, and hydrogen. Thus positive (negative) stretch will increase (decrease) the methane or hydrogen concentration of a lean methane/air or hydrogen/air mixture, but decrease (increase) the propane concentration of a rich propane/air mixture at the flame. Both mixtures are

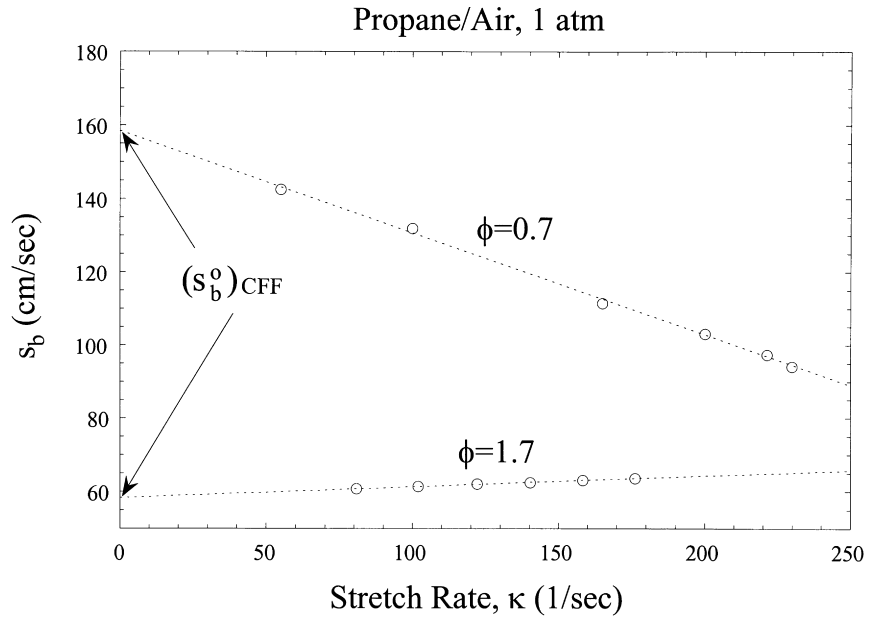

Fig. 15. Calculated s_b for weakly stretched counterflow propane/air flames, showing its linear variation with stretch rate, and the opposite response for lean and rich flames. Also note the opposite response with the counterflow hydrogen/air flames.

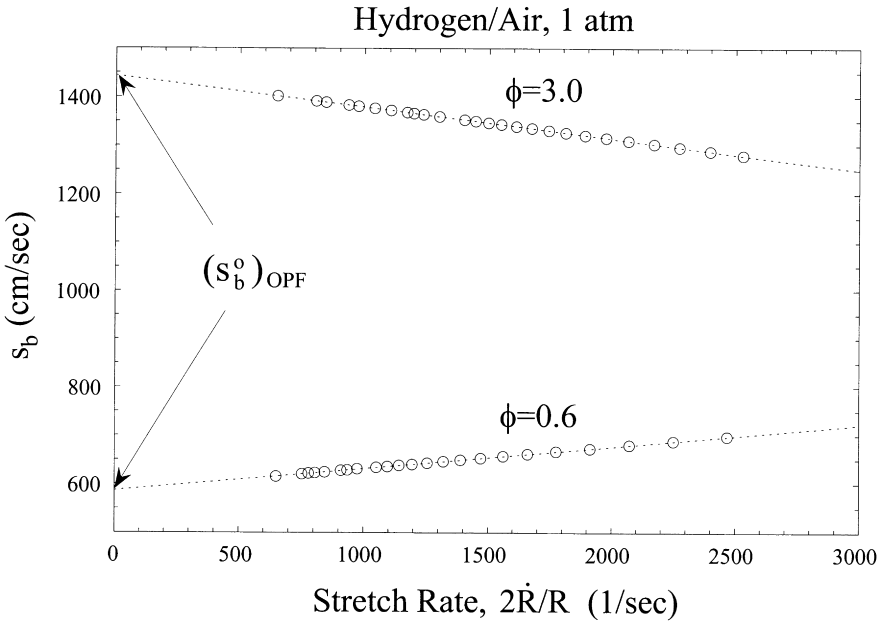

Fig. 16. Calculated s_b for weakly stretched outwardly propagating spherical hydrogen/air flames, showing its linear variation with stretch rate, and the opposite response for lean and rich flames.

consequently rendered more (less) stoichiometric at the flame, leading to enhanced (reduced) burning intensity.

The second group consists of rich hydrogen/air, rich methane/air, and lean propane/air mixtures, whose effective Lewis numbers are greater than unity while positive (negative) stretch also renders the mixture less (more) stoichiometric. Thus the responses of these two groups of mixtures to stretch are expected to be qualitatively opposite.

Experiments and computations have been conducted using these mixtures in flame configurations exhibiting

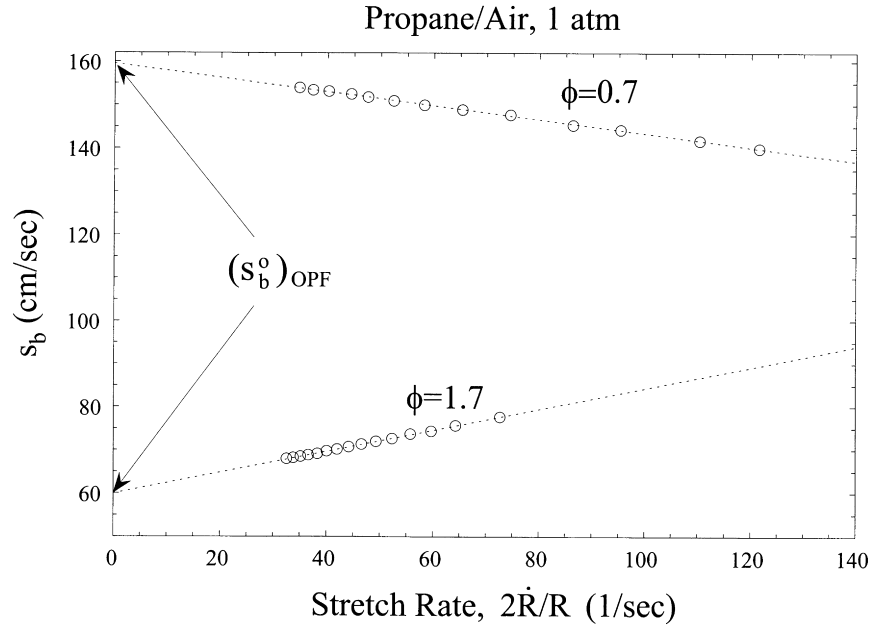

Fig. 17. Calculated s_b for weakly stretched outwardly propagating spherical propane/air flames, showing its linear variation with stretch rate, and the opposite response for lean and rich flames.

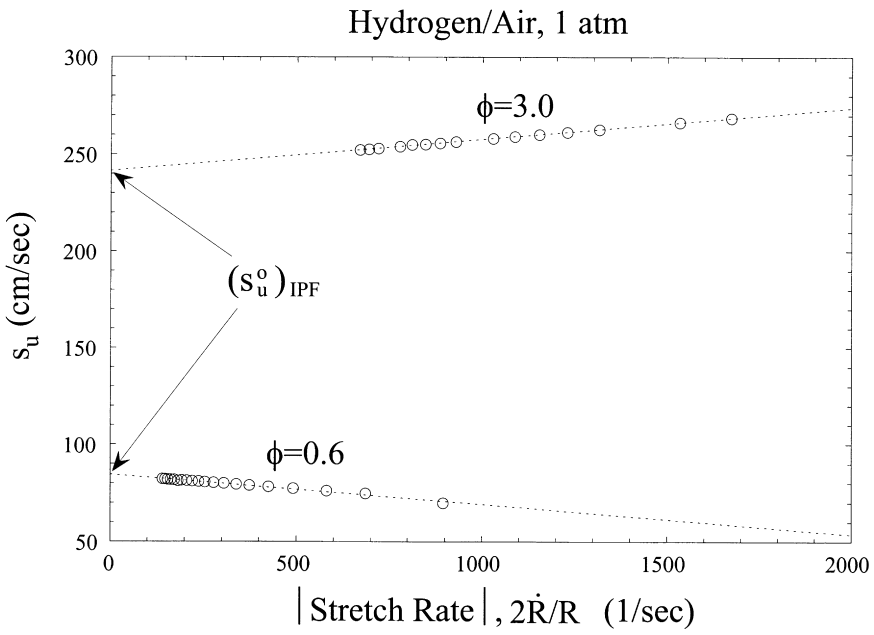

Fig. 18. Calculated s_u for weakly stretched inwardly propagating spherical hydrogen/air flames, showing its linear variation with stretch rate, and the opposite response for lean and rich flames. Also note the opposite response with outwardly propagating flames.

positive and negative stretches. For positive stretch, extensive experiments have been performed by using the symmetrical counterflow flame (CFF) and the outwardly propagating flame (OPF). For negative stretch, the inwardly propagating flame (IPF) and the Bunsen flame (BF) have been used.

Fig. 14 shows the computationally determined [26] s_b as a function of the stretch rate for lean and rich hydrogen/air

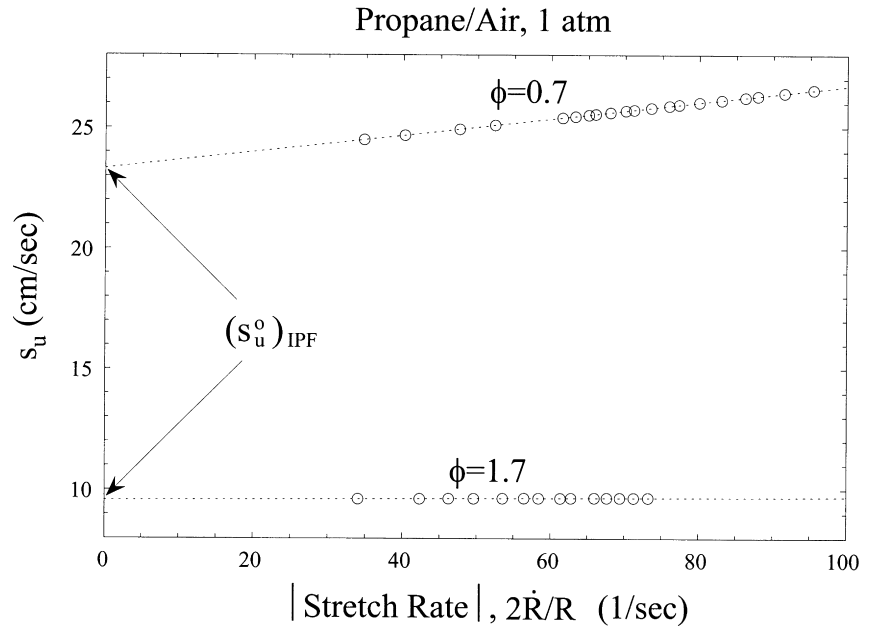

Fig. 19. Calculated s_u for weakly stretched inwardly propagating spherical propane/air flames, showing its linear variation with stretch rate, and the opposite response for lean and rich flames. Also note the opposite response with outwardly propagating flames.

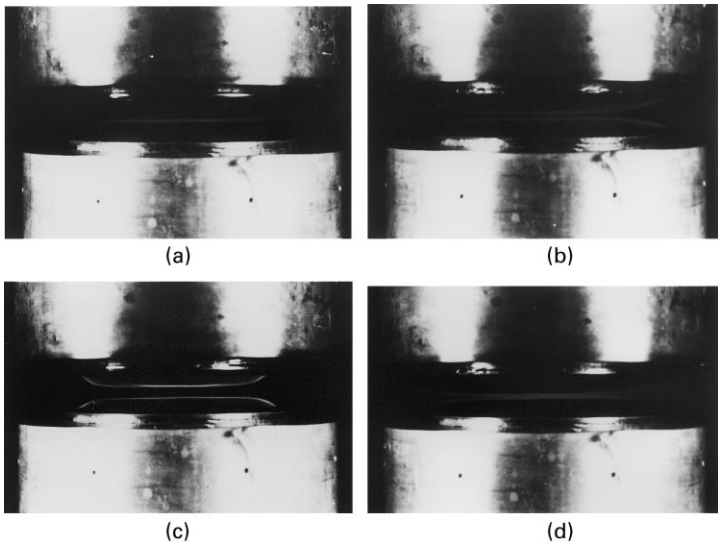

Fig. 20. Counterflow twin flame images just prior to the state of extinction: (a) lean methane/air; (b) rich methane/air; (c) lean propane/air; and (d) rich propane/air.

counterflow flames, with s_b defined as the axial flow velocity at the location of the maximum heat release rate. The use of s_b avoids the ambiguity from choosing the spatial location at which s_u is defined. It is seen that while s_b increases with κ for lean flames, it decreases for rich flames. This is in agreement with the anticipated behavior of the positively stretched flames with *Le* smaller and greater than unity, respectively. The increasing trend for the lean flame due to nonequidiffusion is particularly significant because, as shown in Eq. (56), pure stretch alone would cause s_b to decrease because of flow divergence.

To further demonstrate the importance of nonequidiffusion, Fig. 15 shows the corresponding plot for the lean and rich propane/air flames. Since the *Le* behavior for lean and rich mixtures are switched for hydrogen/air and propane/air flames, it is seen that s_b now exhibits completely opposite behavior, decreasing for lean mixtures while increasing for rich mixtures.

Figs. 16 and 17 show the s_b for the outwardly propagating hydrogen and propane flames; s_b is chosen because the downstream state is stationary for the OPF in the laboratory frame, and as such is well defined. It is seen that since OPF is also positively stretched, the flame responses are qualitatively similar to those for the CFF. However, unlike the CFF whose s_b is affected by both nonequidiffusion and flow divergence, the s_b for the OPF is affected only by nonequidiffusion. Thus the opposite behavior for lean and rich flames here is a clear indication of the influence of nonequidiffusion alone.

Figs. 18 and 19 show the flame speed response for the negatively stretched, inwardly propagating flames. Since the nature of the stretch rate is now reversed as compared to the CFF and OPF, it is seen that the flame response is also reversed, with s_u decreases and increases with increasing stretch rate for the hydrogen/air flames, and increases and decreases for the propane/air flames. We further note that since the upstream state of an IPF is stationary in the laboratory frame, s_u is a more logical choice than s_b in determining the flame speed.

The final point to note is that the variations shown in Figs. 14–19 are all linear, indicating that the flame computed are all weakly stretched and hence can be described by the linear theory presented earlier. It may be noted that although the intensity of stretch cannot be precisely quantified because of the corresponding imprecise definition of the flame thickness and hence the Karlovitz number, it can be assessed by the extent of the deviation of the flame response from that of the unstretched value, obtained by linearly extrapolating the stretched flame speeds to zero stretch. The results of Figs. 14–19 show that such deviations are at most about 20%. The observed linear behavior is therefore consistent with the result of small deviation.

We next examine the role of nonlinear stretch and nonequidiffusion in flame extinction. Fig. 20 shows the photographic images of the binary flame configuration for lean and rich methane/air and propane/air mixtures at the state just prior to extinction if stretch is further increased by increasing the freestream flow velocities [16]. It is seen that while the lean propane/air and rich methane/air flames are quite separated at extinction, implying that the flames are located away from the stagnation surface and hence $x_f > 0$, the lean methane/air and rich propane/air flames merge at extinction, implying $x_f = 0$. This result agrees with our previous discussion that $Le > 1$ flames extinguish while situated away from the stagnation surface, and $Le < 1$

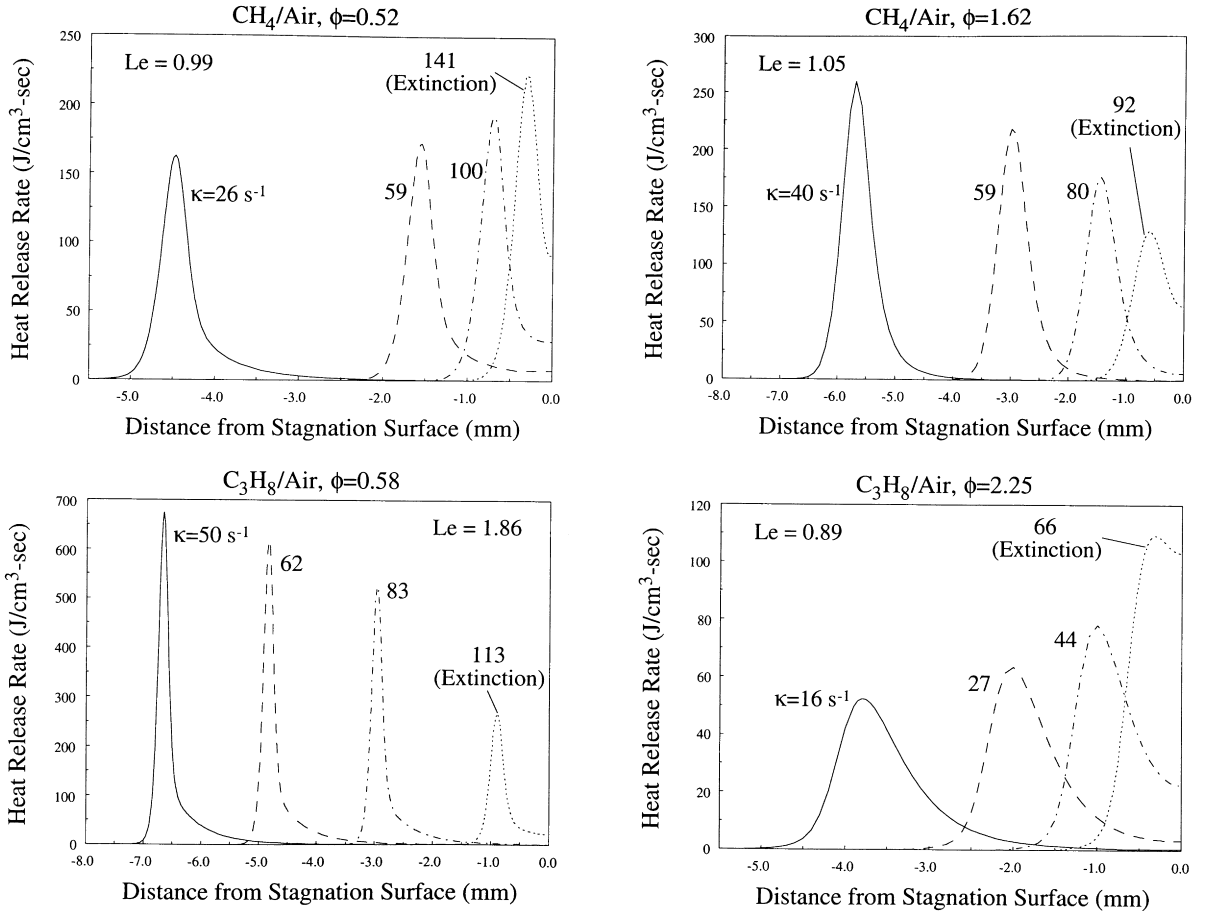

Fig. 21. Computed heat release rate profiles for counterflow twin flames with increasing strain rate: (a) lean methane/air; (b) rich methane/air; (c) lean propane/air; and (d) rich propane/air.

flames extinguish at the stagnation surface because of incomplete reaction.

Fig. 21 shows the computed heat release rate profiles with increasing stretch, for lean and rich methane/air and propane/air flames. The estimated Lewis numbers for the mixtures are also indicated. The stoichiometries are those of the experiments of Tsuji and Yomaoka [17]. It is seen that for the $Le > 1$, rich methane/air and lean propane/air flames, the maximum heat release rate is reduced with increasing stretch. As extinction is approached, the reaction zone can still be considered to be away from the stagnation surface. Furthermore, reaction is "complete", recognizing nevertheless that the slow CO oxidation will always impart some degree of incomplete reaction and hence truncate the reaction rate profile at the stagnation surface. For the $Le <$ 1, lean methane/air and rich propane/air flames, the maximum heat release rate is seen to continuously increase with increasing stretch and the reaction zone profile is truncated at the stagnation surface even for moderate stretch rates, sufficiently in advance of the extinction state.

Fig. 22 shows the computed maximum (flame) temperature, T_b, with strain rate variations for the situations of Fig. 21. The plot exhibits the upper and middle branches of the characteristic S-shaped ignition–extinction curves, with the solid segments corresponding to the physically realistic branches and the dashed segments the unstable branches. Consequently the turning points designate the states of extinction. The behavior of T_b with increasing stretch corroborates the observation of Fig. 21 in that, for the $Le > 1$ flames, T_b monotonically decreases with increasing strain rate, while for $Le < 1$ flames T_b first increases and then decreases as the extinction state is approached. It may also be noted that since the Lewis numbers of the methane/air mixtures are very close to unity, the distinguishing trends between the lean and rich cases are not as prominent as those of the propane/air mixtures.

It is significant to note that the above linear and extinction results have all been observed in experiments involving the counterflow flames [16,17,34] and the outwardly propagating flames [20–22].

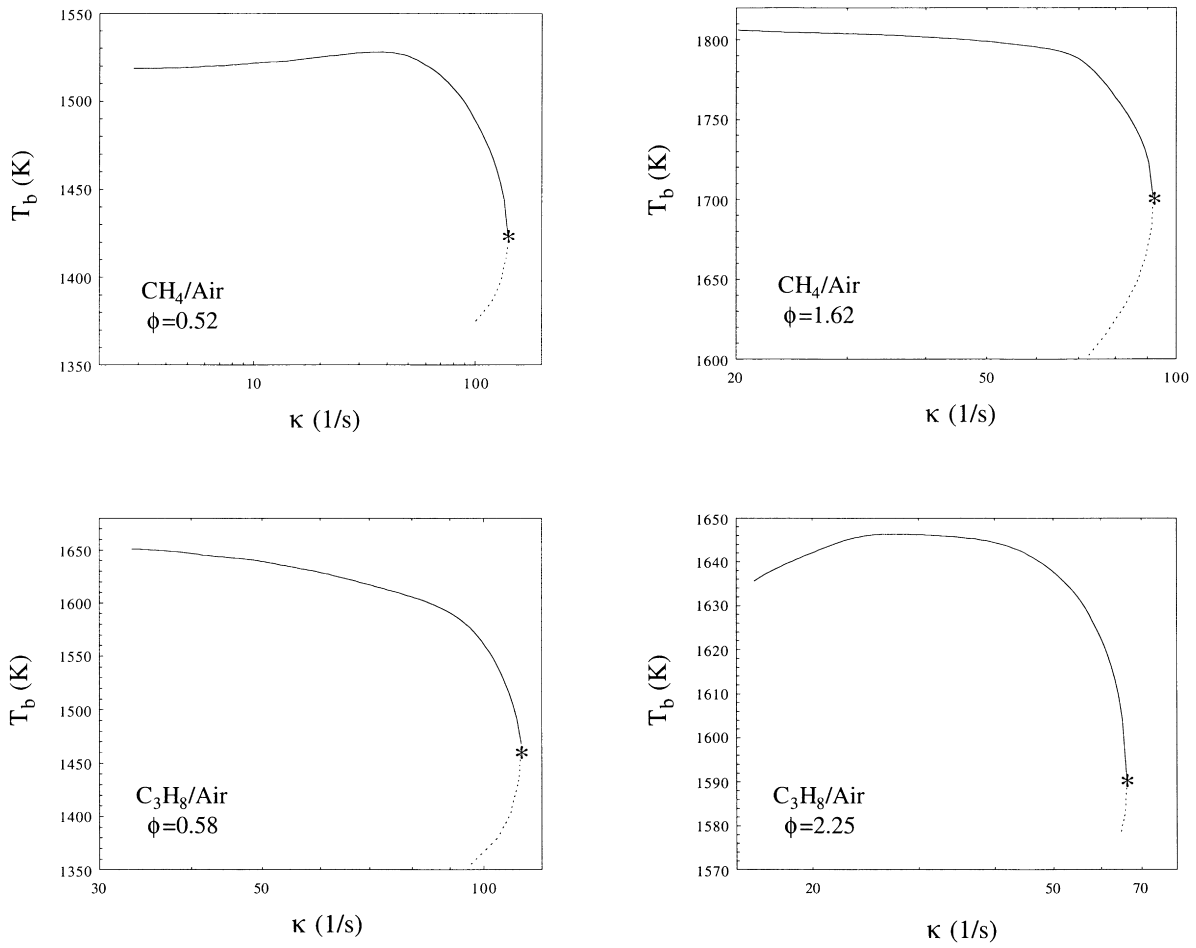

Fig. 22. Computed flame temperatures for counterflow twin flames with increasing strain rate, for the same mixtures as those of Fig. 21. The extinction turning point is designated by " ∗ ".

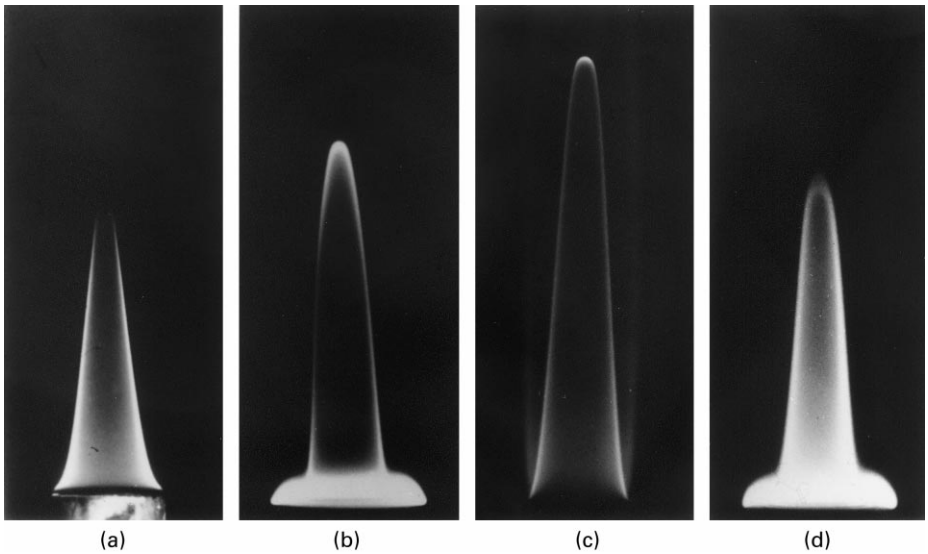

Fig. 23. Images of Bunsen flames of: (a) rich propane/air; (b) lean propane/air; (c) rich methane/air; and (d) lean methane/air mixtures.

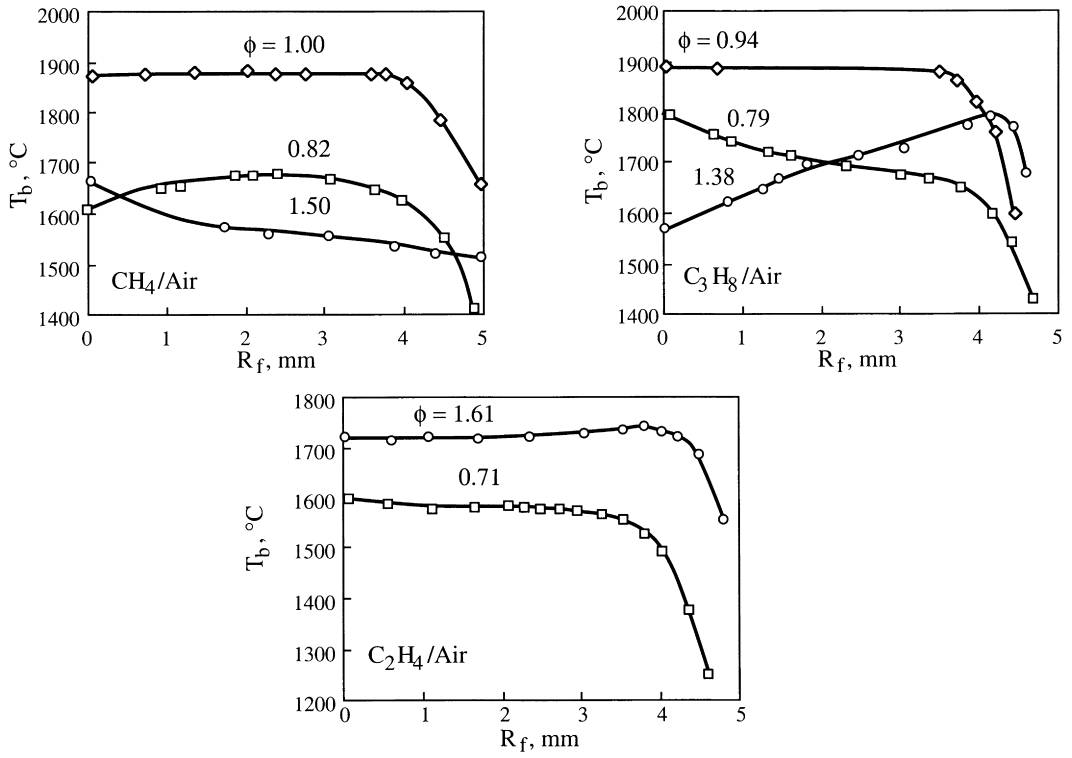

Fig. 24. Flame tip temperatures of methane/air, propane/air and ethylene/air Bunsen flames with various equivalence ratios and hence nature of nonequidiffusion.

Next we examine the flame temperature response to negative stretch, provided by the increasing curvature along the surface of a Bunsen cone. The behavior should be completely opposite to those of the counterflow and outwardly propagating flames. Fig. 23 [35] shows the photographic images of the flame configurations of lean and rich propane/air and methane/air mixtures. It is clear that with increasing curvature, and thereby increasing negative stretch along the surface as the flame tip is approached from the flame base, the burning intensity increases for lean propane/air and rich methane/air mixtures, but decreases for rich propane/air and lean methane/air mixtures. The reduction in the flame temperature can be so severe that extinction occurs at the flame tip that suffers the largest stretch, exhibiting the tip-opening phenomenon.

To quantify the above observation, Fig. 24 shows the measured maximum temperature along the flame surface [18,19]. Excluding the segment near the flame base where burning is weak due to heat loss to the burner rim, it is seen that as we move along the flame towards the flame tip, the flame temperature increases for the rich methane/air and lean propane/air flames, but decreases for the lean methane/air and rich propane/air flames. The neutral compositions are found to be approximately $\phi = 1.00$ and 0.94 for methane/air and propane/air flames, respectively.

Recognizing that the flame responds in opposite trends for methane/air and propane/air mixtures, additional experiments have been conducted for ethylene/air mixtures because the molecular weight of ethylene is between those of methane and propane. Indeed, Fig. 24 shows that for the ethylene/air flame, T_f varies very slightly not only with flame curvature but also for rich and lean mixtures. This is in agreement with the theoretical result that for an equidiffusive mixture, stretch has no effect on the flame temperature.

We further note that since the flame temperature can deviate from the adiabatic flame temperature only in the simultaneous presence of stretch and nonequidiffusion, the deviation should also be suppressed for a nonequidiffusive mixture if the flame is not stretched. By using the shoulder region of a two-dimensional Bunsen flame to simulate such an unstretched flame, Fig. 25 shows that the flame temperature there is indeed minimally affected for the lean and rich methane/air and propane/air flames.

The above results clearly demonstrate that the behavior of the negatively stretched Bunsen flames are completely opposite to those of the positively stretched forward stagnation and outwardly propagating spherical flames. Thus all experimental and computational results are in agreement with the concept of flame stretch in the presence of nonequidiffusion. The effects of pure curvature on the local

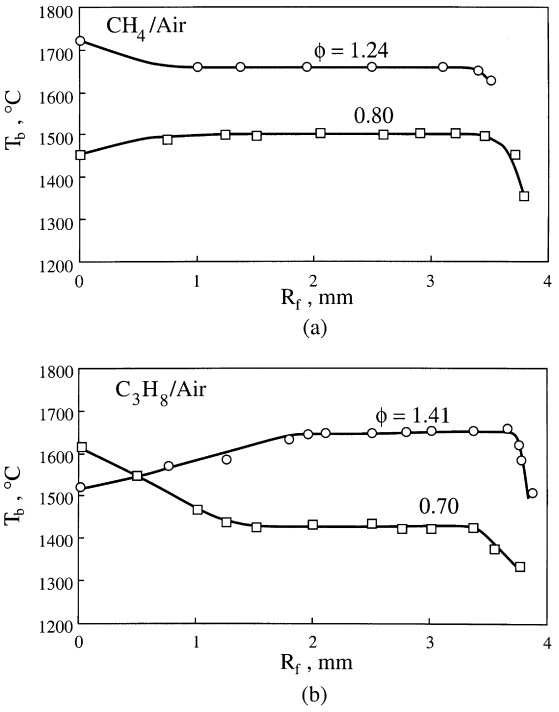

Fig. 25. Temperature profiles over the two-dimensional Bunsen flame surface for methane/air and propane/air flames, showing the absence of stretch effects over the shoulder region of the unstretched flame.

flame speed have also been investigated and are found to qualitatively agree with the theoretical anticipations [32].

6.3. Quantitative extraction of global flame parameters

In addition to understanding the behavior of stretched flames, it is also of interest to be able to quantitatively describe the dynamics and geometry of flame surfaces in nonuniform flow fields through the use of such simple, but generalized, global expressions given in, say Section 5.4. These expressions can then be integrated in the study of complex flame phenomena such as turbulent flames.

An inspection of the general solution of Section 5.4 shows that, in order to evaluate the various stretched flame responses for a given thermodynamic state defined by its temperature, pressure, and composition, and for a given stretch intensity κ, we need to know the laminar flame speed, s_u^o (or s_b^o), the thickness, $\mathcal{L}_D^o$, as well as the global physico-chemical parameters E_a (through Ze) and Le. The thermodynamic parameters of the burnt state, T_b^o and ρ_b^o, can be readily calculated from the upstream state. In the following we use the hydrogen/air and propane/air systems [26] to demonstrate how these various parameters can be determined.

The laminar flame speed can be either calculated, if we know the chemical kinetic mechanism, or experimentally measured. The experimental determination can use either the counterflow flame [36,37] or the outwardly propagating flame [20–22], with linear extrapolation to zero stretch rate as shown in Figs. 14–17. Fig. 26 shows the result of such a linear extrapolation, say by using the OPF. Fig. 27 demonstrates the internal consistency of the concept of linear extrapolation by showing that the extrapolated values obtained by using the CFF, OPF, and IPF all agree with each other as well as the independently calculated laminar flame speed. In Fig. 26 we have also plotted the laminar burning flux in order to emphasize the fact that it is the fundamental eigenvalue of the flame propagation. Specifically, it is seen that while the flame speed decreases with pressure, the burning flux increases with pressure.

Determination of the laminar flame thickness, which provides an indication of the residence time within the flame, is somewhat more uncertain, for two reasons. First, it is well established that the simple relation $\mathcal{L}_D^o \sim (\lambda/c_p)_u/f^o$, based on the characteristic time considerations, yields values which are too small. Thus a reasonably accurate determination requires resolution of at least the thermal profile of the flame, either computationally or experimentally. Secondly, since the flame thickness is definition dependent, there exist considerable uncertainties in the determined values.

To resolve the above uncertainty, the flame thickness has been evaluated using both the gradient definition, $\mathcal{L}_T^o = (T_b^o - T_u)/(dT/dx)_{max}$, as well as the full-width at half-maximum (FWHM) value of the temperature gradient profile. Fig. 28a shows that the flame thicknesses determined using these two definitions are actually quite close to each other, and are therefore self-consistent.

The global parameters E_a and Le need to be extracted from the flame responses. It is important to recognize that they are both physico-chemical properties of the flame. Specially, although E_a is meant to describe the global response of the detailed reaction chemistry, the progress of the individual reactions obviously depends on the availability and concentrations of the intermediates, which in turn depend on the transport aspects of the problem. By the same token, although Le is superficially a parameter representing the transport of the freestream reactants, there are many intermediates, produced through intermediate reactions and with different diffusivities, that could affect the entire reaction progress and manifest their effects through some nonequidiffusive phenomena. As such, E_a and Le are fundamentally flame dependent properties.

The above discussions indicate that E_a and Le are functions of the stretched flame environment, and hence are specific to each stretched flame under study. It is, however, reasonable to expect that the chemical and transport aspects of the flame structure should be insensitive to stretch as far as the influence of E_a and Le is concerned. The following extraction procedure is based on this premise.

From the expression of the laminar flame speed [38],

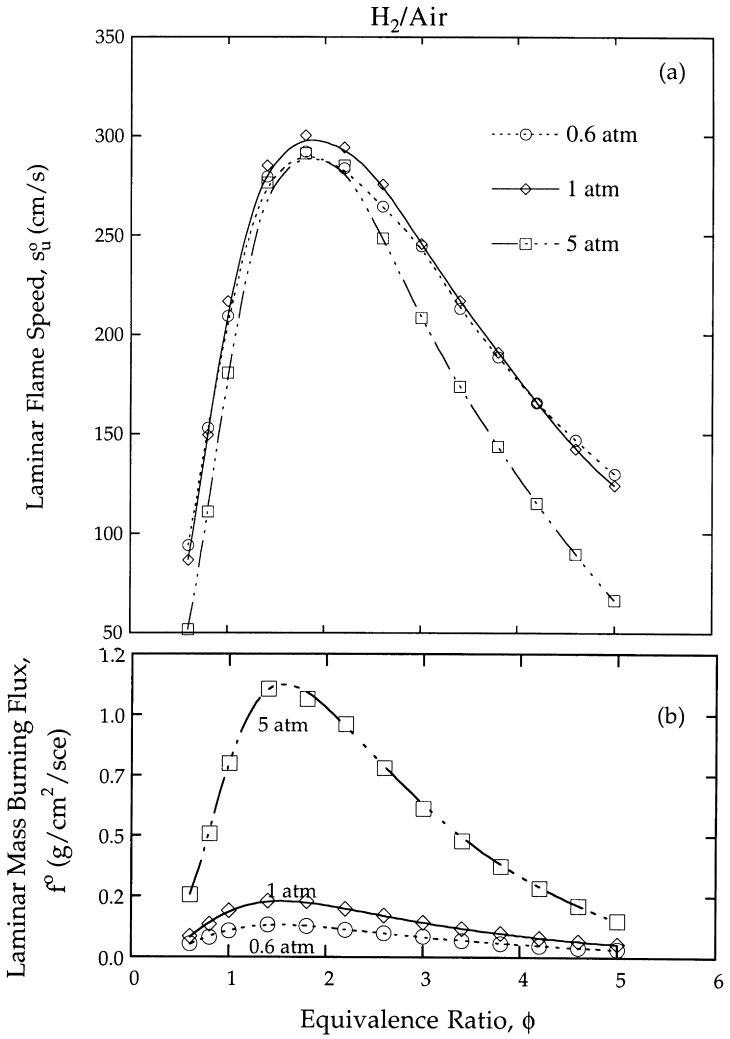

Fig. 26. (a) Laminar flame speed, and (b) laminar mass burning flux of hydrogen/air flames determined through linear extrapolation of the stretched flame speeds of outwardly propagating flames to zero stretch rate. Note the agreement with independently calculated laminar flame speeds denoted by line.

$f^o \sim \exp(-E_a/2\Re T_b^o)$, we have

$$\frac{d\ln f^o}{d(1/T_b^o)} = -\frac{E_a}{2\Re}. \tag{76}$$

Since the basic flame characteristics should be minimally affected when evaluating the differential in Eq. (76), either computationally or experimentally, a viable approach to effect the change in T_b^o, and thereby f^o, is through substitution of a small amount of nitrogen in the mixture by an equal amount of argon. Fig. 28b shows the extracted values for the hydrogen/air flames. It is seen that the extracted E_a has a minimum in ϕ, demonstrating that the progressive reduction in the flame speed, as the mixture becomes either leaner or richer, is due to a decrease in the flame temperature as well as an increase in the chemical activation.

Regarding the extraction of *Le*, we first note that frequently *Le* is calculated as the ratio of the thermal diffusivity of the mixture to the mass diffusivity between the deficient reactant and the abundant species of the mixture, which is usually nitrogen, all based on the freestream mixture properties. Such an approach obviously cannot be used for near-stoichiometric mixtures.

We demonstrate the extraction of *Le* by using the CFF [26]. For this flame, with equidiffusion assumption Eq. (75) degenerates to

$$s_b = s_b^o + \left[\frac{(1-Le)}{2\epsilon^o} - 1\right]\frac{\alpha^o \kappa \ell_T^o}{\beta^o}. \tag{77}$$

From the computed and experimental results such as Fig. 15,

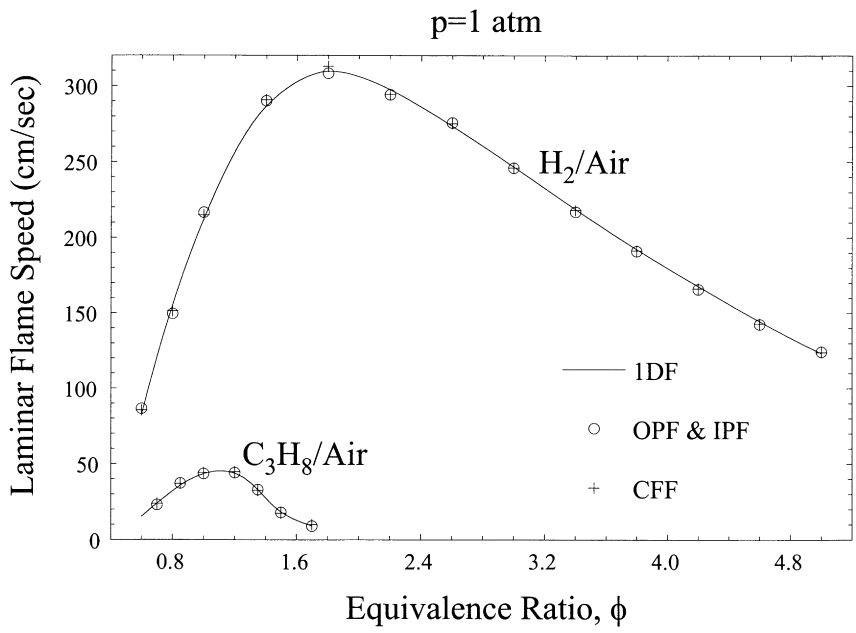

Fig. 27. Laminar flame speed of hydrogen/air and propane/air mixtures determined through linear extrapolation of stretched flame speeds of counterflow, outwardly propagating, and inwardly propagating flame speeds. Note the mutual agreement as well as the agreement with independently calculated laminar flame speeds.

we also have

$$s_b = s_b^o + L_b\kappa. \tag{78}$$

Equating the coefficients of the above two expressions, we have

$$L_b = \left[\frac{(1-Le)}{2\epsilon^o} - 1\right]\frac{\alpha^o}{\beta^o}\ell_T^o, \tag{79}$$

from which Le can be determined for a given ϕ. To increase the accuracy of such a determination, for a given ϕ we can plot $(L_b/\ell_T^o)(\beta^o/\alpha^o) + 1$ versus $1/2\epsilon^o$ for several pressures. It Le is not a sensitive function of pressure, as is reasonable to expect, then such a plot would yield a straight line whose slope is $(1 - Le)$.

Fig. 29c shows that such a linearity indeed exists. Similar extractions can also be performed for the OPF and IPF, as shown in Fig. 29a and b. The extracted Lewis numbers from these three flame configurations are plotted in Fig. 30. It is quite remarkable that they are very close to each other, as is reasonable to expect. Furthermore, for the very lean and very rich mixtures, their values are quite close to those evaluated based on the diffusivities of H_2 and O_2 relative to the mixture, 0.33 and 2.32, respectively. This seems to support the original notion that although the reaction intermediates are crucial elements in the flame structure, it is still the diffusivities of the freestream reactants that control the nonequidiffusive characteristics of stretched flames.

Fig. 30 also shows that while Le appears to merge smoothly with the limiting values 2.32 on the rich side, it decreases rapidly to the limiting values of 0.33 on the lean side. Such a disparate behavior is actually only a consequence of the asymmetrical nature of the definition of the equivalence ratio ϕ, in that ϕ is bounded between 0 and 1 on the lean side, but is "stretched out" between 1 and ∞ on the rich side. To remove this definitional effect, in Fig. 30b Le is plotted as a function of the normalized equivalence ratio $\Phi = \phi/(1 + \phi)$, which is bounded between 0 and 0.5 on the lean side and 0.5 and 1 on the rich side. It is seen that Le now varies in a more gradual manner between the two limits.

In Fig. 30 we have also plotted the mixture Le evaluated using the expression derived by Joulin and Mitani [39] for a two-reactant flame. The evaluation is somewhat involved and the reader is referred to Ref. [26] for details. Such an independent evaluation also yields close agreement with the extracted values.

Fig. 31 presents the corresponding extracted Le for the propane/air flame. The results are consistent with the above discussion on hydrogen/air flames.

Knowing all the parameters discussed above, the response of a stretched flame can be computed using the expressions given in Eqs. (72)–(75). The evaluations should be quite accurate, once the various parameters are extracted, as has been carried out for the hydrogen/air and propane/air flames presented here [26]. A more direct approach, however, is to simply extract a global parameter representing the effects of stretch. For example, the upstream flame speed is given by Eq. (55). Thus once the Markstein number Ma is known, for

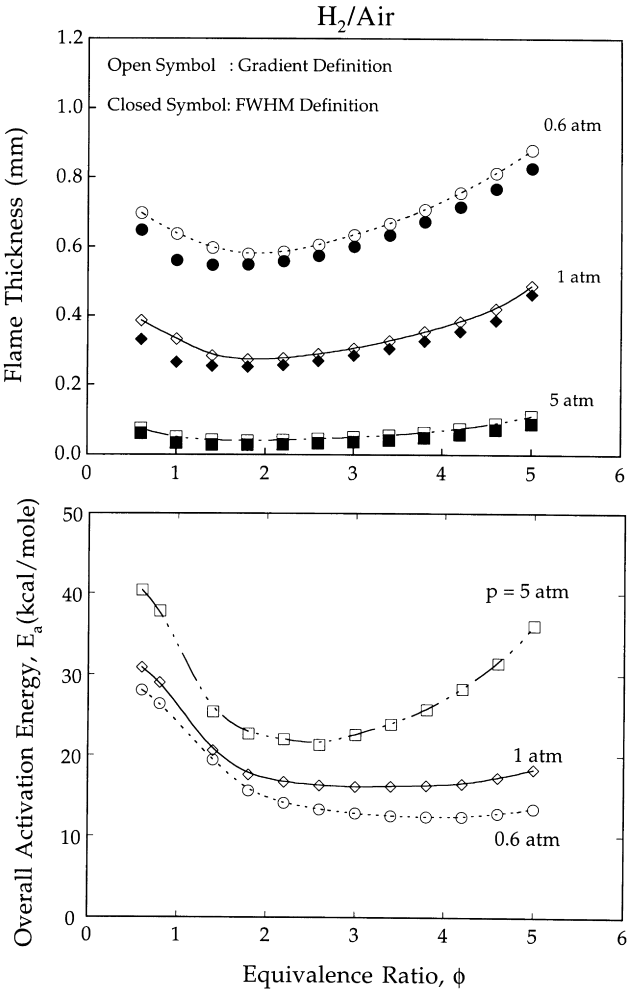

Fig. 28. Calculated (a) flame thicknesses using the gradient and the full-width-at-half-maximum definitions and (b) overall activation energy of hydrogen/air flames.

a given unstretched flame, the stretched flame speed can be evaluated for a given nondimensional stretch rate *Ka*. This bypasses the need to extract E_a and *Le* because they are lumped into *Ma* anyway. As such, there has been substantial activity recently in the determination of *Ma* [21,22].

Two points are worth mentioning. First, it is more direct to simply express the flame speed in terms of the raw, dimensional, physical quantities as

$$s_u = s_u^o + L\kappa, \tag{80}$$

where L has the dimension of a length and can be called a Markstein length. It is simply the slope in the plots of Figs. 14–19 for variations of either s_u or s_b. The advantage of using L and κ over *Ma* and *Ka* is that they are precisely defined while the magnitudes of *Ma* and *Ka* depend on the evaluation of the flame time and hence flame thickness which can be quite uncertain, as discussed earlier. Thus the reported *Ma* and *Ka* in the literature can differ substantially depending on the flame thickness adopted in the nondimensionalization. This can convey different meanings in assessing whether a given stretch is strong or weak, indicated by whether *Ka* is greater or smaller than unity. Thus before this uncertainty is clarified, it is better to using the raw dimensional quantities in the comparison.

Secondly, Eq. (80) shows that the stretched flame expression is general, valid for flames under stretch of different nature, whether it is due to flow nonuniformity, or flame curvature, or flame unsteadiness. However, recent studies have reported the need to use different Markstein numbers of stretches of different nature [40]. The need to do so, however, stems from the incorrect location at which s_u is evaluated. That is, s_u in our general formulation represents the flame speed at the upstream boundary of the flame, which is located at a distance $\mathcal{L}_T$ upstream of the reaction

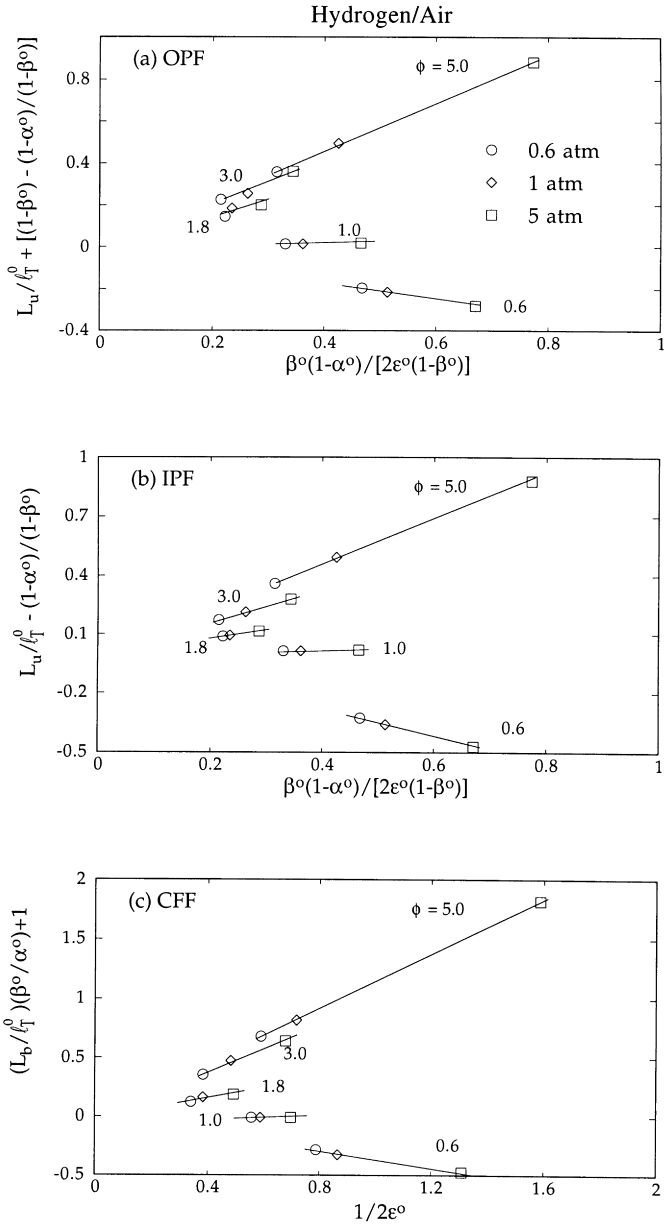

Fig. 29. Extrapolation procedure for the global Lewis number from various flame configurations.

zone. However, if the flame is treated as being infinitesimally thin such that the stretch rates of different nature are indeed evaluated at a flame surface, then s_u should correspond to the local flow velocity obtained by extrapolating the upstream flow velocity from the location of the upstream boundary to that of the (thin) reaction zone. Thus if s_u is corrected for this effect, then the Markstein lengths for flames of different nature indeed agree with each other [26]. This is shown in Figs. 32 and 33 for hydrogen/air and propane/air flames, respectively.

7. Simultaneous considerations of hydrodynamic and flame stretch

Our discussion has demonstrated that while the hydrodynamic stretch affects the geometry of the flame surface, the flame stretch affects the flame structure. These effects, while manifested at different scales, are intimately coupled. One approach through which such a coupling can be effected is the use of the *G*-equation, Eq. (12), with $\tilde{s}_u$ given by, say Eq. (67), recognizing nevertheless that application of the various

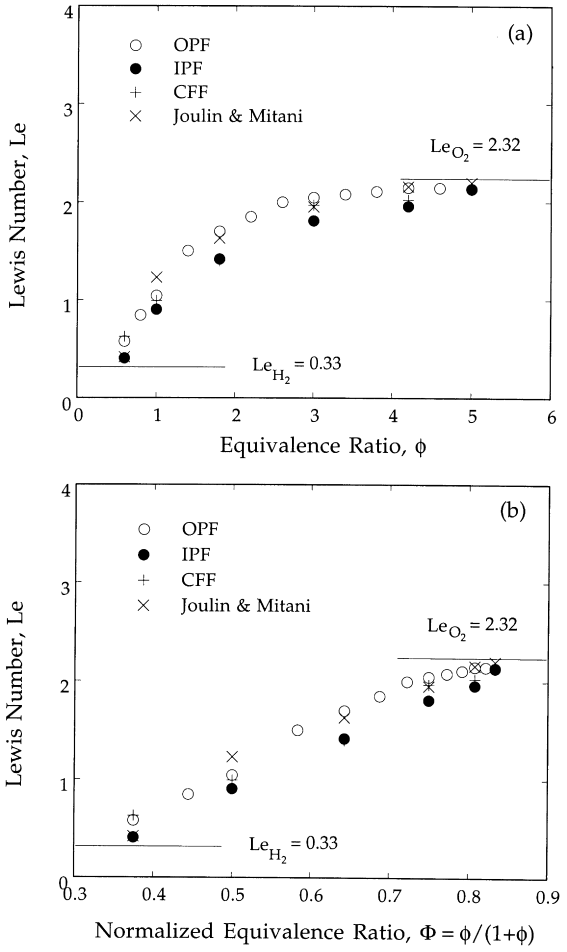

Fig. 30. Extracted global Lewis numbers for hydrogen/air mixtures from various flame configurations.

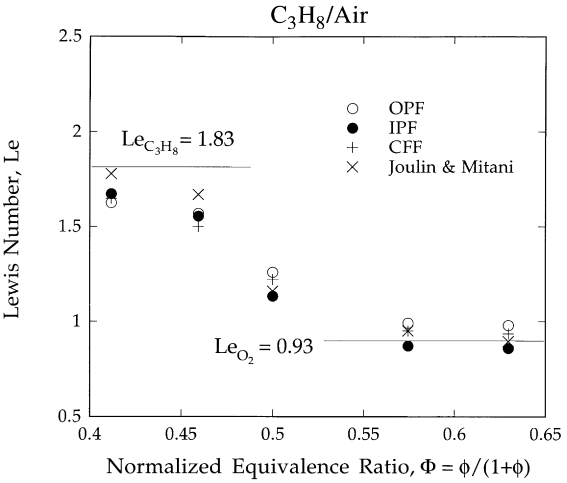

Fig. 31. Extracted global Lewis numbers for propane/air mixtures from various flame configurations.

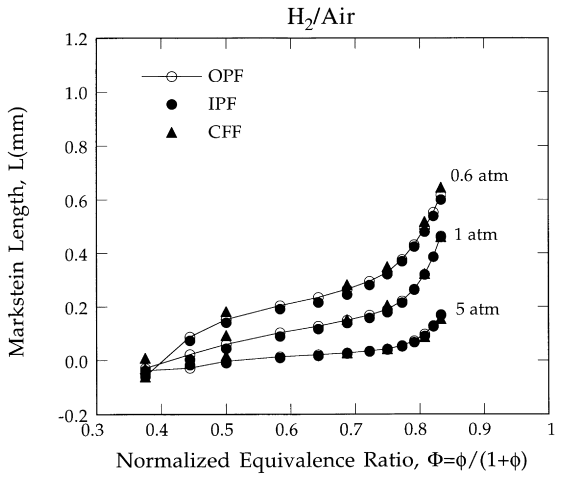

Fig. 32. Extracted Markstein lengths for hydrogen/air mixtures from various flame configurations.

concepts introduced in Section 6.3 could lead to quantitatively more accurate results. In the following we shall study two problems that clearly show the coupling and influences of these two stretch effects, namely the smoothing of flame cusps identified in Section 3.2, and the possible configurations of Bunsen flames. In the next section the combined stretch analysis will also be applied to the phenomena of flamefront instabilities.

7.1. Curvature-induced cusp broadening

In Section 3.2 we have shown the propensity of cusp formation for wrinkled flame surfaces. The flame itself, however, possesses an intrinsic response that tends to inhibit cusp formation. As shown in Section 5.2, the upstream flame

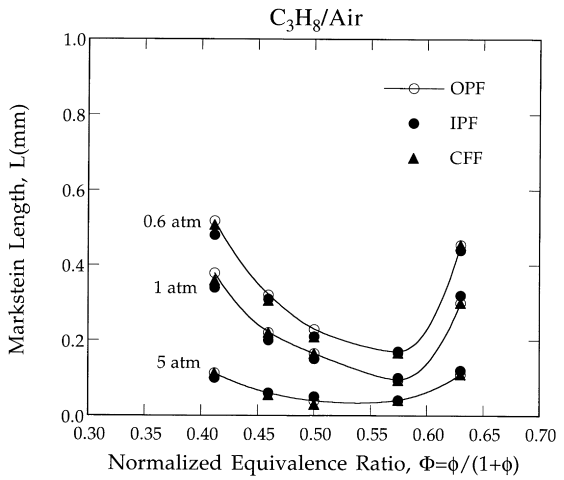

Fig. 33. Extracted Markstein lengths for propane/air mixtures from various flame configurations.

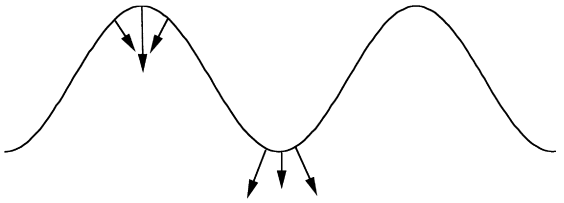

Fig. 34. Schematic showing the smoothing effects of curvature on wrinkled flames.

speed of an equidiffusive mixture in the presence of curvature is modified from $\tilde{s}_u = 1$ for the one-dimensional flame to

$$\tilde{s}_u = 1 - \mathcal{L}_T^o \nabla \cdot \mathbf{n}. \tag{81}$$

Using this curvature-affected flame speed expression in the G-equation, with $v = 0$ for the quiescent flow example, we have [29]

$$\frac{\partial \hat{g}}{\partial \hat{t}} + \frac{\hat{g}}{(1+\hat{g}^2)^{1/2}} \frac{\partial \hat{g}}{\partial \hat{x}} = \frac{\partial}{\partial \hat{x}} \left[\frac{\hat{\mathcal{L}}_T^o}{(1+\hat{g}^2)} \frac{\partial \hat{g}}{\partial \hat{x}} \right], \tag{82}$$

which governs the evolution of the flame surface. Comparing Eq. (82) with Eq. (16), we see that the additional, second-order term assumes the role of viscous action, with a corresponding "viscosity coefficient", given by $\tilde{\mathcal{L}}_T^o/(1+\hat{g}^2)$, that tends to smooth the cusp. Physically, since the negative flame curvature associated with the receding, trough region of the flame (Fig. 34) enhances the flame speed ($\tilde{s}_u > 1$), while the positive curvature in the protruding, crest region tends to reduce the flame speed ($\tilde{s}_u < 1$), the aggravating tendency for the flame segment in the trough region to collide is moderated.

For weakly wrinkled flames ($\hat{g} \ll 1$), Eq. (82) simplifies

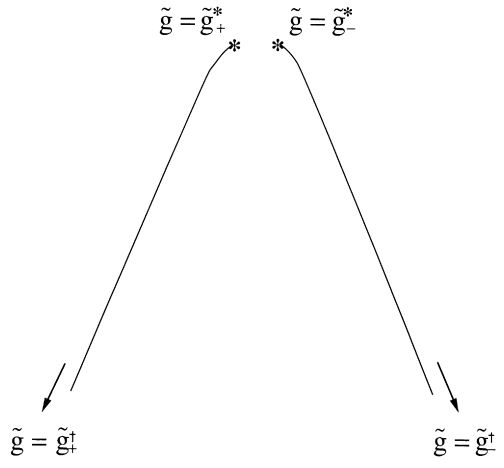

Fig. 35. Analytical prediction of the configuration of an open-tipped Bunsen flame.

to

$$\frac{\partial \hat{g}}{\partial \hat{t}} + \hat{g} \frac{\partial \hat{g}}{\partial \hat{x}} = \hat{\mathcal{L}}_T^o \frac{\partial^2 \hat{g}}{\partial \hat{x}^2}, \tag{83}$$

which is the Burgers equation. Analytical solutions are available for this well-known equation.

For nonequidiffusive mixtures, the flame speed will be further affected by the stretch term σ, which can be either positive or negative depending on the nature of stretch and nonequidiffusion. Thus following similar reasoning for the burning intensity of Bunsen flames (Fig. 7b), for the present wrinkled flame we expect that the tendency to form sharp segments is, respectively, moderated and aggravated for $Le > 1$ and <1 mixtures. Furthermore, when the burning intensity in the trough region is reduced by flame stretch, local extinction may also occur, leading to the formation of "holes" over the flame surface. We shall next demonstrate these phenomena by considering the opening of the Bunsen tip.

7.2. Inversion and tip opening of Bunsen flames

We consider the steady-state configuration of a two-dimensional Bunsen flame situated in a uniform flow of velocity $\mathbf{v} = (0, v)$ [41,42]. With $\mathbf{V}_f = 0$, space variables nondimensionalized by $\mathcal{L}_T^o$, $\tilde{G}(\tilde{x}, \tilde{y}) = \tilde{y} - \tilde{f}(\tilde{x})$, and using the stretch-affected flame speed given by Eq. (67), the G-equation becomes

$$\frac{d\tilde{g}}{d\tilde{x}} = \frac{(1+\tilde{g}^2)^{3/2}[(1+\tilde{g}^2)^{1/2} - \tilde{v}]}{(1+\tilde{g}^2)^{1/2} - Ma\tilde{v}}, \tag{84}$$

which describes the flame configuration for given Markstein number and flow velocity. For this problem we have found it more convenient to reference quantities to the flame scale instead of the hydrodynamic scale. The reason being that the hydrodynamic scale here is the curvature of the flame tip, which however is a response of the analysis. Furthermore, the present reference facilitates analysis of the flame structure and extinction.

Although Eq. (84) can be integrated to yield an analytical solution, the characteristic of the flame configuration can be more clearly illuminated by using the critical-point analysis. Thus setting the numerator and denominator of Eq. (84) to zero, we obtain the critical points

$$\tilde{g}_\pm^\dagger = \pm(\tilde{v}^2 - 1)^{1/2} \text{ and } \tilde{g}_\pm^* = \pm[(Ma\tilde{v})^2 - 1]^{1/2}. \tag{85}$$

The particular value of $\tilde{g}_\pm = \tilde{g}_\pm^\dagger$ corresponds to the Landau limit, which describes the slope of the flame shoulder as shown in Fig. 35 for an open-tipped Bunsen flame. It is also clear that $\tilde{g}_-^\dagger < \tilde{g} < \tilde{g}_+^\dagger$. Further setting $\tilde{g}_\pm^* = 0$ and $\tilde{g}_\pm^* = \tilde{g}_\pm^\dagger$, respectively, yields the following two critical Markstein numbers

$$Ma_1 = \frac{1}{\tilde{v}} \text{ and } Ma_2 = 1, \tag{86}$$

where $0 < Ma_1 < Ma_2 = 1$.

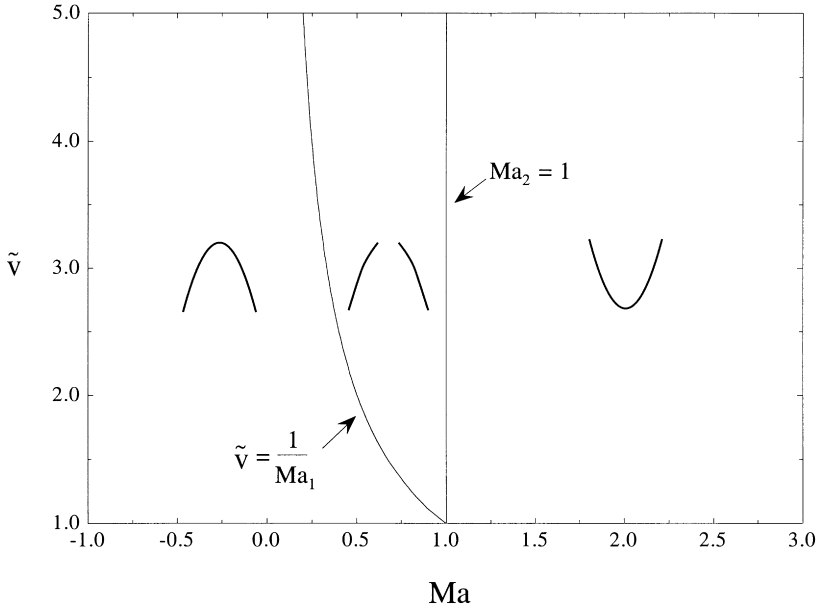

Fig. 36. Regimes with different Bunsen-type flame configurations as functions of flow velocity and Markstein number.

Based on the above critical Markstein numbers, the following observations can be made regarding the possible configurations of Bunsen flames. First,

$$\frac{d\tilde{g}}{d\tilde{x}} > 0 \text{ for } Ma > Ma_2 \tag{87a}$$

$$\frac{d\tilde{g}}{d\tilde{x}} < 0 \text{ for } Ma < Ma_1. \tag{87b}$$

Recognizing that $d\tilde{g}/d\tilde{x}$ is the second derivative of the flame shape function (87a) and (87b) then respectively define regimes for the existence of inverted Bunsen flames and normal Bunsen flames, as shown in Fig. 36. The prediction of inverted Bunsen flames [41,42] is of particular interest

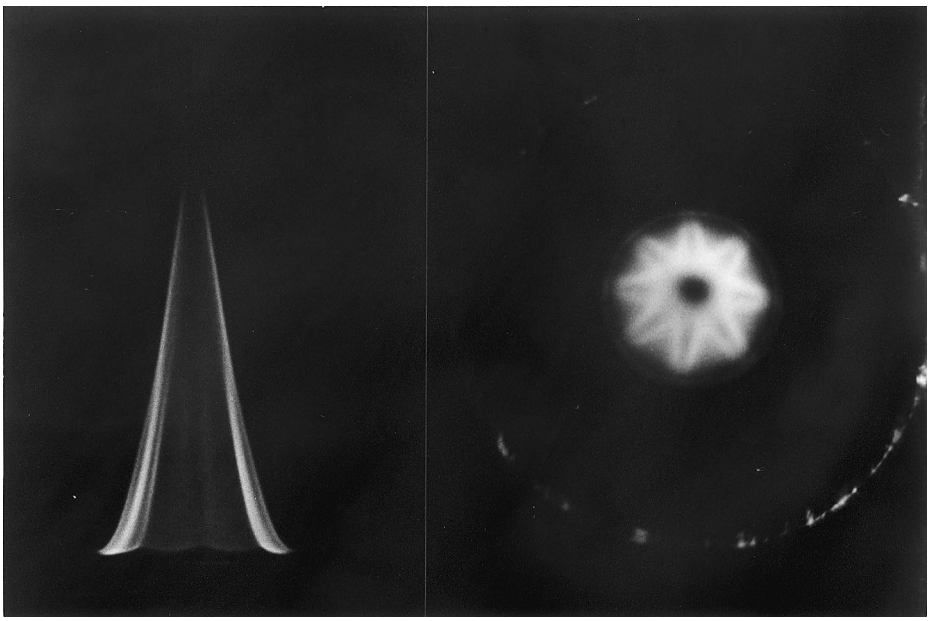

Fig. 37. Frontal and planar photographic images of a polyhedral rich propane/air flame.

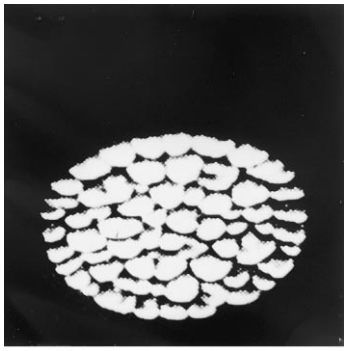

Fig. 38. Photographic image of a cellular rich propane/air/nitrogen flame. Adapted from Ref. [2].

because they have not been experimentally observed. This is not surprising because special stabilization mechanisms are probably needed to hold such freely propagating flames at the base of its shoulder.

In the regime $Ma_1 < Ma < 1$, the behavior is more complex:

$$\frac{d\tilde{g}}{d\tilde{x}} < 0 \text{ when } \tilde{g}^{\dagger}_{-} < \tilde{g} < \tilde{g}^{*}_{-}$$

$$\frac{d\tilde{g}}{d\tilde{x}} > 0 \text{ when } \tilde{g}^{*}_{-} < \tilde{g} < \tilde{g}^{*}_{+} \tag{88}$$

$$\frac{d\tilde{g}}{d\tilde{x}} < 0 \text{ when } \tilde{g}^{*}_{+} < \tilde{g} < \tilde{g}^{\dagger}_{+}.$$

In this intermediate regime of the Markstein number, the differential equation is singular at $\tilde{g} = \tilde{g}^{*}_{\pm}$, where $|\tilde{g}^{*}_{\pm}| < |\tilde{g}^{\dagger}_{\pm}|$. Consequently, integration starting from $\tilde{g} = \tilde{g}^{\dagger}_{\pm}$ at the shoulder will stop at $\tilde{g}^{*}_{\pm}$. The flame front takes the shape of an open tip Bunsen flame which is concave towards the unburnt mixture (Figs. 35 and 36). Moreover, since increasing either Ma or $\tilde{\nu}$ causes $|\tilde{g}^{*}_{\pm}|$ to increase, the opening becomes wider with the increasing flow velocity and decreasing mixture diffusivity. The above characteristics of tip opening have all been experimentally observed [35].

8. Flamefront cellular instabilities

Perhaps one of the most beautiful and fascinating phenomena in flame dynamics is the presence of instabilities in the form of cells and ridges of characteristic sizes over the flame surface. These non-planar flame patterns, which represent alternating regions of intensified and weakened burning, can be either stationary or non-stationary; in the latter case they can also be either steadily or chaotically evolving [4,6,43,44].

The earliest observation of flamefront instability is that of the polyhedral flame, manifested by the presence of regularly spaced ridges over a Bunsen flame in which the deficient reactant is also the lighter one. Fig. 37 shows the front and top views of such a flame, obtained by burning a rich propane/air mixture. The flame pattern consists of petals of flame surfaces separated by extinguished regions of ridges, with the petals being convex towards the unburnt mixture. For a given tube diameter, the number of ridges varies with the mixture concentration and the flow velocity [45]. Furthermore, the polyhedral pattern can also spin about its vertical axis, with a circumferential speed that sometimes can even exceed the laminar flame speed of the mixture. The

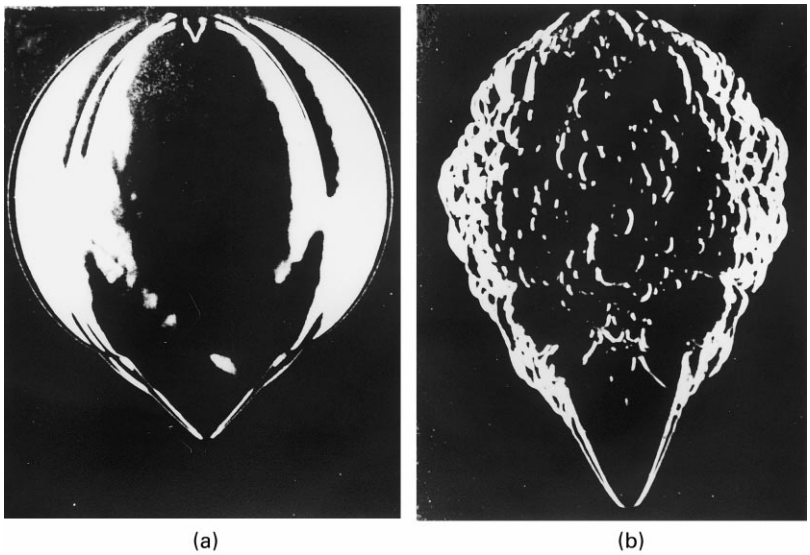

Fig. 39. Photographic images of expanding flames of: (a) lean butane/air; and (b) lean hydrogen/air mixtures, showing that the former is cellularly stable while the latter cellularly unstable.

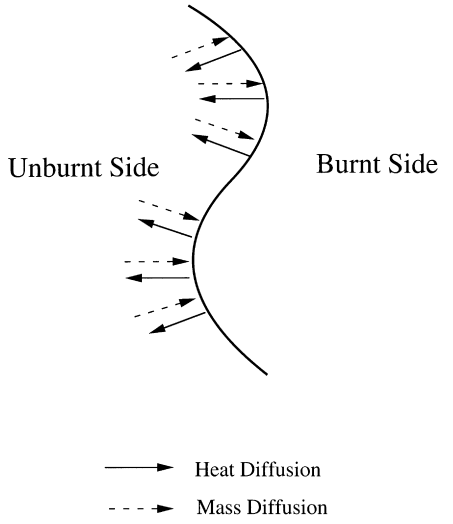

Fig. 40. Schematic showing the mechanism of diffusional–thermal cellular instability.

spinning, however, does not appear to have any preference for either the clockwise or counter-clockwise direction. It is also seen that the tip is extinguished for the present $Le < 1$, negatively stretched flame in accordance with the discussions in the previous section.

Fig. 38 shows the cellular pattern of a rich propane/air/nitrogen mixtures burning in a quasi-stabilized manner in vertical wide tubes of about 10 cm in diameter [2]. The cells are typically centimeter in size, being one order larger than the thickness of the flame, and were observed to be in continuous motion, consisting of the growth of large cells at the expense of smaller ones. These large cells would then split up into two or more smaller ones. The cells are again convex towards the unburnt mixture. Ref. [46] shows the time-resolved development of the cells as the flame propagates outward, at atmospheric as well as elevated pressure environments.

Finally, Fig. 39 shows outwardly propagating flames in a low-speed laminar flow, initiated by a spark discharge [47]. It is seen that the lean butane/air flame is largely cellularly stable, except for some large-scale sharp folds that we shall discuss later, while the lean hydrogen/air flame is clearly cellularly unstable.

We shall now present the phenomenology of the different modes of the observed cellular instability.

8.1. Phenomenology

From our understanding of the behavior of nonequidiffusive stretched flames, it is reasonable to expect that those cellular flame phenomena that depend on whether the mixture is lean or rich must in turn depend on the diffusive aspects of the flame, and thereby the flame structure itself. Indeed, if we perturb an initially planar flame into one consisting of alternating convex and concave segments towards the unburnt mixture (Fig. 40), then the subsequent evolution of these flame segments can be considered in the same manner as that for the intensification or weakening of the Bunsen flame tip (Fig. 7b). Specifically, for a $Le > 1$ flame, the burning is intensified at the concave segment and weakened at the convex segment, leading to smoothing of the wrinkles. Consequently such a flame is cellularly stable. Conversely, by the same reasoning an $Le < 1$ flame is cellularly unstable. This phenomenon can of course also be interpreted on the basis of the different diffusivities of the deficient and abundant species. We shall call this mode of instability as the nonequidiffusive instability. Since the instability is caused by the active modification of the

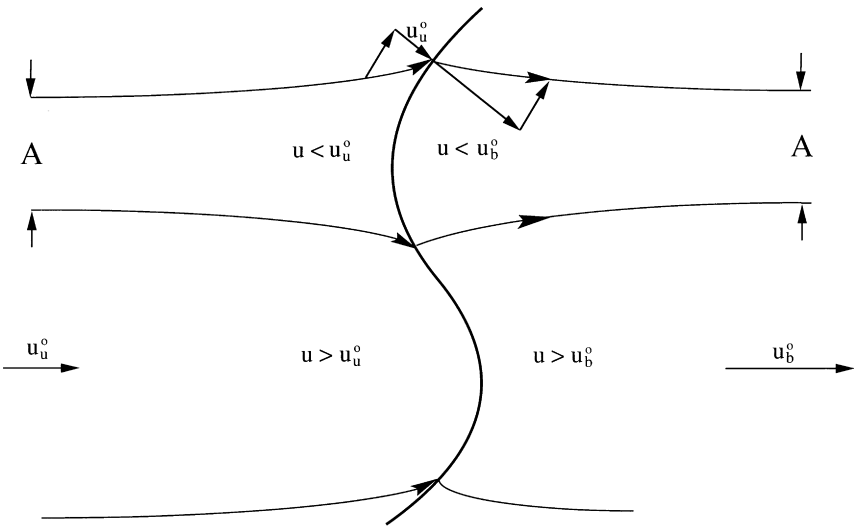

Fig. 41. Schematic showing the mechanism of hydrodynamic cellular instability.

diffusive structure of the flame, the cell size is expected to be one order larger than the flame thickness, as experimentally observed.

In addition to nonequidiffusion, we have shown that the upstream flame speed can also be modified by pure curvature effects. Thus if we again consider Fig. 40, but for an equidiffusive mixture, it is apparent that since the flame speed is reduced for the convex segment and increased for the concave segment, curvature tends to stabilize the flame. This is expected to shift the stability boundary based on nonequidiffusion considerations away from $Le = 1$ to smaller values of Le. We shall call the combined nonequidiffusive and pure curvature instabilities as the diffusional–thermal instability.

Cells of much larger sizes, of the order of 10 cm for atmospheric flames, have also been observed for large scale flames which are cellularly stable in terms of the diffusive–thermal instability; an example is the sharp folds shown in Fig. 39b. Since the scale of the cells is now much larger than the flame thickness, one may expect that the cause of flamefront instability is hydrodynamic instead of diffusive-thermal in nature. To identify the mechanism associated with this hydrodynamic instability, let us again perturb a planar flame (Fig. 41), recognizing that the flame thickness is now much smaller than the extent of wrinkling such that the flame structure is minimally affected. We can therefore treat the entire flame as a surface, with the flame speed s_u remaining at its unperturbed value, s_u^o, and that the gas densities for the upstream and downstream regions at their respective unburnt and burnt values, ρ_u and ρ_b^o. Further recognizing that the areas of the streamtube should remain the same both far upstream and downstream of the flame because of the lack of disturbance there, that because the normal component of the downstream flow velocity at the flame surface is larger than that of the upstream velocity due to thermal expansion, and that the tangential components of the upstream and downstream velocities should be continuous, the streamlines must therefore assume the pattern as shown. Thus for the convex segment of the flame, the widening of the streamtube upon approaching the flame causes the flow to slow down. However, since the flame speed remains unaffected, the local velocities of the approach flow and the flame can no longer balance each other in the manner of the planar configuration. This then results in further advancement of the convex segment into the unburnt mixture. A similar argument for the concave segment shows that it will further recede into the burnt mixture. Thus this hydrodynamic mode of instability is absolutely unstable. Furthermore, since the above discussion does not involve any length scales, we expect that the flame is unstable to perturbations of all wavelengths. This hydrodynamic instability is also called Landau–Darrieus instability.

A third mode of flamefront instability is that of Rayleigh–Taylor for fluids which have negative density stratification in the direction of a body force such as gravity. Thus an upwardly propagating flame is buoyantly unstable because the denser, unburnt mixture is over the lighter, burnt product, while the converse holds for a downwardly propagating flame. Furthermore, since an accelerating flame experiences a body force directed from the unburnt to the burnt mixtures, it is also subjected to this mode of body force instability.

8.2. Analysis

Because of the disparate scales associated with hydrodynamic and diffusive–thermal instabilities, a general analysis can be mathematically quite involved [44,48]. Thus it has been found expedient to separately analyze their linear stability in terms of the stability boundaries and the dispersion relations. Thus for the hydrodynamic instability, Landau and Darrieus [4] treated the flame as a surface of discontinuity moving with the constant laminar flame speed s_u^o everywhere over its surface, viz. the Landau limit of flame propagation. Since diffusive transport is suppressed, the density remains constant on either side of the flame sheet while variations of the flow velocity and pressure are described by the Euler equation. For the diffusive–thermal instability, an analysis of the flame structure is necessary and frequently the assumption of constant density, which implies small heat release, is made to facilitate the analysis.

In the following we shall adopt an approximate, though analytically and conceptually more apparent, analysis which incorporates the three modes of instabilities mentioned above. The approach, first used by Markstein [2], involves analyzing the stability of flame surfaces in the manner of Landau and Darrieus, but allowing the flame speed to be affected by flame stretch. Consequently both the large-scale hydrodynamic and body-force instabilities, and the small-scale diffusive–thermal instabilities, are captured. The analysis is that of linear stability, relevant for the initial growth of the disturbance and hence small departure of the flame surface configuration from the planar one. Such an analysis yields the stability boundaries and the dispersion relations of a given system. For simplicity we shall also restrict the analysis to two-dimensional disturbances.

The analysis involves applying a small disturbance to a planar flame, and determining whether this disturbance will cause the instantaneous flame surface $f(x, t)$, along with other quantities, to grow or decay.

On the unburnt and burnt sides of the flame, respectively designated by the subscripts $(-)$ and $(+)$, the densities are uniform, given by

$$\hat{\rho}_- = \hat{\rho}_u = 1 \text{ and } \hat{\rho}_+ = \hat{\rho}_b^o = \beta^o < 1, \tag{89}$$

where $\beta^o = 1/(1 + \tilde{q}_c)$ is the density ratio. The velocity and pressure variations for the inviscid and incompressible flows are governed by continuity and the Euler equation

$$\hat{\nabla}\cdot\tilde{\mathbf{v}}_{\mp} = 0 \tag{90}$$

$$\hat{\rho}_{\mp}\left(\frac{\partial\tilde{\mathbf{v}}_{\mp}}{\partial\hat{t}} + \tilde{\mathbf{v}}_{\mp}\cdot\hat{\nabla}\tilde{\mathbf{v}}_{\mp}\right) = -\hat{\nabla}\tilde{p}_{\mp} + \hat{\rho}_{\mp}\hat{g}\mathbf{e}_{\mathrm{g}}, \tag{91}$$

where $\mathbf{e}_{\mathrm{g}}$ is the unit vector in the direction of gravity. In the above, length, velocity, time, ρ, p, g and the heat of reaction $\tilde{q}_{\mathrm{c}}$ are, respectively, nondimensionalized by the physical quantities $\mathscr{L}_{\mathrm{H}}$, $s_{\mathrm{u}}^{\mathrm{o}}$, $\mathscr{L}_{\mathrm{H}}/s_{\mathrm{u}}^{\mathrm{o}}$, ρ_{u}, $\rho_{\mathrm{u}}(s_{\mathrm{u}}^{\mathrm{o}})^2$, $(s_{\mathrm{u}}^{\mathrm{o}})^2/\mathscr{L}_{\mathrm{H}}$ and $c_{\mathrm{p}}T_{\mathrm{u}}/Y_{\mathrm{u}}$. We further require that the upstream and downstream solutions must be bounded as $\hat{y}\to\pm\infty$, and that they are related to each other across the flame sheet through the conservation of mass and the normal and tangential momenta:

$$[\hat{\rho}(\tilde{\mathbf{v}}-\tilde{\mathbf{V}})\cdot\mathbf{n}] = 0, \tag{92}$$

$$[\hat{\rho}(\tilde{\mathbf{v}}-\tilde{\mathbf{V}})\cdot\mathbf{n}(\tilde{\mathbf{v}}\cdot\mathbf{n}) + \tilde{p} - \hat{\rho}\hat{g}(\hat{f}-\hat{y})] = 0, \tag{93}$$

$$[\tilde{\mathbf{v}}\times\mathbf{n}] = 0, \tag{94}$$

where $[\phi] = \phi(\hat{y}=\hat{f}_{+}) - \phi(\hat{y}=\hat{f}_{-})$ for the quantity ϕ. The jump relation (94) states that the tangential components of the velocities are continuous across the flame.

The problem is completed by specifying the upstream flame speed, $\tilde{s}_{\mathrm{u}}$, needed for the G-equation. Landau and Darrieus assumed $\tilde{s}_{\mathrm{u}}=1$. We shall, however, use the general expression for the stretched flame, Eq. (67). When expressed in the hydrodynamic scale $\mathscr{L}_{\mathrm{H}}$, this expression can be written as

$$\tilde{s}_{\mathrm{u}} = 1 + \hat{\mathscr{L}}_{\mathrm{T}}^{\mathrm{o}}(-\hat{\nabla}\cdot\mathbf{n} + Ma\hat{K}a), \tag{95}$$

where the Karlovitz number $\hat{K}a$ is now measured in units of $\mathscr{L}_{\mathrm{H}}$ and therefore differs from the previous definition by the factor $\hat{\mathscr{L}}_{\mathrm{T}}^{\mathrm{o}} = \mathscr{L}_{\mathrm{T}}^{\mathrm{o}}/\mathscr{L}_{\mathrm{H}}$, which compares the flame thickness to the hydrodynamic scale.

The steady one-dimensional solution of the above problem, corresponding to a planar flame front with the velocity field $\tilde{\mathbf{v}} = \tilde{\mathbf{v}}_0 = (\tilde{u}_0, 0)$, is given by

$$\tilde{u}_0 = \begin{cases} 1 \\ 1+\tilde{q}_{\mathrm{c}} \end{cases}, \quad \tilde{p}_0 = \begin{cases} -\hat{g}\hat{y} & \hat{y}<0 \\ -\tilde{q}_{\mathrm{c}} - \hat{g}\hat{y}/(1+\tilde{q}_{\mathrm{c}}) & \hat{y}>0 \end{cases}, \tag{96}$$

where the subscript "0" designates this basic solution, $\hat{g}>0$ corresponds to a downward propagating flame, and we have also located the planar flame front at $\hat{y}=0$.

To perform a linear stability analysis to determine the response of this solution to small arbitrary disturbances, we represent the disturbed quantities as $\tilde{\mathbf{v}} = \tilde{\mathbf{v}}_0 + \tilde{\mathbf{v}}'$, $\tilde{p} = \tilde{p}_0 + \tilde{p}'$, and $\hat{f} \equiv \hat{f}$, where $\tilde{\mathbf{v}}' = (\tilde{u}', \tilde{v}')$ and the perturbations are assumed to be small compared to the basic state solution. Substituting these expressions into Eqs. (90) and (91), and linearizing about the basic state, we obtain

$$\hat{\nabla}\cdot\tilde{\mathbf{v}}'_{\mp} = \frac{\partial\tilde{u}'_{\mp}}{\partial\hat{x}} + \frac{\partial\tilde{v}'_{\mp}}{\partial\hat{y}} = 0 \tag{97}$$

$$\hat{\rho}_{\mp}\left(\frac{\partial\tilde{\mathbf{v}}'_{\mp}}{\partial\hat{t}} + \tilde{\mathbf{v}}_{0,\mp}\cdot\hat{\nabla}\tilde{\mathbf{v}}'_{\mp} + \tilde{\mathbf{v}}'_{\mp}\cdot\hat{\nabla}\tilde{\mathbf{v}}_{0,\mp}\right) = -\hat{\nabla}\tilde{p}'_{\mp}. \tag{98}$$

Similar linearization of the flame speed expression (95), the G-equation (12), and the jump relations (92)–(94) then respectively yield

$$\tilde{s}_{\mathrm{u}} = 1 - \hat{\mathscr{L}}_{\mathrm{T}}^{\mathrm{o}}\frac{\partial^2\hat{f}}{\partial\hat{x}^2} + \hat{\mathscr{L}}_{\mathrm{T}}^{\mathrm{o}}Ma\frac{\partial^2\hat{f}}{\partial\hat{x}^2} = 1 - (1-Ma)\hat{\mathscr{L}}_{\mathrm{T}}^{\mathrm{o}}\frac{\partial^2\hat{f}}{\partial\hat{x}^2} \tag{99}$$

$$\tilde{u}'_{-}(0) = \frac{\partial\hat{f}}{\partial\hat{t}} - (1-Ma)\hat{\mathscr{L}}_{\mathrm{T}}^{\mathrm{o}}\frac{\partial^2\hat{f}}{\partial\hat{x}^2} \tag{100}$$

$$[\tilde{u}'] = -\tilde{q}_{\mathrm{c}}(1-Ma)\hat{\mathscr{L}}_{\mathrm{T}}^{\mathrm{o}}\frac{\partial^2\hat{f}}{\partial\hat{x}^2} \tag{101}$$

$$[\tilde{p}'] = 2\tilde{q}_{\mathrm{c}}(1-Ma)\hat{\mathscr{L}}_{\mathrm{T}}^{\mathrm{o}}\frac{\partial^2\hat{f}}{\partial\hat{x}^2} - \frac{\hat{g}\tilde{q}_{\mathrm{c}}\tilde{f}}{(1+\tilde{q}_{\mathrm{c}})} \tag{102}$$

$$\tilde{q}_{\mathrm{c}}\frac{\partial\hat{f}}{\partial\hat{x}} + [\tilde{v}'] = 0. \tag{103}$$

To solve Eqs. (96) and (98) subject to Eqs. (99)–(103), we look for solution of the form

$$\tilde{u}'_{\mp} = \bar{\tilde{u}}_{\mp}(\hat{y})\exp(\hat{\omega}\hat{t} + \mathrm{i}\hat{k}\hat{x}), \quad \tilde{v}'_{\mp} = \bar{\tilde{v}}_{\mp}(\hat{y})\exp(\hat{\omega}\hat{t} + \mathrm{i}\hat{k}\hat{x})$$

$$\tilde{p}'_{\mp} = \bar{\tilde{p}}_{\mp}(\hat{y})\exp(\hat{\omega}\hat{t} + \mathrm{i}\hat{k}\hat{x}), \quad \hat{f} = \hat{A}\exp(\hat{\omega}\hat{t} + \mathrm{i}\hat{k}\hat{x}). \tag{104}$$

The solution procedure is straightforward. It can thus be shown that for a nontrivial solution to exist, $\hat{\omega}$ must satisfy the following dispersion relation

$$(2+\tilde{q}_{\mathrm{c}})\hat{\omega}^2 + 2(1+\tilde{q}_{\mathrm{c}})\hat{k}\hat{\omega} - \tilde{q}_{\mathrm{c}}(1+\tilde{q}_{\mathrm{c}})\hat{k}\left\{\hat{k} - \frac{2(1-Ma)\hat{\mathscr{L}}_{\mathrm{T}}^{\mathrm{o}}(1+\tilde{q}_{\mathrm{c}})}{\tilde{q}_{\mathrm{c}}}\hat{k}^2 - \frac{\hat{g}}{(1+\tilde{q}_{\mathrm{c}})}\right\} = 0, \tag{105}$$

which possesses two roots. The first has a negative real part, and therefore it does not predict instability. The second root is given by

$$\hat{\omega} = \frac{(1+\tilde{q}_{\mathrm{c}})}{(2+\tilde{q}_{\mathrm{c}})}\left\{-\hat{k} + \sqrt{\left[1 + \frac{\tilde{q}_{\mathrm{c}}(2+\tilde{q}_{\mathrm{c}})}{(1+\tilde{q}_{\mathrm{c}})}\right]\hat{k}^2 - 2(2+\tilde{q}_{\mathrm{c}})(1-Ma)\hat{I}_{\mathrm{T}}^{\mathrm{o}}\hat{k}^3 - \frac{\tilde{q}_{\mathrm{c}}(2+\tilde{q}_{\mathrm{c}})}{(1+\tilde{q}_{\mathrm{c}})^2}\hat{g}\hat{k}}\right\}. \tag{106}$$

We now study the implication of the dispersion relation (106) for the real values of $\hat{\omega}$.

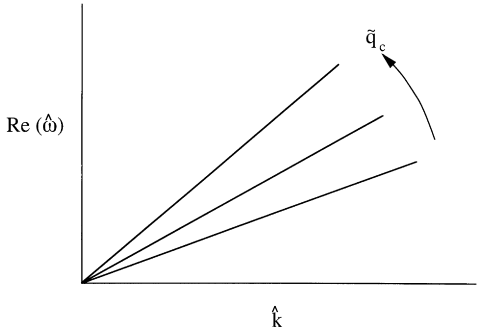

Fig. 42. Stability diagram for the hydrodynamic instability.

We first examine the Landau limit, corresponding to the hydrodynamic instability. Setting $\hat{\mathcal{L}}_T^o \equiv 0$ and $\hat{g} = 0$, Eq. (106) becomes

$$\hat{\omega} = \frac{(1+\hat{q}_c)}{(2+\hat{q}_c)}\left\{-1+\sqrt{1+\frac{\hat{q}_c(2+\hat{q}_c)}{(1+\hat{q}_c)}}\right\}\hat{k}. \tag{107}$$

Since $\hat{\omega} > 0$ for all $\hat{q}_c > 0$, Eq. (107) shows that the flame is unconditionally unstable to disturbances of all wavelengths. As discussed earlier, this mode of hydrodynamic instability is caused by the thermal expansion of the gas upon crossing the flame. Consequently, the instability grows faster with increasing $\tilde{q}_c$ and hence thermal expansion, as shown in Fig. 42.

Since smooth laminar flames are routinely observed in the laboratory, there must exist alternate mechanisms that can counteract the hydrodynamic instability and thereby stabilize the flame surface. One such mechanism is buoyancy. Specifically, for an upward propagating flame in the presence of gravity, $\hat{g} < 0$ and we again have $\hat{\omega} > 0$ from Eq. (106) for $\hat{\mathcal{L}}_T^o \equiv 0$. Such flames are exposed to both the hydrodynamic instability as well as the body-force, Rayleigh–Taylor instability. However, for a downward propagating flame, $\hat{g} > 0$ and the above root possesses both real and imaginary parts. The real part passes through zero at the critical value $\hat{k}_g = \hat{g}/(1+\tilde{q}_c)$. Since in the radical term the gravity term varies with $\hat{k}$ while the thermal expansion term varies with $\hat{k}^2$, the gravity term dominates for small $\hat{k}$. The flame is therefore unstable to short wavelength disturbances with $\hat{k} > \hat{k}_g$, and stable to long wave disturbances with $\hat{k} < \hat{k}_g$, as shown in Fig. 43. Thus buoyancy can stabilize long wave disturbances for downwardly propagating flames.

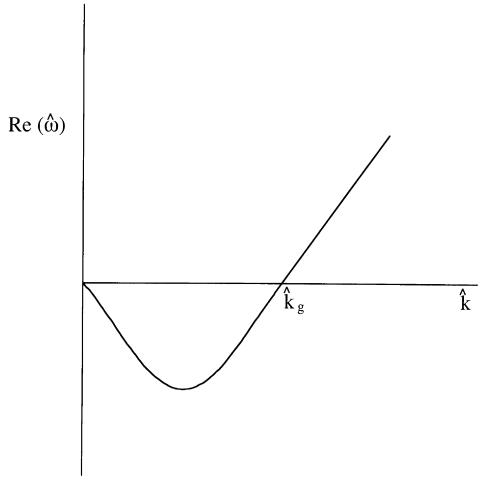

Fig. 43. Stability diagram for the hydrodynamic instability in the presence of a stabilizing body force.

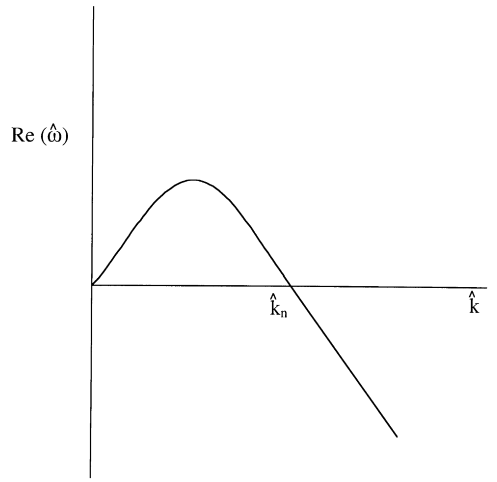

Fig. 44. Stability diagram showing the stabilizing influence of the pure curvature effect on the hydrodynamic instability.

We next study the pure flame curvature effect by setting $Ma = 0$ (and $\hat{g} = 0$) in Eq. (106). It is seen that the term representing its influence in the radical term is always negative, and hence tends to moderate the destabilizing effect of thermal expansion. Furthermore, since this curvature term varies with $\hat{k}^3$ as compared to the $\hat{k}^2$ variation of the thermal expansion term, we expect that the flame is rendered stable by curvature for short wave disturbances with $\hat{k} > \hat{k}_n = \tilde{q}_c/[2\hat{\mathcal{L}}_T^o(1+\tilde{q}_c)]$, as shown in Fig. 44. This is in agreement with our earlier anticipations.

We finally study the nonequidiffusive instability, as determined by the term in Eq. (106) with the factor $Ma = (Le^{-1} - 1)/2\epsilon^o$. Since this term is positive for $Ma > 0$ and hence $Le < 1$, the flame is rendered unstable for $Le < 1$ mixtures. The converse holds for $Le > 1$ mixtures. Stability is promoted for short wave disturbances in the same manner as the pure curvature effect. All these results are again in agreement with our earlier discussions.

By combining the pure curvature and nonequidiffusive effects as represented by the factor $(1 - Ma)$ for the

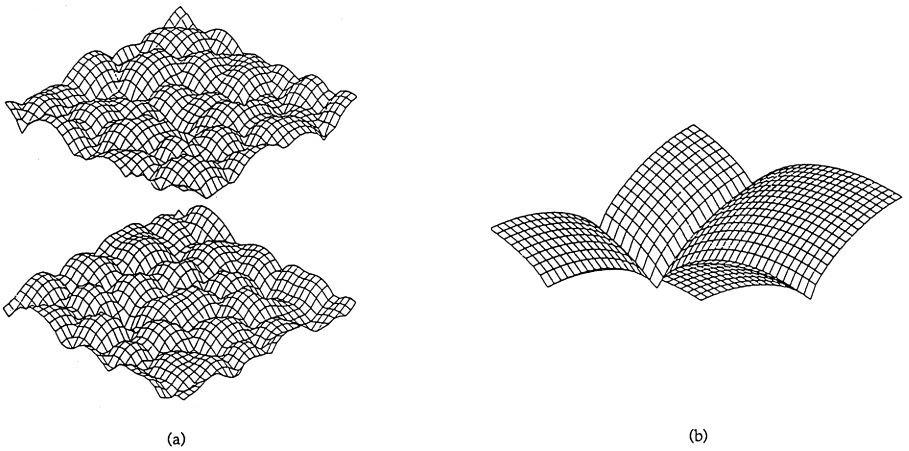

Fig. 45. Numerical simulation of the cellular flame structure exhibiting: (a) diffusional–thermal instability; and (b) hydrodynamic instability. Note the chaotic nature of the former and the regular folds of the latter.

diffusive–thermal instability, it is clear that their influence is destabilizing for $Ma > 1$, or $Le < 1/(1 + 2\epsilon^o) \approx (1 - 2\epsilon^o)$, and stabilizing otherwise. Thus the pure curvature effect extends the regime of stabilizing Lewis number by $2\epsilon^o$ in that, without considering it, the flame will lose stability for $Le < 1$.

In summary, we have shown that while thermal expansion is destabilizing for all wavelengths, its effects can be counteracted by those of other processes. For long wave disturbances, relevant for large-scale flame phenomena, buoyancy provides a stabilizing influence when the flame propagates downward. For short wave disturbances, pure curvature is always stabilizing. This tendency is further enhanced for mixtures whose *Le* is larger than $1 - 2\epsilon^o$.

8.3. Additional considerations

There are two other major processes which can affect the flame burning rate and hence its propensity to destabilize. The first is heat loss. Diffusional-thermal stability analyses have been performed for the doubly infinite flame with volumetric heat loss [49]. Results show that such a heat loss tends to increase the critical Lewis number of stability from the adiabatic value of $1 - 2\epsilon^o$, and hence narrows

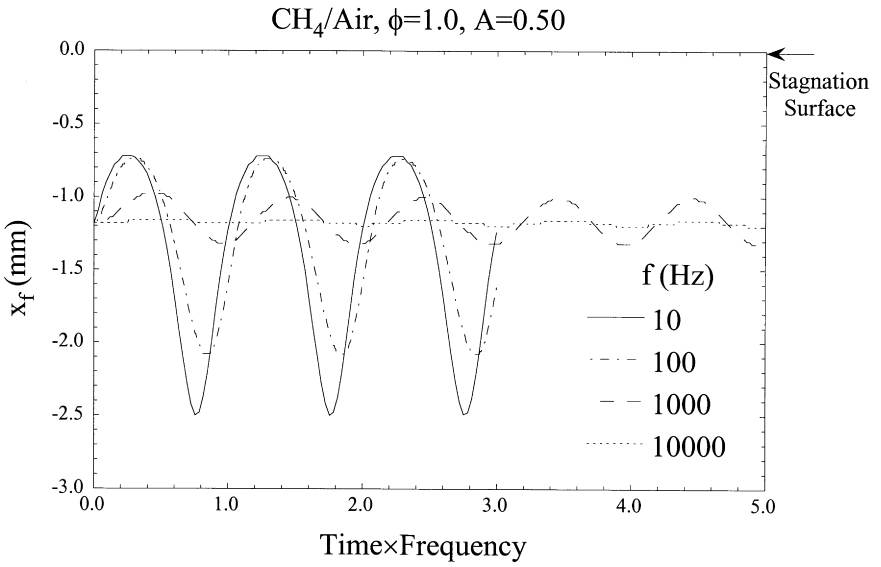

Fig. 46. Location of an oscillated counterflow methane/air flame, showing the reduced response with increasing frequency.

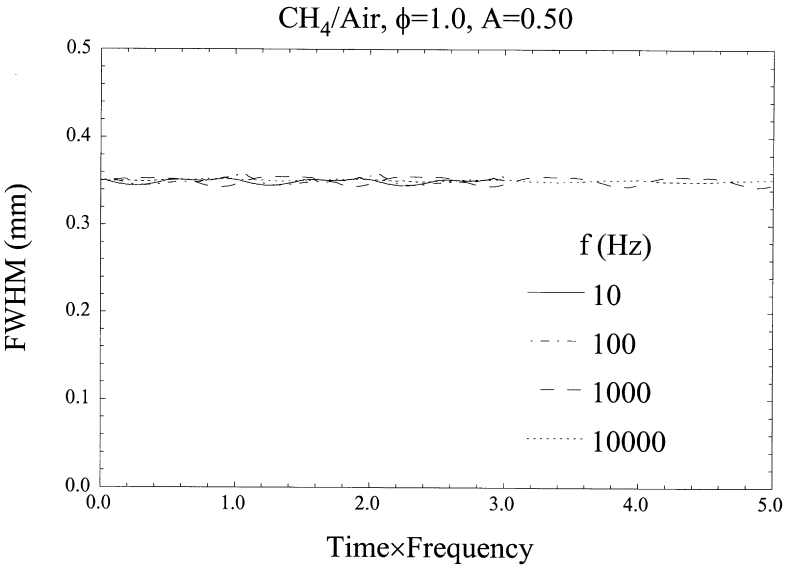

Fig. 47. Thickness of the oscillated counterflow methane/air flame of Fig. 46, showing its insensitivity to oscillations at all frequencies.

the regime of stability. This outcome is reasonable if we consider that the effect of heat loss from the flame is to reduce the flame temperature and hence the rate of heat diffusion. Since the mass diffusion rate is fixed, the flame is rendered unstable.

The second process is bulk aerodynamic stretching, which has been found to be stabilizing if it is positive, and destabilizing if otherwise [50,51]. Conceptually, a positively stretched flame such as the counterflow flame and the outwardly expanding flame tends to continuously "stretch out" and "carry away" any wrinkles which may develop over the flame surface. Experimentally it has been found for stagnation flows that for low rates of stretch, the flame exhibits the same cellular structure as observed for non-stretched flames. However, with increasing stretch, the instability in the radial direction is first suppressed, resulting in ridges emanating in the radial direction. With strong enough stretching, even these radial ridges are suppressed. By the same reasoning, we then expect that flamefront instability tend to be aggravated in a compressive flow whose stretch is negative.

The linear stability analysis discussed above only describes the initial response of the flame. Nonlinear analyses, frequently aided by numerical solutions, are needed to trace through the development of the instabilities until the formation of the cellular flame pattern. Such numerical simulation [48] have found that diffusive-thermal instability generates cells of a chaotic nature (Fig. 45a), while hydrodynamic instability generates steady cells of regular sizes and shapes (Fig. 45b). It has thus been suggested that diffusive–thermal instability can lead to self-turbulization of a flame.

9. Unsteady dynamics

The review so far has been concerned with steady state or quasi-steady flames, such as the counterflow and Bunsen flames for the former, and the spherically propagating flame for the latter. In this section we shall discuss flame dynamics which are oscillatory in nature and hence are fundamentally unsteady. The oscillatory response can be either caused by externally applied, forced oscillatory motion [52–56], or is intrinsic in the flame propagation mode [57–64].

9.1. Forced oscillation

Studies of effects of aerodynamic oscillation on the response of strained laminar flames are of relevance to the understanding of turbulent flames and acoustic combustion instabilities. Since flamelets constituting the bulk flame are subjected to fluctuating flows with various intensities of straining, it is reasonable to expect that they would respond differently in an oscillating strained flow field than a steady strained flow field.

There are two parameters that characterize the influence of flow oscillation, namely the frequency of the oscillation as compared to (the inverse of) the characteristic flame time, and the amplitude of the oscillation. Fig. 46 shows the

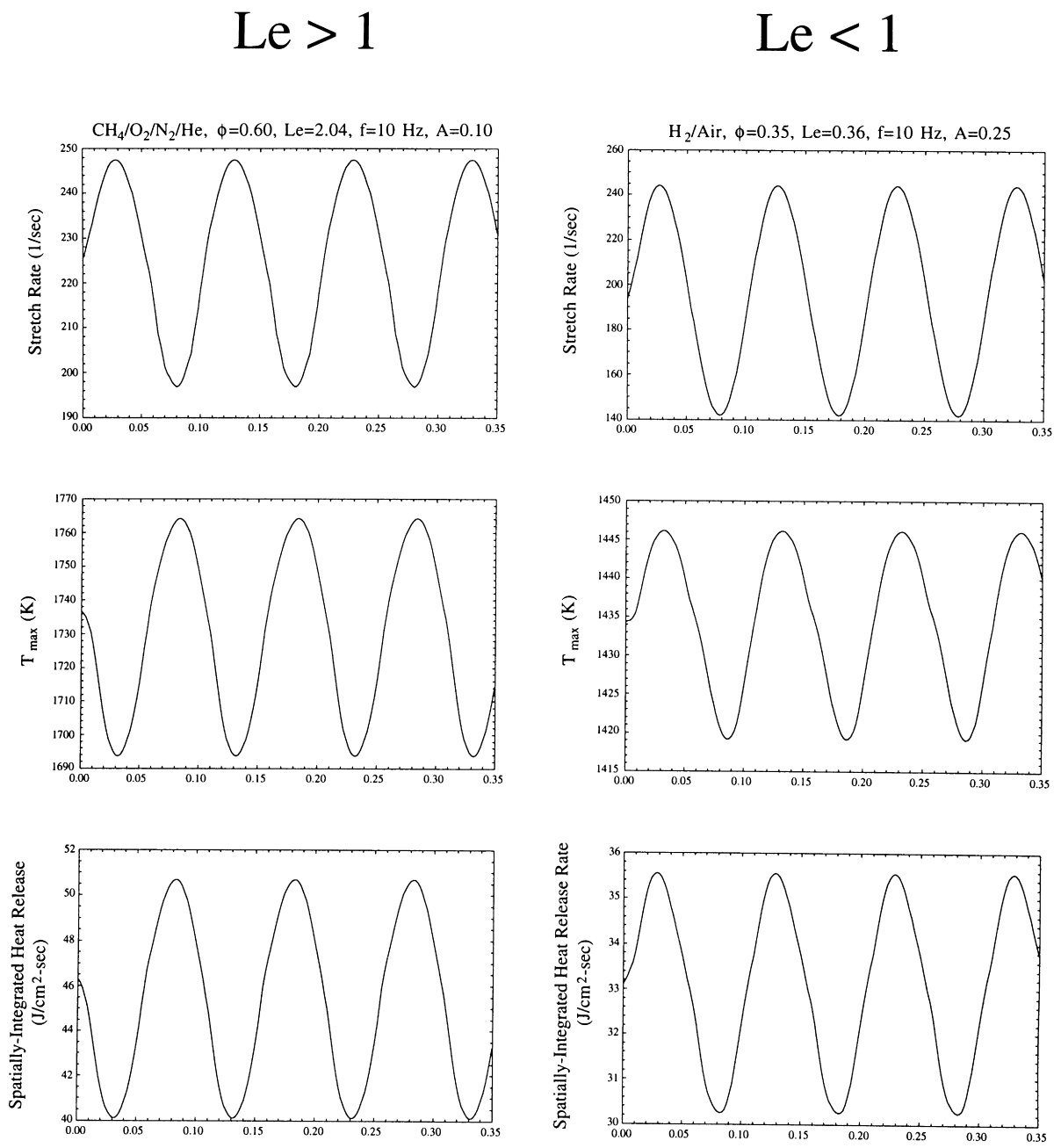

Fig. 48. Phase relations between imposed strain and flame burning intensity: (a) out of phase for $Le > 1$ flames; (b) in phase for $Le < 1$ flames.

temporal variation of the location of a counterflow, near-equidiffusive, methane/air flame with $\phi = 1$, when it is subjected to an oscillation amplitude of approximately 0.5 relative to a steady strain rate. Since a premixed flame can freely adjust its location in response to changes in the flow so as to achieve dynamic balance, provided there is enough time to achieve the re-location, Fig. 46 shows that for low frequencies the flame indeed translates readily and hence exhibits large movements. However, for high-frequency oscillation, the flame does not have enough time to adjust to changes in the flow field and its movement is considerably restrained.

Fig. 47 shows the corresponding variation of the flame thickness in terms of the FWHM value. It is seen that the flame thickness is not sensitive to the oscillation frequency for all frequencies. This interesting behavior is because of

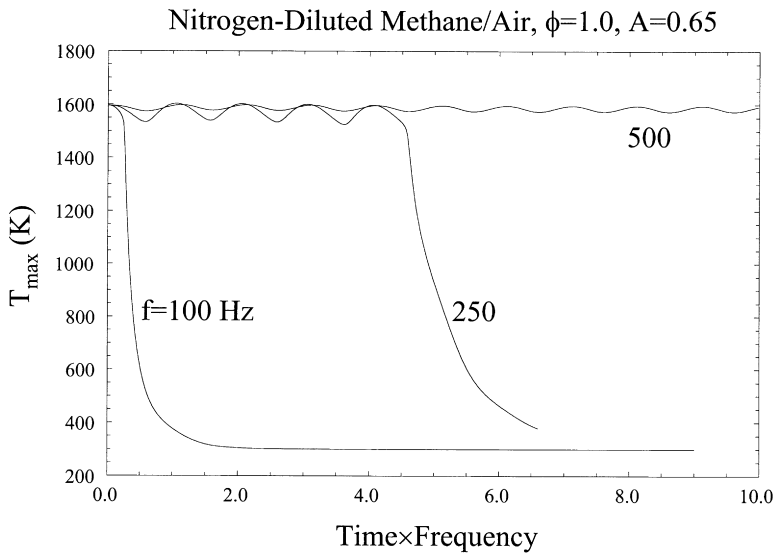

Fig. 49. Cycle variations of maximum flame temperature, T_{max}, with various frequencies of oscillation, for a nitrogen-diluted stoichiometric methane mixture, whose mole fraction is methane:oxygen:nitrogen = 1:2:12.12, with 0.65 amplitude perturbation.

the fact that, for a near-equidiffusive mixture, the flame thickness is basically invariant to strain rate variations in the steady, and hence low frequency limit, while it is also insensitive to high frequency oscillations because of the reduced response time.

The effects of nonequidiffusion are illustrated in Fig. 48 for two mixtures whose Lewis numbers are, respectively, larger and smaller than unity. It is seen that while the maximum flame temperature and heat release rate are out of phase with the imposed oscillatory strain rate for the $Le > 1$ flame, the behavior is reversed for the $Le < 1$ flame. This result is in agreement with the understanding from the steady state response that shows that, for mixtures with Le greater or smaller than unity, the burning intensity, respectively, decreases and increases with increasing strain rate. The practical implications of this result in combustion instability within combustion chambers can be quite significant.

Based on the concept of *quasi-steadiness*, an oscillating flame extinguishes if the instantaneous strain rate increases beyond the steady-state extinction strain rate at any instant during a cycle of oscillation. On the other hand, when such a state is not attained during the cycle, then extinction cannot be achieved. As a result, if quasi-steady extinction were to occur, it must occur during the first cycle. Fig. 49 demonstrates that, for a nitrogen-diluted, stoichiometric methane/

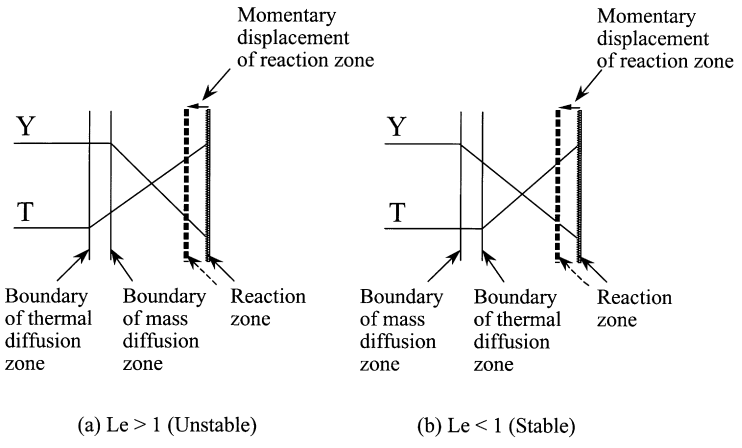

Fig. 50. Schematic showing the mechanism of diffusional–thermal pulsating instability: (a) $Le > 1$ (unstable); (b) $Le < 1$ (stable).

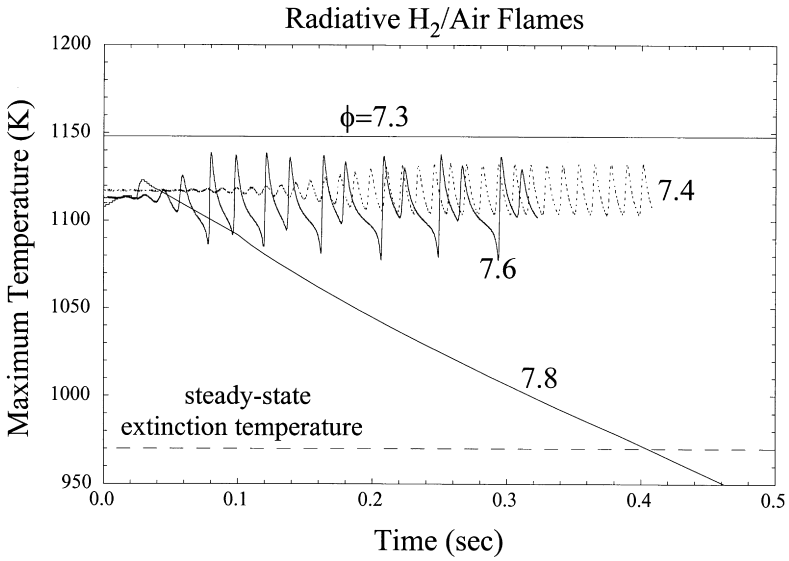

Fig. 51. Various pulsating modes for near-limit rich hydrogen/air flames.

air mixture and given amplitude fraction of 0.65, extinction occurs within one cycle for an $f = 100$ Hz oscillation. However, extinction is delayed with increasing frequency (e.g. $f = 250$ Hz) in that the system can persist over several cycles, with progressive reduction in the peak flame temperature, before extinction takes place. With even higher frequencies, for example $f = 500$ Hz, the unsteady flame eventually achieves permanent oscillation without extinction. Thus, quasi-steadiness obviously does not hold for the imposition of high-frequency oscillation.

9.2. Intrinsic pulsating instability

In addition to cellular instability, a flame can also propagate in a pulsating or spinning mode due to temporal instability. The controlling factor in inducing the pulsating instability is again diffusional-thermal in nature, and the mechanism is depicted in Fig. 50, for a planar flame. Specifically, consider a disturbance momentarily applied to the reaction zone, causing it to move forward. Because of the larger inertia of the thermal and mass diffusion zones

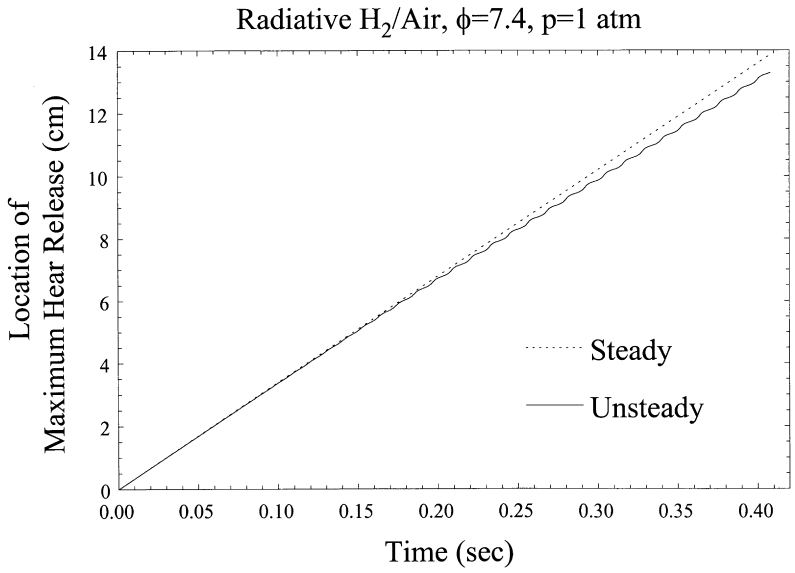

Fig. 52. Trajectory of steady and pulsating flames, showing slower propagation rate for the latter.

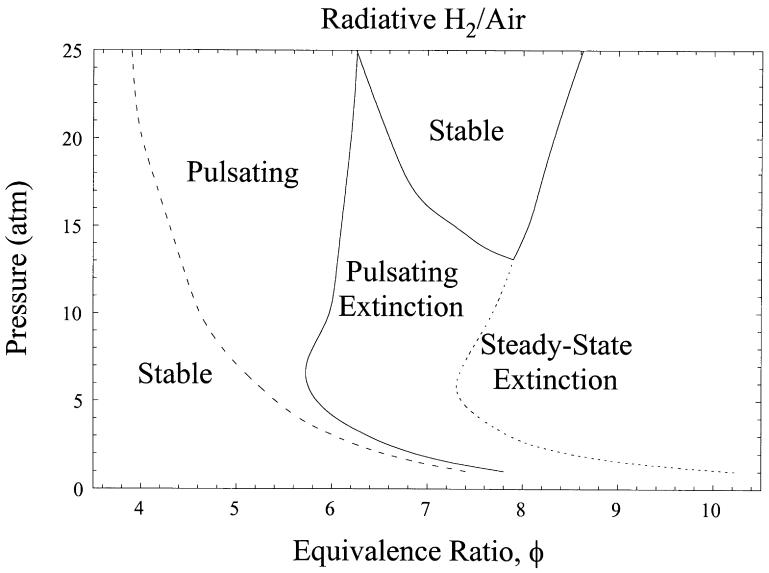

Fig. 53. Calculated pulsating stability and extinction boundaries of rich hydrogen/air flames from 1 to 20 atm.

relative to that of the reaction zone, the flame structure and hence thickness cannot instantaneous relax to accommodate such a disturbance. Consequently the diffusion zone becomes thinner, and the corresponding temperature and concentration gradients also steepen. For an $Le > 1$ flame, since the thermal diffusion zone is initially thicker than the mass diffusion zone, a reduction of their respective thicknesses by the same amount implies that the thermal gradient suffers relatively less steepening than the concentration gradient. Thus the reaction becomes stronger because it now gains more reactant from the freestream than loses heat to it, causing it to further move forward. By the same reasoning, if the reaction zone is displaced backward, the burning will be weakened, causing it to further lag behind. Thus $Le > 1$ flames can be pulsatingly unstable. Similarly it can be reasoned that $Le < 1$ flames are pulsatingly stable. This dependence on *Le* is completely opposite to that of cellular diffusional–thermal instability in that cellular instability is promoted for $Le < 1$ flames and suppressed for $Le > 1$ flames.

Asymptotic analysis assuming negligible heat release [58] shows that a flame is pulsatingly unstable for $Ze(Le - 1) > 4(1 + \sqrt{3}) \approx 10.9$, which we shall call the Sivashinsky criterion. Since *Ze* for many practical flames are actually not too large, typically smaller than six or seven, and since *Le* for gaseous mixtures are close to unity, the tendency for gaseous flames to exhibit pulsating instability is actually not strong. Thus studies of pulsating instability have focused on solid flames [43,65–71] which are of interest to materials synthesis, for which *Le* is very large. Here pulsating or spinning modes of propagation are frequently observed, resulting in undesirable laminated synthesized products.

Recently the possible existence of pulsating instability in gaseous mixtures has regained interest [60–64] for weakly burning flames, especially in its role in causing flame extinction. That is, when a flame is near the extinction state, its global activation energy and hence *Ze* are expected to increase substantially such that the Shivashinsky criterion can be satisfied. The possible onset of pulsating instability near the extinction state can have profound impact on our understanding of the extinction mechanism and prediction of the extinction limit. For example, if a flame is susceptible to pulsating instability, will it extinguish in steadily or pulsatingly propagating mode? If it is the latter, will the steady extinction limit be widened or contracted?

The above possibility has been computationally investigated for the planar freely propagating rich hydrogen/air flames with radiative heat loss [63,64]. A steady state calculation allowing for radiative heat loss shows that the flame extinguishes at $\phi = 10.4$ through the turning point criterion. However, when unsteadiness is allowed in the calculation, a rich variety of propagation modes is captured, as shown in Fig. 51. It is seen that while at $\phi = 7.3$ the flame is still stable, at $\phi = 7.4$ it loses stability and propagates in an oscillatory mode, with a single frequency. The overall propagation rate, however, is slower, as shown in Fig. 52, because the flame spends more time in the negative phase of the oscillation than the positive phase. At $\phi = 7.6$ the propagation mode transitions to that of period doubling, with two frequencies. Finally, the flame fails to propagate at $\phi = 7.8$. These results clearly show that the flame extinguishes in the pulsating mode, and that the extinction limit is narrowed due to pulsation. The reason that pulsation promotes extinction is that while the positive phase of the oscillation enhances the intensity of the flame that is already burning anyway, the

negative phase can reduce the burning intensity to a state of temporary extinction which, however, is unrecoverable.

By using globally extracted E_a and *Le*, it has been found that the computationally calculated limit at which the flame becomes unstable agrees closely with that given by the Shivashinsky criterion. Furthermore, it is also recognized that the net effect of the hydrogen oxidation mechanism is quite nonlinear in that, for a given temperature, by progressively increasing the pressure the reaction intensity is first weakened through the $H + O_2$ chemistry, and then enhanced through the HO_2 and H_2O_2 chemistry. As such, it is reasonable to expect that, with increasing pressure, the global E_a will first increase and then decrease. This in turn implies that the propensity to pulsate will first increase and then decrease. Fig. 53 [64] shows the calculated stability diagram in terms of ϕ and pressure, indicating the respective limits for the onset of pulsation, extinction in the steady mode, and extinction in the pulsating mode. It is seen that while pulsation is indeed promoted with increasing pressure for the lower pressure range, a regime of stability is identified at higher pressures.

While rich hydrogen/air mixtures may not be too practically relevant, except perhaps in the mixing region of a nonpremixed hydrogen/air system, further studies [72] have shown that pulsating instability also occurs for lean heptane/air flames. Consequently, the practical implications of pulsation, and hence pulsation induced flame extinction, take on a new dimension of importance.

Finally, it has also been found that positive stretch, in the form of counterflow [73] or outwardly propagating flames [74], promotes pulsation while negative stretch, in form of inwardly propagating flames [75], suppresses it. This is completely opposite to the effects of stretch on cellular flames.

10. Concluding remarks

The present review has demonstrated that there now exists a basic framework for the description of the dynamics and geometry of flame surfaces in general flow fields, and consequently a solution procedure for chemically reacting flows in which the nonequilibrium processes of diffusion and reaction take place through laminar flamelets. This is achieved by incorporating the *G*-equation as part of the solution for the conservation equations of heat, mass, and momentum, treating the flame surfaces, known as flamelets, as sources of heat and sinks for reactants. These flamelets actively propagate with stretch-affected velocities, and at the same time are also passively convected by the local dynamics of the flow.

We have also shown that this description, at both the linear level of flame propagation and nonlinear level of flame extinction, can be made quantitatively accurate, and hence meaningful, by using such global flame parameters as the unstretched flame speed s_u^o, the flame thickness, the activation energy, the Lewis number, and the Markstein length. These global flame parameters are defined and can be empirically determined, either experimentally or computationally, if the chemical kinetic mechanism is known for a fuel/oxidizer system and a given thermodynamic state of temperature, pressure, and reactant concentration.

The materials presented in this review demonstrate the significant progress that has been made on the structure and dynamics of laminar premixed flames in the past 25 years or so. There are, however, still some crucial issues that require further investigation. Some of them are discussed in the following.

1. The quasi-one-dimensional analysis shows that the temperature of a nonequidiffusive stretched flame can deviate from the adiabatic flame temperature due to the local stratification of the energy and species contents from the freestream values. This stratification occurs within the transport zone and the changes in these contents are supposed to be transported in the tangential direction of the flame segment under consideration. One would then expect that they would eventually cross the reaction zone at some neighboring flame segments. In other words, while total energy conservation based on the freestream values may not hold locally, it must hold when summed over the entire flame surface. In particular, segments of energy deficit must be balanced by segments of energy excess for overall energy conservation. However, experimental results on, say the counterflow and Bunsen flames, seem to show that the same stretch-affected behavior prevails throughout the entire flame surface. This “unpleasant” result, even at the conceptual level, needs to be resolved. A satisfactory investigation may require two-dimensional analysis.
2. Most analyses on stretched flames have assumed quasi-steadiness in the flame structure. There are, however, strong transients in combustion processes that can intrude into the flame structure. Examples are pressure and velocity oscillations within combustion chambers in the form of combustion instabilities, and high-intensity turbulent flows in which the local conditions fluctuate rapidly. We also note that our analysis of the flamefront instability using the *G*-equation and the quasi-steady stretched flame expression did not capture pulsating instability. Results from recent studies on unsteady flame dynamics, some of them are discussed in this review, need to be integrated into the description of flame dynamics in an essential manner.
3. Practically all of the previous analytical and computational studies based on the *G*-equation have neglected density variations across the flame. While this assumption decouples the description of the flame dynamics from that of the flow field, it is clearly not satisfactory considering the significant density jump across the flame due to the large amount of heat release. This restriction needs to be removed. Computationally, special numerical

front-tracking techniques need to be developed to describe the flamefrot movement in complex flow fields.

4. Laminar flamelet is a meaningful concept only if the flame thickness is much thinner than that of the aerodynamic scale. In a turbulent flow this would require that the flame thickness be smaller than the Kolmogorov scale of the turbulence, which may not be always satisfied. To circumvent this difficulty, we may treat the much thinner reaction zone as the G surface, and let the preheat zone be part of the flow field to be calculated. It may be noted that generalized jumps relations across such reaction surfaces have been derived [76,77].
5. It is anticipated that there will be increased activities in the use of the G-equation in the description of chemically reacting turbulent flows, especially when density jump is accounted for. Many issues related to stretched flames assume special significance in turbulent flames, such as self-laminarization through heat release, self-turbulization through triggering of the various modes of flamefront instabilities, the ignition, extinction, and re-ignition criteria and processes, the formation of islands of unburnt mixtures through flame folding, and the concentration stratification within turbulent eddies and how it affects the oxidative and pollutant chemistry.

Acknowledgements

It is a pleasure to acknowledge the support of our research activities on flames by the Air Force Office of Scientific Research and the National Aeronautics and Space Administration.

References

[1] Lewis B, von Elbe B. Combustion, flames and explosions of gases. 3rd ed. New York: Academic Press, 1987.
[2] Markstein GH. Nonsteady flame propagation. New York: Pergamon Press, 1964.
[3] Buckmaster JD, Ludford GSS. Theory of laminar flames. Cambridge: Cambridge University Press, 1983.
[4] Williams FA. Combustion theory. 2nd ed. Reading, MA: Addison-Wesley, 1985.
[5] Law CK. Proc Combust Inst 1988;22:1381–402.
[6] Clavin P. Prog Energy Combust Sci 1985;11:1–59.
[7] Matalon M. Combust Sci Technol 1983;31:169–81.
[8] Chung SH, Law CK. Combust Flame 1984;55:123–5.
[9] Goey LPH, Boonkkamp T, Ten JHM. Combust Sci Technol 1997;122:399–405.
[10] Sivashinsky GI. Acta Astronautica 1976;3:889–918.
[11] Pelce P, Clavin P. J Fluid Mech 1982;124:219–37.
[12] Clavin P, Williams FA. J Fluid Mech 1982;116:251–82.
[13] Matalon M, Matkowsky BJ. J Fluid Mech 1982;124:239–59.
[14] Chung SH, Law CK. Combust Flame 1988;72:325–36.
[15] Kerstein AR, Ashurst WT, Williams FA. Phys Rev A 1988;37:2728–31.
[16] Ishizuka S, Law CK. Proc Combust Inst 1982;19:327–35.
[17] Tsuji H, Yamaoka I. Proc Combust Inst 1982;19:1533–40.
[18] Mizomoto M, Asaka Y, Ikai S, Law CK. Proc Combust Inst 1984;20:1933–9.
[19] Law CK, Cho P, Mizomoto M, Yoshida H. Proc Combust Inst 1986;21:1803–9.
[20] Dowdy DR, Smith DB, Taylor SC, Williams A. Proc Combust Inst 1990;23:325–32.
[21] Kwon S, Tseng LK, Faeth GM. Combust Flame 1992;90:230–46.
[22] Tseng LK, Ismail MA, Faeth GM. Combust Flame 1993;94:410–26.
[23] Law CK, Sung CJ, Yu G, Axelbaum RL. Combust Flame 1994;98:139–54.
[24] Kee RJ, Miller JA, Evans GH, Dixon-Lewis G. Proc Combust Inst 1988;22:1479–94.
[25] Dixon-Lewis G. Proc Combust Inst 1990;23:305–24.
[26] Sun CJ, Sung CJ, He L, Law CK. Combust Flame 1999;118:108–28.
[27] Matkowsky BJ, Sivashinsky GI. SIAM J Appl Math 1979;37(3):686–99.
[28] Shy SS, Ronney PD, Buckley SG, Yakhot V. Proc Combust Inst 1992;24:543–51.
[29] Sung CJ, Sun CJ, Law CK. Combust Flame 1996;107:114–24.
[30] Eng JA, Law CK, Zhu DL. Proc Combust Inst 1994;25:1711–8.
[31] Klimov AM. Zhur Prikl Mekh Tekhn Fiz 1983;3:49–58.
[32] Echekki T, Mungal MG. Proc Combust Inst 1990;23:455–61.
[33] Sun CJ, Law CK. Combust Flame 2000;121:236–48.
[34] Sung CJ, Liu JB, Law CK. Combust Flame 1996;106:168–83.
[35] Law CK, Ishizuka S, Cho P. Combust Sci Technol 1982;28:89–96.
[36] Wu CK, Law CK. Proc Combust Inst 1984;20:1941–9.
[37] Zhu DL, Egolfopoulos FN, Law CK. Proc Combust Inst 1988;22:1539–45.
[38] Egolfopoulos FN, Cho P, Law CK. Combust Flame 1989;76:375–91.
[39] Joulin G, Mitani T. Combust Flame 1981;40:235–46.
[40] Bray KNC. Proc R Soc London A 1990;431:315–35.
[41] Sivashinsky GI. J Chem Phys 1975;62(2):638–43.
[42] Sung CJ, Yu KM, Law CK. Combust Sci Technol 1994;100:245–70.
[43] Margolis SB. Prog Energy Combust Sci 1991;17:135–62.
[44] Matalon M, Matkowsky BJ. Combust Sci Technol 1983;34:295–316.
[45] Sohrab SH, Law CK. Combust Flame 1985;62:243–54.
[46] Tse SD, Zhu DL, Law CK. Proc Combust Inst 2000;28 (in press).
[47] Strehlow RA. Combustion fundamentals. New York: McGraw-Hill, 1984.
[48] Sivashinsky GI. Ann Rev Fluid Mech 1983;15:123–204.
[49] Joulin G, Clavin P. Combust Flame 1979;35:139–53.
[50] Sivashinsky GI, Law CK, Joulin G. Combust Sci Technol 1982;28:155–9.
[51] Bechtold JK, Matalon M. Combust Flame 1987;67:77–90.
[52] Rutland CJ, Ferziger JH. Combust Sci Technol 1990;73:305–26.
[53] Egolfopoulos FN. Proc Combust Inst 1994;25:1365–73.
[54] Im HG, Bechtold JK, Law CK. Combust Flame 1996;105:358–72.
[55] Petrov CA, Ghoniem AF. Combust Flame 1995;102:401–7.

[56] Sung CJ, Law CK. Thirty-Sixth Aerospace Sciences Meeting. AIAA Paper No. 98-0555, 1998.
[57] Sivashinsky GI, Int J. Heat Mass Transfer 1974;17:1499–506.
[58] Sivashinsky GI. Combust Sci Technol 1977;15:137–46.
[59] Rogg B. In: Peters N, Warnatz J, editors. Numerical methods in laminar flame propagation, Braunschweig: Vieweg, 1982. p. 38–48.
[60] Kailasanath K, Ganguly K, Patnaik G. Progress in astronautics and aeronautics, vol. 151. Washington, DC: AIAA, 1993. p. 247–62.
[61] Goyal G, Maas U, Warnatz J. Combust Sci Technol 1995;105:183–93.
[62] He L, Clavin P. Combust Flame 1993;93:408–20.
[63] Christiansen EW, Sung CJ, Law CK. Proc Combust Inst 1998;27:555–62.
[64] Christiansen EW, Sung CJ, Law CK. Steady and pulsating propagation and extinction of rich hydrogen/air flames at elevated pressures. Combust Flame (in press).
[65] Merzhanov AG, Borovinskaya IP. Combust Sci Technol 1975;10:195–201.
[66] Matkowsky BJ, Sivashinsky GI, SIAM. J Appl Math 1978;35:465–78.
[67] Maksimov YuM, Merzhanov AG, Pak AT, Kuchkin MN. Combust Explos Shock Waves 1981;17:393–400.
[68] Bayliss A, Matkowsky BJ. J Comp Phys 1987;71:147–68.
[69] Margolis SB, Williams FA, SIAM. J Appl Math 1989;49:1390–420.
[70] Makino A, Law CK. Proc Combust Inst 1996;26:1867–74.
[71] Makino A, Law CK. Proc Combust Inst 1998;27:2469–76.
[72] Christiansen EW, Sung CJ, Law CK. Proc Combust Inst 2000;28 (in press).
[73] Sung CJ, Law CK. Thirty-eighth Aerospace Sciences Meeting. AIAA Paper No. 2000-0577, 2000.
[74] Farmer JR, Ronney PD. Combust Sci Technol 1990;73:555–74.
[75] Sung CJ, Sun CJ, Law CK. Combust Sci Technol Comm 2000 (in press).
[76] Liñán A. Acta Astronautica 1974;1:1007–39.
[77] Law CK, Chao BH, Umemura A. Combust Sci Technol 1992;88:59–88.